



# 1 Ozone trends in homogenized Umkehr, Ozonesonde, and COH 2 overpass records

3 Irina Petropavlovskikh<sup>1,2</sup>, Jeannette D. Wild<sup>3,4</sup>, Kari Abromitis<sup>1,2</sup>, Peter Effertz<sup>1,2</sup>, Koji Miyagawa<sup>5</sup>,  
4 Lawrence E. Flynn<sup>4</sup>, Eliane Maillard-Barras<sup>6</sup>, Robert Damadeo<sup>7</sup>, Glen McConville<sup>1,2</sup>, Bryan  
5 Johnson<sup>2</sup>, Patrick Cullis<sup>2</sup>, Sophie Godin-Beckmann<sup>8</sup>, Gerard Ancellet<sup>8</sup>, Richard Querel<sup>9</sup>, Roeland  
6 Van Malderen<sup>10</sup>, Daniel Zawada<sup>11</sup>

7 <sup>1</sup> CIRES, University of Colorado, Boulder, CO, USA

8 <sup>2</sup> NOAA, Global Monitoring Lab, Boulder, CO, USA

9 <sup>3</sup> University of Maryland, Earth System Science Interdisciplinary Center (ESSIC), College Park, MD, USA

10 <sup>4</sup> NOAA/NESDIS/Center for Satellite Applications and Research (STAR), College Park, MD, USA

11 <sup>5</sup> NEIS, Tsukuba-City, Japan

12 <sup>6</sup> Federal Office of Meteorology and Climatology, MeteoSwiss, Payern, Switzerland

13 <sup>7</sup> NASA Langley Research Center, Hampton, VA, USA

14 <sup>8</sup> LATMOS Sorbonne Université, UVSQ-CNRS/INSU, Paris, France.

15 <sup>9</sup> National Institute of Water & Atmospheric Research (NIWA), Lauder, New Zealand

16 <sup>10</sup> Royal Meteorological Institute of Belgium, Uccle (Brussels), Belgium

17 <sup>11</sup> University of Saskatchewan, Saskatoon, SK, Canada

18 *Correspondence to:* Irina Petropavlovskikh (Irina.petro@Noaa.gov)

19 **Abstract.** This study presents an updated evaluation of stratospheric ozone profile trends at  
20 Arosa/Davos/Hohenpeißenberg, Switzerland/Germany, Observatory de Haute Provence (OHP), France, Boulder,  
21 Colorado, Mauna Loa Observatory (MLO) and Hilo, Hawaii, and Lauder, New Zealand with focus on the ozone  
22 recovery period post 2000. Trends are derived using vertical ozone profiles from NOAA's Dobson Network via the  
23 Umkehr method (with a recent new homogenization), ozonesondes, and the NOAA COHesive SBUV/OMPS satellite-  
24 based record (COH) sampled to match geographical coordinates of the ground-based stations used in this study.  
25 Analyses of long-term changes in stratospheric ozone time series were performed using the updated version (0.8.0) of  
26 the Long-term Ozone Trends and Uncertainties in the Stratosphere (LOTUS) Independent Linear Trend (ILT)  
27 regression model. This study finds a consistency of the trends derived from the different observational records, which  
28 is a key factor to the understanding of the recovery of the ozone layer after the implementation of the Montreal Protocol  
29 and its amendments that control ozone-depleting substances production and release into the atmosphere. The Northern  
30 Hemispheric Umkehr records of Aros/Davos, OHP, and MLO all show positive trends in the mid to upper stratosphere  
31 with trends peaking at  $\sim +2\%$ /decade. Although the upper stratospheric ozone trends derived from COH satellite  
32 records are more positive than those detected by the Umkehr system, the agreement is within the two **sigma**  
33 uncertainty. Umkehr trends in the upper stratosphere at Boulder and Lauder are positive but not statistically significant,  
34 while COH trends are larger and statistically significant (**within 2 sigma**). In the lower stratosphere, trends derived  
35 from Umkehr and ozonesonde records are mostly negative (except for positive ozonesonde trends at OHP), however  
36 the uncertainties are quite large. Additional dynamical proxies were investigated in the LOTUS model at five ground-  
37 based sites. The use of additional proxies did not significantly change trends, but equivalent latitude reduced the  
38 uncertainty of the Umkehr and COH trends in the upper stratosphere and at higher latitudes. In lower layers, additional  
39 predictors (tropopause pressure for all stations, two extra components of Quasi-Biennial Oscillation at MLO, Arctic



40 Oscillation at Arosa/Davos, OHP and MLO) improve the model fit and reduce trend uncertainties as seen by Umkehr  
41 and sonde.

## 42 **1 Introduction**

43 The WMO Ozone Assessments (WMO, 2018; WMO, 2022), indicate that for some geographical regions, the  
44 stratospheric ozone layer is recovering in accordance with the reduction of ozone depleting substances (ODS) whose  
45 production was restricted by the Montreal Protocol and its amendments. The US Clean Air Act requires NOAA to  
46 monitor prohibited chemicals and the ozone layer to ensure the success of the Montreal Protocol. NOAA's long-term  
47 network of measurements helps to interpret total column and vertically resolved ozone changes and link ozone  
48 recovery to the reduction of ODS levels in the stratosphere, changes in the lower stratosphere that are associated with  
49 climate changes, and to the increases in the troposphere that are influenced by the stratosphere/troposphere exchange  
50 and long-range transported pollution. The ongoing recovery of the stratospheric ozone layer is of great importance to  
51 human health (i.e. cancer from enhanced UV exposures, Madronich et al., 2021), the sustained production of crops,  
52 and the success of fisheries (dangerous algae blooms). For more information see the Environmental Effects  
53 Assessment Panel 2022 Quadrennial Assessment (EEAP, 2023).

54 Studies of ozone recovery require long-term datasets often consisting of data merged from several instruments, or  
55 from a single instrument type on multiple satellite platforms, or at a ground-based (GB) station. 2011 saw the initiation  
56 of the SPARC/IO3C/IGACO-O3/NDACC (SI2N) activity to evaluate ozone trends in the depletion and recovery  
57 phases using both GB and merged satellite observations. The resulting report (Harris et al., 2015) emerged near the  
58 release of the 2014 WMO Ozone Assessment (WMO, 2014). The two studies resulted in broadly similar trend values  
59 in both the depletion and recovery phases. But the WMO report determined the recovery trends to be statistically  
60 significant, whereas the SI2N study did not. The discrepancy centered on differing error analysis techniques for the  
61 merged datasets: SI2N using distribution of the individual variances around the mean and WMO using weighted mean  
62 of the individual standard deviations.

63 The Long-term Ozone Trends and Uncertainties in the Stratosphere (LOTUS) study sought to reconcile the differences  
64 between the WMO Assessment and the SI2N study. Phase 1 focused on developing best practices for data merging,  
65 trend determination and error analyses. Results focused on analysis of broad latitudinal regions, near global, Northern  
66 and Southern Hemisphere, and Tropics as were used in the SI2N studies. Results are found in the 2019 report  
67 (SPARC/IO3C/GAW, 2019). Phase 2 refined the trend models, and extended the study to gridded, and GB ozone data  
68 sets. The development of methods used in trend detection is built on the community knowledge gained during the  
69 Tiger Team project in early 1990s (Reinsel et al., 2005), collaborations through the SPARC, WMO and IO3C  
70 supported LOTUS activity (Hassler et al., 2014; Harris et al., 2015; Godin-Beekmann et al., 2022) and the most recent  
71 contributions to the WMO Ozone assessment analyses published in Chapter 3, "Update on Global Ozone: Past, Present  
72 and Future" (Hassler et al., 2022).

73 Understanding the causes of the differences between GB and satellite records can create improvements not only in the  
74 internal consistency of data sets, but also in the uncertainties of overall ozone trends. Further, development of  
75 techniques to directly assess uncertainties in the merged records resulting from discrepancies that cannot be completely



76 reconciled, such as small relative drifts and differences resulting from coordinate transformations and sampling  
77 differences, allows for a more precise estimate of significance of the mean trends. For the GB and satellite data used  
78 in the 2019 LOTUS Report, information on stability and drifts of the measurement was incomplete. The  
79 homogenization of many ozonesonde records was recently addressed and data were reprocessed (Tarasick et al., 2016;  
80 Van Malderen et al., 2016; Witte et al., 2017; Sterling et al., 2018; Witte et al., 2018; Ancellet et al., 2022) while some  
81 instrumental artifacts still need to be addressed (Smit, 2021).

82 The first attempt to evaluate representativeness of the trends derived from GB station records in the middle and upper  
83 stratosphere using SBUV data was done as a part of the LOTUS activity and was discussed in the 2019 LOTUS report.  
84 Comparisons of trends derived from satellite data sub-sampled at the station location (overpass) to those derived from  
85 the relevant zonal average provide a measure of potential sampling errors when comparing satellite and GB trends  
86 (Zerefos et al., 2018; Godin-Beekmann et al., 2022). This paper continues that work by comparing trends derived from  
87 several GB and satellite records that are matched spatially. We further investigate the impact of temporal matching on  
88 trends.

89 The common statistical linear regression trend model used in the 2019 LOTUS Report and the 2022 update (Godin-  
90 Beekmann et al., 2022) was optimized for analyses of the zonally averaged satellite data sets. However, analyses of  
91 the GB and satellite overpass ozone profile data may require reconsideration of additional proxies and optimization  
92 methods to improve interpretation of the processes that impact ozone changes over limited geophysical regions and  
93 reduce trend uncertainties. An assessment of model sensitivities to uncertainties in the volcanic aerosols, solar cycle,  
94 QBO, El Nino Southern Oscillation (ENSO) and other mechanisms also need to be considered in the GB and satellite  
95 overpass record trend analysis. The localized time series for the assessment of dynamical and chemical proxies can  
96 improve attribution of ozone variability, especially in the lower stratosphere, thus reducing uncertainties in the derived  
97 trends. This paper provides an assessment of uncertainties in the derived trends from the NOAA ground-based,  
98 ozonesonde and SBUV/OMPS (zonally averaged and overpass) records and reports improvements in the Multiple  
99 Linear Regression (MLR) trend uncertainties with addition of proxies representing interannual dynamical variability  
100 or long-term changes in atmospheric circulation.

101 In the LOTUS report, the ozone trends were analyzed at low and middle latitudes, with a focus on the upper and  
102 middle stratosphere. This paper includes middle and low latitude trends assessed in the lower stratosphere and thus  
103 offers an opportunity to test the additional proxy of the tropopause pressure (Thompson et al., 2021).

## 104 **2 Data**

### 105 **2.1 Umkehr and Ozonesonde Records at NOAA**

106 The Dobson Ozone Spectrophotometer has been used to study total ozone since its development in the 1920s  
107 (Staehelin et al., 2018). Dobson records are regularly used in satellite record validation (Bai et al., 2015; Koukouli et  
108 al., 2016; Boynard et al., 2018) and the development of global combined ozone data records (Fioletov et al., 2008;  
109 Hassler et al., 2018). The NOAA Dobson ozone record was homogenized in 2017 to account for inconsistencies in  
110 past calibration records, data processing methods and selection of representative data (Evans et al., 2017). NOAA



111 Dobson instruments at 4 stations and MeteoSwiss at Arosa/Davos also measure Umkehr profiles, which are derived  
112 as partial column ozone amounts in ~5 km layers. Profiles are derived using an optimum statistical inversion of Dobson  
113 measurements taken continuously at different solar zenith angles (SZAs) (Petropavlovskikh, 2005; Hassler, 2014).  
114 These Umkehr data were recently homogenized to assure the removal of small but significant instrumental artifacts  
115 that can impact the accurate detection of stratospheric ozone trends (Petropavlovskikh et al., 2022, Maillard Barras et  
116 al., 2022). This study focuses on Umkehr records from the MeteoSwiss station of Arosa/Davos, Switzerland, and on  
117 Umkehr records from the NOAA stations of Boulder, Colorado, Mauna Loa Observatory (MLO), Hawaii, Lauder,  
118 New Zealand, and the Umkehr record from Observatory de Haute Provence (OHP), France). NOAA/GML for Umkehr  
119 data means that the NOAA optimization process was applied to the operational records (N-values) prior to the retrieval  
120 of ozone profiles. The source data used in this study are available at  
121 <https://gml.noaa.gov/aftp/data/ozwv/Dobson/AC4/Umkehr/Optimized/>. See **Table 1** for details on the GB datasets,  
122 locations, source of data and temporal extent of data used. Umkehr measurements are typically made twice per day  
123 when there is no cloud obstruction.

124 The ozonesonde instrument has been flown at 4 NOAA stations since the 1980s. Evolving instrumentation and  
125 standard operating procedures led to the development of data homogenization methods by NOAA and the international  
126 community (i.e., ASOPOS-1, Smit, 2014) to resolve record inconsistencies in the NOAA (Sterling et al., 2018),  
127 Canadian (Tarasick et al., 2016) and SHADOZ (Southern Hemisphere Additional Data from Ozonesonde) networks  
128 (Witte et al., 2017; Witte et al., 2018). The effort was extended in the ASOPOS-2 (Smit et al., 2021) activity and  
129 included a larger group of stations that are part of the NDACC (Network for Detection of Atmospheric Composition  
130 Change) and WMO GAW (World Meteorological Organization Global Atmosphere Watch program) networks. The  
131 error budget for each profile is calculated and included in the archived files (Sterling, 2018). Modern ozonesonde  
132 instruments measure ozone at high vertical resolution, on the order of 100 m (Thompson et al., 2019) depending on  
133 the altitude.

134 The sondes constitute an essential component of satellite calibration and cross-calibration (Hubert et al., 2016),  
135 verification and improvement of climate chemistry and chemistry-transport models (Wargan et al., 2018; Stauffer et  
136 al., 2019). The Dobson total ozone, Umkehr and ozonesonde profile records provide key measurements for upper and  
137 middle stratospheric ozone trend calculations, and are part of the NOAA benchmark network for stratospheric ozone  
138 profile observations (SPARC/IO3C/GAW, 2019; Godin-Beekmann et al., 2022; WMO, 2022).

139 The ozonesonde data are used for trend analyses from OHP, Boulder, and Lauder stations where we have Umkehr  
140 observations. Ozonesondes are launched at Hilo, Hawaii, which is nearly co-located with MLO. Ozonesonde data  
141 for the Arosa/Davos panel are selected from Hohenpeißenberg (HOH), Germany station that is in close vicinity to  
142 Arosa/Davos station. Sonde measurements are typically measured once or twice per week, varying somewhat with  
143 station operational procedures.

144 Data for the NOAA GML ozonesonde records are publicly available from the NOAA Global Monitoring Lab (GML)  
145 at <https://gml.noaa.gov/aftp/data/ozwv/Ozonesonde/>. We use the '100 Meter Average Files' in each station directory.  
146 Other sonde datasets used in this study are also available at several other data centers including the World Ozone and  
147 Ultraviolet Radiation Data Centre (WOUDC, [www.woudc.org](http://www.woudc.org)), Network for the Detection of Atmospheric



148 Composition Change (NDACC, [www.ndacc.org](http://www.ndacc.org)) data centers, or at the Harmonization and Evaluation of Ground-  
 149 based Instruments for Free-Tropospheric Ozone Measurements (HEGIFTOM, <https://hegiftom.meteo.be/>) archive.

150 **Table 1 denotes the source of each dataset used in this study.**

151 The ozonesonde data is of significantly higher vertical resolution (even when used as 100 m averages) than the Umkehr  
 152 data layers of approximately 5000 m. In order to create a dataset with comparable resolution, we use the Umkehr  
 153 averaging kernels (AK) to smooth the sonde data. Details appear in Appendix A. We cap the sonde profile at Umkehr  
 154 layer 5 (16–32 hPa) as there is not sufficient sonde information at higher altitudes to meet the requirements of the AKs  
 155 for layers 6 and above. We further match the ozonesonde data to the dates when both Umkehr and sonde data are  
 156 available using  $\pm 24$  hours to find a match, then generate the ozonesonde monthly mean. Appendix D explores the  
 157 impact of temporal sampling on trends. The final matched dataset, with AK averaging, is publicly available at  
 158 [https://gml.noaa.gov/aftp/ozwv/Publications/2023\\_Umkehr\\_Ozone\\_Trends\\_Paper/](https://gml.noaa.gov/aftp/ozwv/Publications/2023_Umkehr_Ozone_Trends_Paper/).

159

Location	WUOD C Station #	Instrument	Date Range used in trend calculations	Source
Arosa/Davos Arosa, Switzerland (46.8° N, 9.7° E) Davos, Switzerland (46.8° N, 9.8° E)	035	Umkehr	1980 – 2018 2018 – 2020	Optimization by NOAA/GML
Hohenpeißenberg (HOH), Germany (47.8° N, 11.0° E)	099	Ozonesonde	1980 – 2020	NDACC
Observatory de Haute Provence (OHP), France (43.9°N, 5.8° E)	040	Umkehr	1983 – 2020	NOAA/GML
		Ozonesonde	1991 – 2020	NDACC (same as HEGIFTOM)
Boulder, Colorado (40.0° N, 105.3° W)	067	Umkehr	1980 – 2020	NOAA/GML
		Ozonesonde	1980 – 2020	NOAA/GML - 100m average data
Mauna Loa Observatory (MLO), Hawaii (19.5°N, 155.6°W)	031	Umkehr	1982 – 2020	NOAA/GML



Hilo, Hawaii (19.7° N, 155.1° W)	109	Ozonesonde	1982 – 2020	NOAA/GML - 100m average data
Lauder, New Zealand (45.0°S, 169.7°E)	256	Umkehr	1987 – 2020	NOAA/GML
		Ozonesonde	1987 – 2020	NDACC

160

161 **Table 1: GB datasets, location, instrument type, temporal extent, data record source. For the trend calculations we remove**  
 162 **data during volcanic periods from 1982–1984 and 1991–1994.**

163 **2.2 The NOAA Cohesive (COH) Station Overpass Ozone Profile Datasets**  
 164

165 NASA and NOAA have produced satellite measurements of ozone profiles through the Solar Backscatter Ultraviolet  
 166 (SBUV) on the sequence of Polar Orbiting Environmental Satellites (POES) since 1978. This measurement series is  
 167 extended with the related Ozone Mapping and Profiler Suite (OMPS) nadir profiler (NP) instruments using similar  
 168 measurement techniques and retrieval algorithms. These combine to provide nearly 45 years of continuous data (1978  
 169 – present). This single instrument type dataset eliminates many homogeneity issues including varying vertical  
 170 resolution, or instrumentation differences. Version 8.6 SBUV data incorporates additional calibration adjustments  
 171 beyond the Version 8 release (McPeters et al., 2013). Small but evident biases remain (Kramarova et al., 2013a).  
 172 Several methods have been historically used to combine these datasets into a continuous series. The NASA MOD  
 173 version 1 dataset based on SBUV and OMPS v8.6 (Frith, 2014) combines data from all available satellites with no  
 174 modification or bias adjustments. NASA has developed an alternate processing for the SBUV and OMPS data (v8.7)  
 175 which incorporates new calibrations at the radiance level, and updated a priori with improved troposphere.  
 176 Additionally, the a priori is chosen to be representative of the local solar time of the measurement. MOD v2 is based  
 177 on the v8.7 processing (Frith et al., 2020), and further applies an adjustment to the v8.7 data to shift all measurements  
 178 to a nominal measurement time of 1:30 PM local time.

179 The NOAA SBUV/2 and OMPS Cohesive dataset (further referred to as COH) combines data from the SBUV/2 and  
 180 OMPS instruments using NASA’s version 8.6 for the SBUV/2 data and NOAA/NESDIS version 4r1 for the OMPS  
 181 Suomi National Polar-orbiting Partnership (SNPP) data. This dataset uses correlation-based adjustments providing  
 182 an overall bias adjustment plus an ozone-dependent factor (Wild et al., 2016) to moderate the remaining biases  
 183 between instruments in the series. The resulting profile product is a set of daily or monthly zonal means and is publicly  
 184 available at [https://ftp.cpc.ncep.noaa.gov/SBUV\\_CDR](https://ftp.cpc.ncep.noaa.gov/SBUV_CDR). Zones are 5° wide in latitude, identified by the central latitude  
 185 (2.5°, 7.5°, etc.). Contributing satellites and their period of use is shown in Table 2.

186

Satellite	Dates
Nimbus 07	10/1978 – 5/1989
NOAA 11	6/1989 – 12/1993



NOAA 09	1/1994 – 6/1997
NOAA 11	7/1997 – 12/2000
NOAA 16	1/2001 – 12/2003
NOAA 17	1/2004 – 12/2005
NOAA 18	1/2006 – 12/2010
NOAA 19	1/2011 – 12/2013
SNPP	1/2014 – present

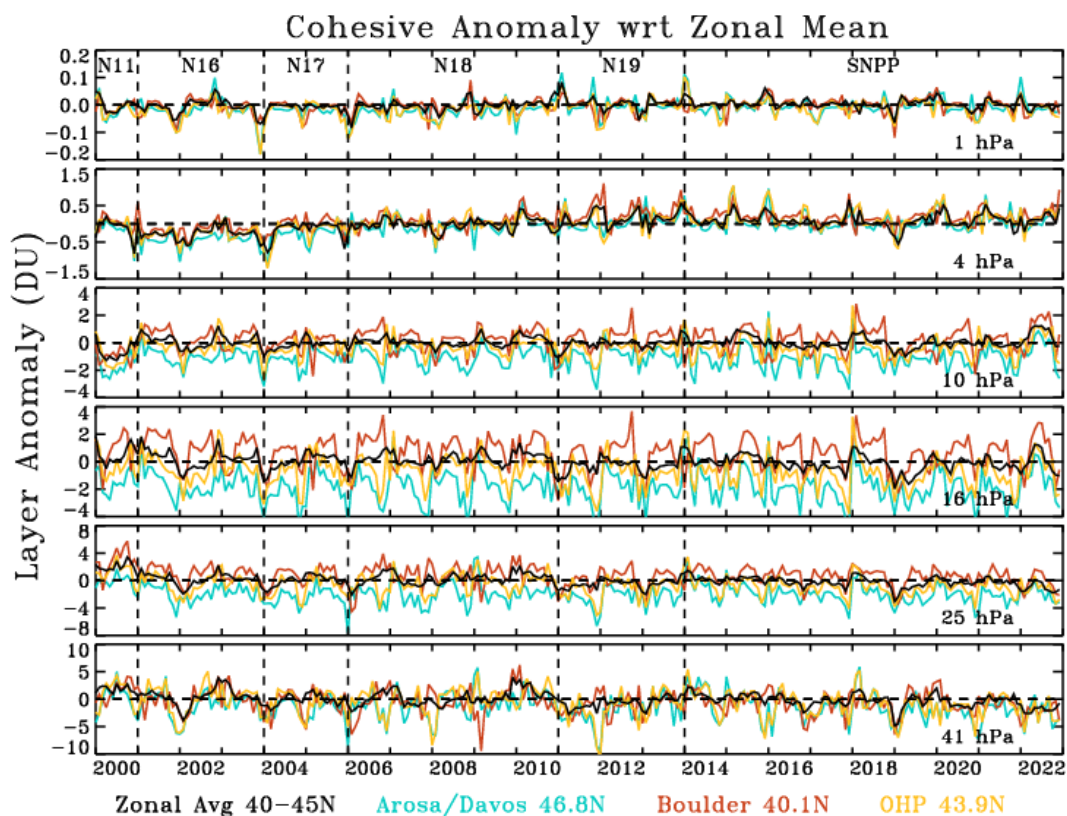
187 **Table 2: Satellite mapping for COH data series**

188 A previous version of this dataset using OMPS v3r2 has been used in climate reviews and trend studies (Godin-  
 189 Beekmann et al., 2022; Weber et al., 2022a, 2022b) including Chapter 3 of the WMO Ozone Assessment (Hassler et  
 190 al., 2022). Appendix B examines the differences between the data versions. The impact on trends is limited to less  
 191 than 1% per decade, well within the precision of the trend results.

192 We create the overpass data at a ground station by collecting all profiles from a satellite within a  $\pm 2/20^\circ$   
 193 latitude/longitude box centred on the station. The box size is chosen to ensure that one to four points are found per  
 194 day. Fewer points are found if the orbit passes directly over the station; more points are found if the orbits straddle  
 195 the station. The collected profiles are inverse-distance weighted to the station location and averaged. COH style  
 196 adjustments are applied (Wild et al., 2016) creating a COH overpass time series from 1978 to present. This dataset is  
 197 available on the NOAA website at [https://ftp.cpc.ncep.noaa.gov/SBUV\\_CDR/overpass](https://ftp.cpc.ncep.noaa.gov/SBUV_CDR/overpass).

198 Figure 1 shows the ozone anomaly time series for the 40–45° N zonal average data, and for the data at 3 stations in or  
 199 near the zone. Anomalies are calculated with respect to the zonal average climatology. The series shown are for the  
 200 layer data with the bottom pressure of the layer displayed on the right side of the graph. This depiction retains the  
 201 information about the relative differences between the stations and the zonal average. In the mid-stratosphere (25–10  
 202 hPa) the biases between the stations are most pronounced with Arosa/Davos usually showing less ozone and Boulder  
 203 usually showing more ozone. At the uppermost layers (1 and 4 hPa), and the lowest layer (41 hPa) the bias between  
 204 stations is reduced. The anomalies for Arosa/Davos and OHP, which are geographically closer than Boulder, are often  
 205 nearly anticorrelated with the Boulder anomalies especially in the second half of the year. Indeed at 16 hPa in  
 206 particular, one can see that often the Boulder anomalies are positive when the Arosa/Davos and OHP anomalies are  
 207 negative.

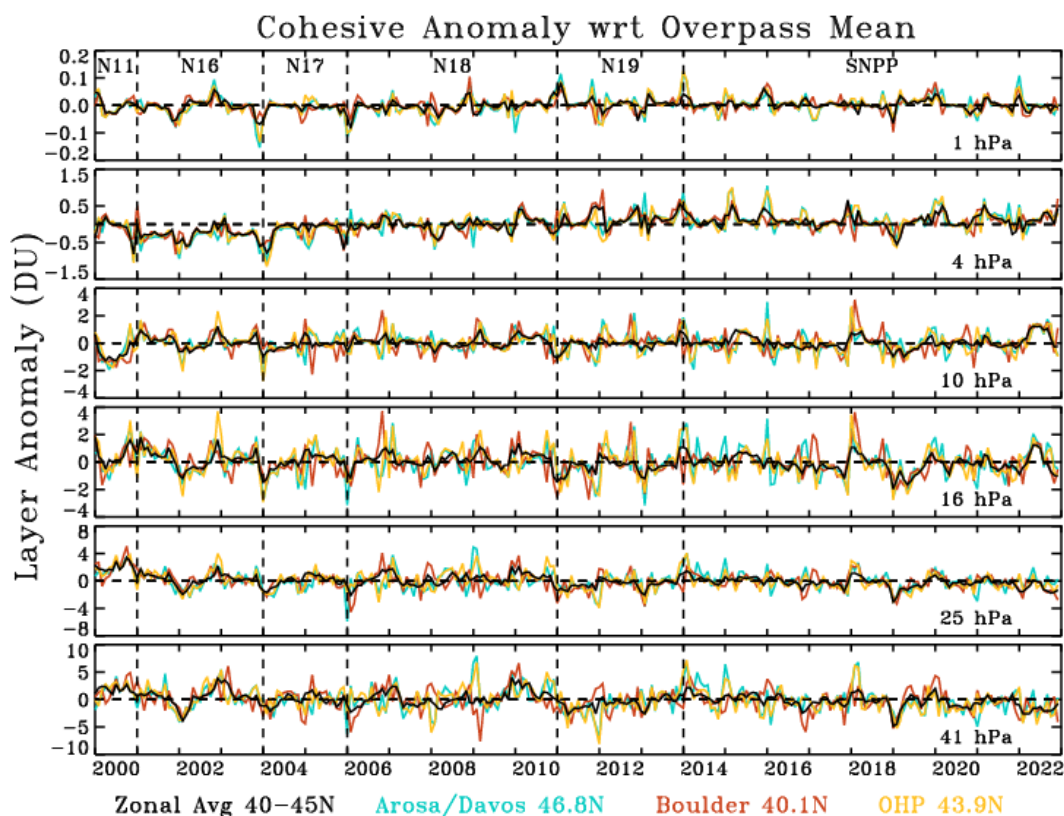
208



209

210 **Figure 1. Monthly ozone anomaly relative to the zonal mean monthly averages. This process leaves intact the trend for**  
 211 **each site and the zone, and accentuates the differences between the station values since all anomalies are referenced to the**  
 212 **zonal product. Evident at 4 hPa is a positive trend from 2002 to 2013, then a levelling out after.**

213 Figure 2 also shows the anomalies for the 40–45° N zonal average with the station anomalies, but each anomaly is  
 214 now created using the climatology derived from each separate dataset. This removes the bias between the stations and  
 215 the zones. At 1 hPa, Arosa/Davos appears to display the most variation (largest peaks and dips) in the anomalies.  
 216 Since the anomaly for each site is now based on the seasonality of each site’s data the structure in the anomalies is  
 217 more uniform. For example, now at 16 hPa, the difference between Boulder and the two sites Arosa/Davos and OHP  
 218 in the latter half of the year is removed. In 2012, where the Boulder anomaly was positive with respect to the zonal  
 219 average seasonal value, and the Arosa/Davos and OHP sets were negative with respect to the zonal seasonal average,  
 220 all are now of the same sign with respect to their own seasonal averages. Nonetheless, there are events where one  
 221 station shows opposite anomalies to the other two, for example early 2009 at 41 hPa, when the Boulder anomaly is  
 222 negative, and Arosa/Davos and OHP are positive. Thus, it is noted that when comparing daily or monthly data values  
 223 from GB and satellite data, the overpass data will reveal a different structure than the zonal data. The trend calculations  
 224 in this paper are based on the datasets of Fig. 2, where the seasonal behavior is removed using the station seasonality.  
 225



226

227

228

229

230

**Figure 2. Monthly ozone anomaly relative to the monthly climatology for each station overpass dataset. This process leaves intact the trend for each site and the zone, and shows the consistency among the stations when each station climatology is removed. This dataset is used for the trends calculations. Evident at 4 hPa is a positive trend from 2002 to 2013, then a leveling out after. Trends are run on this dataset.**

231

232

233

234

235

236

237

238

239

240

241

242

The COH overpass and zonal datasets have a similar vertical granularity as the Umkehr dataset, but use somewhat different pressures for the demarcation of the top and bottom of each layer. Since no additional smoothing is required, we simply use interpolation and integration to convert the COH layer profiles to the Umkehr layers. We exclude layers 1 to 4 since there is little sensitivity in SBUV and OMPS NP in these layers (Kramarova et al., 2013b). The overpass monthly-mean dataset in this study uses all COH data matched to dates when Umkehr data also exists. This dataset is publicly available at [https://gml.noaa.gov/aftp/ozwv/Publications/2023\\_Umkehr\\_Ozone\\_Trends\\_Paper/](https://gml.noaa.gov/aftp/ozwv/Publications/2023_Umkehr_Ozone_Trends_Paper/). Appendix D explores the impact of temporal sampling on trends.

This study also uses a specialized zonal monthly-mean COH product which is the average of all daily profiles with an Umkehr match at the associated GB station. Zones used for most stations are the 5° wide zone which includes the geographic station latitude (Arosa/Davies: 47.5° N, OHP: 42.5° N, MLO: 17.5° N). Boulder and Lauder, however, are located directly on the border of two zones, so the zonal product in this study is the mathematical average of the two adjacent zones (Boulder: 37.5° N and 42.5° N, Lauder 42.5° S and 47.5° S).



243 **3 Methods**

244 **3.1 LOTUS Model overview - the Reference Model**

245 The Long-term Ozone Trends and Uncertainties in the Stratosphere (LOTUS) activity is a project of SPARC  
 246 (Stratosphere-Troposphere Processes and their Role in Climate) and has produced a statistical Multiple Linear  
 247 Regression (MLR) model called the LOTUS model (<https://usask-arg.github.io/lotus-regression/index.html>).

248 The 2019 LOTUS report (SPARC/IO3C/GAW, 2019) and update (Godin-Beekmann et al., 2022) have quantified  
 249 stratospheric ozone trends and evaluated their uncertainties. The LOTUS model is a general-least-squares approach  
 250 MLR model. This study uses version 1 (v 0.8.0) with the independent linear trends (ILT) configuration. The  
 251 independent linear terms represent the ozone depletion period (pre-1997), the ozone recovery period (post-2000) and  
 252 an optional gap period (1997–2000). We will call the terms “pre”, “post” and “gap” for short. The version 0.8.0 adds  
 253 an option to enforce continuity across the gap period which is used in this study. The regression uses an interactive  
 254 procedure (Cochrane and Orcutt, 1949) and the autocorrelation coefficient is adjusted with each iteration. The  
 255 covariance matrix is modified accordingly to account for measurement gaps (Savin and White, 1978).

256 The LOTUS model (further referred as reference model in this study) is written here:

257 
$$\hat{y}(t, z) = \beta_0(t, z)C_{pre}(t) + \beta_1(t, z)C_{post}(t) + \beta_2(t, z)Linear_{pre}(t) + \beta_3(t, z)Linear_{post}(t) + \sum_{i=1}^n \beta_i X_i(t, z) + \epsilon(t, z) \quad (1)$$

258 where  $\hat{y}(t, z)$  is the estimated ozone at time  $t$  and altitude  $z$ ;  $\beta$  are the fitted coefficients of the model; the residual  
 259 term,  $\epsilon(t, z)$  is the difference between the LOTUS model and the input data.  $C_{pre}$  and  $C_{post}$  are the constant terms as  
 260 defined by:

261 
$$Constant_{pre} = \begin{cases} 1 & \text{for } t < 1997\text{-Jan} \\ 1 - mt & \text{for } 1997\text{-Jan} \leq t < 2000\text{-Jan} \\ 0 & \text{for } t \geq 2000\text{-Jan} \end{cases}$$

262 
$$Constant_{post} = \begin{cases} 0 & \text{for } t < 1997\text{-Jan} \\ mt & \text{for } 1997\text{-Jan} \leq t < 2000\text{-Jan} \\ 1 & \text{for } t \geq 2000\text{-Jan} \end{cases}$$

263 where  $0.29135$  and  $t = \text{month}$  starting in January 1980 and ending in December 2020. Indeed, the constant terms are  
 264 only constant in the “pre” and “post” periods. The 3-year “gap” period is represented by a line of slope  $m$  connecting  
 265 the two constant (pre and post period bias) terms.

266 The linear terms of the model are defined as:

267 
$$linear_{pre} = \begin{cases} mt - b & \text{for } t < 1997\text{-Jan} \\ 0 & \text{for } t \geq 1997\text{-Jan} \end{cases}$$

268 
$$linear_{post} = \begin{cases} 0 & \text{for } t < 2000\text{-Jan} \\ mt & \text{for } t \geq 2000\text{-Jan} \end{cases}$$

269 where  $m=0.008487$ ,  $b = -1.700240$ , and  $t = \text{month}$  starting in January 1980 and ending in December 2020.

270 Natural variability is a complicating factor in deriving trends associated with the changes in the ozone depleting  
 271 chemistry. LOTUS fits predictor variables as proxies for natural variability to the ozone data so that one can interpret  
 272 the resulting linear trend as a trend due to the changes in chemistry. The summation term is the summation of the  
 273 predictors used as a proxy for the dynamical induced ozone variability.



274 The natural variability proxies in the LOTUS model v 0.8.0 are Aerosol Optical Depth (AOD), El Niño/ Southern  
275 Oscillation (ENSO), and the Quasi-Biennial Oscillation (QBO) in the form of the first two principal components (also  
276 known as an empirical orthogonal function analysis). The data sources for each are described in Table 3.

277 Large SO<sub>2</sub> levels after volcanic eruptions can impact the validity of sonde ozone retrievals (Yoon et al., 2022). Both  
278 Umkehr and satellite ozone profiles from SBUV and OMPS are highly uncertain and/or biased because of high aerosol  
279 load during volcanic eruptions (DeLuisi et al, 1989; Petropavlovskikh et al., 2005, 2022; Bhartia et al, 1993, Torres  
280 et al., 1995, Bhartia et al, 2013). It is recommended that the data for 2 to 3 years after the El-Chichon and Pinatubo  
281 large volcanic eruptions should not be used in trend analyses. Therefore, we exclude data during the volcanic periods  
282 (1982–1983 and 1991–1993) from the analyzed time series. Moreover, this study is focused on the linear trend  
283 analyses after 2000 when there are no large stratospheric aerosol perturbations that significantly influence  
284 stratospheric ozone variability over the middle latitudes and therefore impact trend and uncertainty estimates. Since  
285 we have eliminated the data during the volcanic period, this study does not include the AOD proxy in the calculations.

286 We define the ‘reference’ model (RM) as the proxies most commonly used for the dynamical proxies which is  
287 equivalent to the LOTUS model v 0.8.0 minus the AOD term. The representative equation is:

$$288 \sum_{i=1}^n \beta_i(t, z) X_i(t) = \beta_4(t, z) QBO_A(t) + \beta_5(t, z) QBO_B(t) + \beta_6(t, z) ENSO(t) + \beta_7(t, z) Solar(t) \quad (2)$$

289 The Quasi-biennial Oscillation (QBO) is derived from the Singapore radiosonde profiles (1979–2020) that detect  
290 variability in the direction of the tropical winds in the lower stratosphere. It also shows that zonal wind variation  
291 propagates downward with an average period of ~28 months [Wallace, 1973]. The principal component analysis of  
292 the 100–10 hPa zonal winds can describe the majority of the wind variability. The reference model (and LOTUS v  
293 0.8.0) use the two leading modes of the calculated empirical orthogonal functions (EOF) for trend analyses [Wallace  
294 et al., 1993].

295 The El Niño/ Southern Oscillation (ENSO) is a periodic mode of climate variability of the atmosphere and sea surface  
296 temperatures associated with the equatorial Pacific Ocean with periods ranging from 2–8 years. The Multivariate  
297 ENSO index (MEI) is produced by the NOAA Physical Sciences Laboratory and is derived from the EOF analysis of  
298 sea surface temperature, sea level pressure, outgoing terrestrial radiation, and surface winds in the area of the Pacific  
299 basin from 30° S to 30° N and from 100° E to 70° W (Wolter and Timlin, 2011). Temperature anomalies in the  
300 troposphere with corresponding stratospheric temperature anomalies during El Niño/ La Niña events modulate the  
301 tropical upwelling of the Brewer-Dobson circulation (BDC) and thus the meridional transport of ozone in the  
302 stratosphere. (Diallo et al., 2018).

303 The solar cycle is the 11-year periodic cycle of solar activity and solar irradiance that reaches the Earth’s atmosphere.  
304 The change in UV radiation that is absorbed by the atmosphere, most notably in the upper stratosphere, leads to  
305 changes in atmospheric temperature and the photochemistry which produces ozone. (Lee and Smith, 2003). The 10.7  
306 cm solar radio flux data is used as the proxy for the solar cycle in the LOTUS model.

307 Seasonal components in the form of Fourier harmonics were added into the LOTUS model with version 0.8.0. Godin-  
308 Beekman et al. (2022) showed in their Fig. 7 that the model fit for the ozone profile satellite and model records is  
309 improved by adding seasonal components to the proxies, increasing the adjusted R-squared (R<sup>2</sup>) from 0.3 or less to  
310 0.3 to 0.5. The seasonality and relevant contributions of some predictor’s variables are compensated in this study by



311 adding the seasonal components to the fitted predictors. Seasonal components are represented in the model by sine  
312 and cosine functions with periods of 12 and 6 months that describe the variability of the proxies on these timescales.  
313 So, for each fitted predictor in the model

314  $\beta_i X_i(t, z)$  where  $i > 1$

315 a seasonal variation in the form of Fourier components is added as follows:

316 
$$\beta_m(t, z) = \beta_{m,0}(z) + \sum_{i=1}^2 \beta_{m,1,i}(z) \sin\left(\frac{2\pi i t}{12}\right) + \sum_{i=1}^2 \beta_{m,2,i}(z) \cos\left(\frac{2\pi i t}{12}\right)$$

### 317 3.2 The Extended Model - Adding Predictors

318 Recent publications (i.e. Petropavlovskikh et al., 2019; Szelag et al., 2020; Godin-Beekmann et al, 2022; Millan et al.  
319 2024) highlight the need to reduce the trend uncertainties in the lower stratosphere (LS). There is still a discrepancy  
320 between modeled and observed ozone trends in the LS but large uncertainties make comparisons difficult. In this  
321 study, we test additional predictors in the model to account for dynamical variability of ozone in the stratosphere, thus  
322 improving the model performance and reducing the uncertainty of the trends. The argument for additional predictors  
323 is that the LOTUS model was developed for the regression of zonally averaged ozone data, which reduces some  
324 variability that might be impacting the ground-based records on regional bases. Impact of additional proxies in trend  
325 analyses were reported in other publications (Weber et al, 2022a, Bernet, 2023 and references therein), and were  
326 mostly found to improve the statistical model fit at high latitudes where the impact of the descending branch of the  
327 Brewer-Dobson circulation and Arctic/Antarctic oscillations has contributed to additional variability in stratospheric  
328 ozone records.

329 In what we define as the ‘extended’ model, we add single additional predictors (one at a time) in the model as such:

330 
$$\sum_{i=1}^n \beta_i(t, z) X_i(t, z) = \beta_4(t, z) QBO_A(t) + \beta_5(t, z) QBO_B(t) + \beta_6(t, z) ENSO(t) + \beta_7(t, z) Solar(t) + \beta_8(t, z) X_{predictor}(t, z)$$

331 The fitted predictors contain Fourier components, like in the reference model, to allow for seasonal variation.

332 We test the following additional predictors as described below to assess the impact on trends and uncertainties:

333

334 • Quasi-Biennial Oscillation (QBO): Two notable disruptions to the otherwise relatively periodic QBO have  
335 occurred during the study period: 2015–2016 and in 2020 (Diallo, et. al 2022). Two additional leading modes  
336 of the calculated empirical orthogonal functions (EOF) are tested to improve the trend model fit during the  
337 anomalous QBO years.

338 • Arctic/Antarctic Oscillation (AO/AAO): the pattern of surface air pressure anomalies in the polar region and  
339 certain mid-latitude regions. The AO/AAO has strong correlations (Lawrence et al 2020) with stratospheric  
340 ozone through the strength of the polar vortex. The positive phase of the AO or AAO in the winter months  
341 is associated with low activity in the vertically propagating planetary Rossby waves, a strong polar vortex, a  
342 low vortex wavenumber, and low stratospheric temperatures. Thus, the positive (negative) phase of the  
343 AO/AAO is correlated to low (high) ozone anomalies especially in the winter months (Lawrence et al, 2020).



- 344
- 345
- 346
- 347
- 348
- 349
- 350
- 351
- 352
- 353
- 354
- 355
- 356
- 357
- 358
- 359
- 360
- 361
- 362
- 363
- 364
- 365
- 366
- 367
- North Atlantic Oscillation (NAO): Similar to the Arctic Oscillation, this is a pattern of surface air pressure anomalies between certain regions in the high altitudes of the North Atlantic Ocean. This index is calculated by the pressure difference between the Azores high and the subpolar low.
  - Eddy Heat Flux (EHF): The flux of heat through a zonal plane by transport due to the Brewer-Dobson circulation, here averaged from 45–75° N/S (use EHF S for Lauder only). This represents the planetary wave activity that drives transport of ozone.
  - Tropopause Pressure (TP): Pressure level of boundary between the troposphere and the stratosphere. In this study, we use the monthly mean pressure level of the tropopause from the NOAA National Centers for Environmental Prediction (NCEP) reanalysis product. As the troposphere warms due to release of GHGs and the stratosphere cools due to ODSs destroying stratospheric ozone, the tropopause is rising (Meng et al., 2021). Thompson et al, (2021) and Stauffer et al., (2023) found that the lower stratospheric ozone trends in tropics become slightly positive when recomputed with respect to the tropopause height (which has its own trend). This finding indicates that ozone depletion in the lower stratosphere (i.e. Ball et al., 2020) is driven by climate-change-related changes in transport and mixing in the lower stratosphere. Therefore, we are testing the TP proxy in the model to account for non-chemical ozone losses in order to assess chemical attribution of ozone trends.
  - Equivalent Latitude (EqLat): Geographical latitude of the isoline encircling the area of equal Potential Vorticity (PV) (Lary et al, 1995). The EqLat normalizes the range of PV values that change with season and interannual and makes it convenient for interpretation of ozone variability and trends (i.e. Wohltmann et al 2005). The dataset was generated from GMI CTM analyses (private communications with Susan Strahan, June 2021) for each ground-based station overpass criteria (latitude and longitude envelope, see above) and at several altitude levels coincident with Umkehr ozone profile layers. Appendix C discusses a COH dataset based on EqLat instead of geometric latitude. No advantage was found by using the EqLat coordinate system for the COH zonal dataset.

368 Source datasets for all predictors in the reference and extended models are shown in Table 3.

Predictor	Description	Source
ENSO	El Nino/Southern Oscillation	Monthly Mean Multivariate ENSO Index <a href="https://psl.noaa.gov/enso/mei.old/">https://psl.noaa.gov/enso/mei.old/</a> <sup>1</sup>
Solar	Solar 10.7cm flux	<a href="https://spaceweather.gc.ca/forecast-prevision/solar-solaire/solarflux/sx-5-en.php">https://spaceweather.gc.ca/forecast-prevision/solar-solaire/solarflux/sx-5-en.php</a>



<b>QBO</b>	<b>Quasi-Biennial Oscillation</b>	<b>Principal Component Analysis of the Monthly Mean Zonal Wind</b> <a href="https://www.geo.fu-berlin.de/met/ag/strat/produkte/qbo/qbo.dat">https://www.geo.fu-berlin.de/met/ag/strat/produkte/qbo/qbo.dat</a>
<b>AOD</b>	<b>AOD is included in the LOTUS model, but not used in this study</b>	
AO	Arctic Oscillation, Monthly Mean index	<a href="http://www.cpc.ncep.noaa.gov/products/precip/CWlink/daily_ao_index/monthly.ao.index.b50.current.ascii">http://www.cpc.ncep.noaa.gov/products/precip/CWlink/daily_ao_index/monthly.ao.index.b50.current.ascii</a>
AAO	Antarctic Oscillation, Monthly Mean index	<a href="https://www.cpc.ncep.noaa.gov/products/precip/CWlink/daily_ao_index/aa/ao.aao.shtml">https://www.cpc.ncep.noaa.gov/products/precip/CWlink/daily_ao_index/aa/ao.aao.shtml</a>
NAO	The North Atlantic Oscillation, monthly mean index	<a href="https://www.cpc.ncep.noaa.gov/products/precip/CWlink/pna/norm.nao.monthly.b5001.current.ascii.table">https://www.cpc.ncep.noaa.gov/products/precip/CWlink/pna/norm.nao.monthly.b5001.current.ascii.table</a>
EHF	Eddy Heat Flux	Cumulative Mean (from September to April) of Heat Flux at 100 hPa from MERRA2 reanalysis averaged over 45–75° N (45–75° S for Lauder), deseasonalized. It is kept constant from April to Sep. <a href="https://acd-ext.gsfc.nasa.gov/Data_services/met/ann_data.html">https://acd-ext.gsfc.nasa.gov/Data_services/met/ann_data.html</a>
TP	Tropopause Pressure	Monthly Mean NCEP-NCAR reanalysis (Kalnay et al., 1996); Tropopause pressure at the lat/lon of each station, deseasonalized.  <a href="ftp://ftp.cdc.noaa.gov/Datasets/ncep.reanalysis.derived/tropopause/pres.trop.mon.mean.nc">ftp://ftp.cdc.noaa.gov/Datasets/ncep.reanalysis.derived/tropopause/pres.trop.mon.mean.nc</a>
EqLat	Equivalent Latitude	Monthly Mean equivalent latitude derived from MERRA2 -GMI CTM potential vorticity (PV) contours on 31 potential temperature surfaces [Susan Strahan, private communication, 8/24/2022]. The PV at each station is determined by a 1/distance weighted average of the values in a ± 2 lat, ± 2 lon grid, then converted to EqLat on the Umkehr layers.



369 **Table 3: List of predictors either previously used (bolded) in the LOTUS 0.8.0 (reference) model and additional predictors**  
370 **evaluated in this study for a future use in the extended LOTUS trend regression model. Note, two components of the QBO**  
371 **predictors were used in the reference model (i.e. Godin-Beekmann et al., 2022). We added two more components in the**  
372 **extended model for tests described in this paper.**

373 <sup>1</sup> Since the incorporation of the ENSO index into the LOTUS model, NOAA GSL has updated the index to v1.2.  
374 <https://psl.noaa.gov/enso/mei/>. However, for consistency with results from the Godin-Beekmann (2022) paper we use the  
375 old MEI index that is part of the LOTUS v 0.8.0 package.

376 All proxies are used as is. No de-trending (removal of the long-term trend in proxy) is applied to the proxies. Therefore,  
377 we interpret any changes to the trends derived with additional proxies as approximations of trends driven by chemistry  
378 and transport related to climate change. These are rough approximations as some feedbacks are known to impact  
379 chemistry (e.g. changes in stratospheric temperature).

### 380 **3.3 The Full Model - Combining Additional Predictors**

381 After we have determined the impact of the additional predictors singly, we discern which predictors should be  
382 combined to constitute the 'Full Model'. Prior to selecting additional predictors for the 'Full Model', we perform  
383 correlation tests to identify any cross correlations between predictors. We select predictors that are not highly  
384 correlated (less than +/- 0.2) to ensure that all predictors are largely independent. We use the square of the Pearson  
385 correlation coefficient **R2** for each pair of the predictors to test our assumptions. We find that ENSO, Solar, QBO  
386 (1,2,3,4), AAO, AO, EHF (N and S), and TP (at each station) have correlations less than +/- 0.2 (with the exception  
387 of R2 = 0.3 for EHF (N) and AO). Therefore, any of these predictors can be combined in the 'Full Model'. We find  
388 that NAO has a correlation of .38 with AO so we do not use these two predictors in the same model.

389 We also test the independence of EqLat proxies calculated at several geographic locations (defined by the latitude and  
390 longitude of each Umkehr station) and by selecting a proxy at several altitude levels centered in the middle of Umkehr  
391 layers 3–9. We find that the R2 between the TP and EqLat in the lower stratosphere (Umkehr layer 3) can be large but  
392 anticorrelated -0.7 (Boulder), moderate 0.4 (MLO and Lauder), while close to zero at Arosa/Davos and low at OHP  
393 (-0.2). In the middle and upper stratosphere, the R2 varies from -0.5 to -0.4 (MLO), 0.2 to 0.3 (Arosa/Davos and  
394 OHP), 0.5 to 0.6 (Boulder), and 0.4 to 0.7 (Lauder). EqLat has mostly low correlations ( $< \pm 0.3$ ) with all other proxies  
395 except for higher correlations with QBO B in layers 5 (-0.3) and 6 (-0.4), and QBO A in layer 7 (0.3) at MLO; and  
396 with AO in layer 8 (0.3) at OHP and Arosa/Davos. Also, EqLat has no correlation with the TP proxy in layer 4 in  
397 Boulder, in layer 9 at Lauder, and in layers 8 and 9 at OHP. Since there are occasional high correlations between  
398 EqLat and TP proxies, we do not use them together in the 'Full trend Model'.

## 399 **4 Results**

### 400 **4.1 Reference Model Trend Results**

401 First, we discuss the reference model trends derived from the COH overpass, Umkehr and ozonesonde records at 5  
402 geographic locations. All datasets are deseasonalized with a climatology computed from a subset of data taken from  
403 1998–2008 prior to the trend analysis. Trend results are presented in Fig. 3 and organized in 5 panels. Each panel  
404 shows trends at selected pressure/altitude levels detected from Umkehr (green), COH (orange) and ozonesonde (blue)



405 records at Arosa/Davos, OHP, Boulder, MLO/Hilo and Lauder ground-based stations. Ozonesonde data for the  
406 Arosa/Davos panel are selected from Hohenpeißenberg, Germany station that is in close vicinity to Arosa/Davos  
407 station. We show trends for layers where the measurement is of highest quality: Umkehr (layer 3 through 8), COH  
408 (layers 5 through 9) and ozonesonde (layers 3 through 5) records.

409 The Umkehr data used in this analysis is the monthly mean of all available Umkehr data (one or two measurements  
410 per day). The sonde and COH monthly means use only those profiles that have corresponding Umkehr measurements  
411 on that date. We explore the impact of temporal sampling on trends in Appendix D. For COH with the Umkehr  
412 matched data, trends are slightly larger at OHP but well within the error bars. At all other stations the COH trends are  
413 not impacted by sampling. At OHP the ozonesonde trends matched to Umkehr are slightly larger at layer 4 only and  
414 well within the error bars; while at Lauder in layers 4 and 5 trends are smaller, but barely within the error bars.

415 In the upper (above 10 hPa) stratosphere, Umkehr (green) and COH (orange) trends are positive and agree within the  
416 error bars ( $\pm 2$  standard errors). The exception is found at 8–2 hPa pressure level over the Lauder station, where  
417 Umkehr trends are near zero and COH trends are  $\sim +3$ –4 %/decade. The error bars show  $\pm 2$  standard errors, and the  
418 fact that they do not overlap suggests that the differences in trends are statistically significant. This could be related  
419 to the relatively large uncertainties in the instrumental corrections applied to homogenize the Umkehr record  
420 (Petropavlovskikh et al, 2022). Björklund (2023) discusses relative drifts in Umkehr, ozonesonde, FTIR and MW  
421 ozone records over Lauder. The authors are not able to identify instrumental artifacts that may have caused the  
422 discrepancies in the co-located records, but point out that it is not related to the sampling biases.

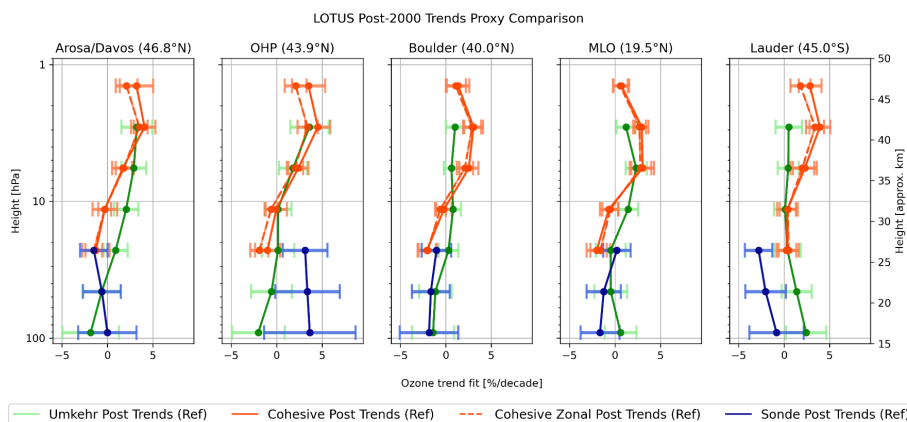
423 In the middle stratosphere (60–10 hPa) agreement between Umkehr and COH is within uncertainty of the trend except  
424 at Arosa/Davos where COH trends are statistically different from Umkehr trends at 16–8 hPa. COH trends at 32–16  
425 hPa are mostly negative ( $-2$ –3 %/decade) with the exception of Lauder where trends are near zero and similar to  
426 Umkehr trends. Umkehr trends between 32–16 hPa are close to zero. The ozonesonde trends (blue) agree with COH  
427 (orange) and Umkehr (green) trends in layer 63–16 hPa at Arosa/Davos, Boulder and MLO. However, at OHP  
428 (Lauder) the ozonesonde trends are found to be positive at  $+3 \pm 3$  %/decade (negative at  $-3 \pm 1.5$  %/decade) and  
429 significantly different from the near-zero trends seen in the COH and Umkehr results.

430 In the lower stratosphere (125–63 hPa), Umkehr trends vary between small positive ( $+1$ –2 %/decade at Hilo and  
431 Lauder) and negative ( $-2$ –3 %/decade at Arosa/Davos, OHP and Boulder); however, trend uncertainties are the largest  
432 (2 standard errors are 2–3 %/decade, (see Table 4 below) in comparison to the middle and upper stratospheric trends.  
433 Ozonesonde trends at OHP station are positive ( $+4$  %/decade), and negative over Lauder ( $-2$  %/decade). They also  
434 feature large uncertainties ( $\pm 5$  %/decade) that are larger than the uncertainties found in Umkehr trends which could  
435 be caused by the limited sampling (see Appendix D). Sonde trends at Hilo show negative trend values with large  
436 uncertainties. But the data in this study at Hilo is not corrected for the ozonesonde drop off after 2014 known to occur  
437 at this station (Stauffer, 2022), so the deviation from the Umkehr results at these levels may be misleading.

438 Figure 3 also shows trends derived from the zonal-mean COH data associated with each station (orange dashed line).  
439 These are shown for comparison with the overpass COH data (solid line) to study the impact of the spatial sampling  
440 biases on the trends. Though Figs. 1 and 2 show clear interannual differences between the records from the individual  
441 stations, and the associated zonal average, we find very small differences in trends (mostly in the upper stratosphere



442 at middle latitude stations). Therefore, the station overpass sampling provides trends that are representative of the  
 443 zonal averaged trends (Zerefos, 2018) and the discrepancies in trends between GB and satellite records do not strongly  
 444 depend on the spatial sampling differences.  
 445



446  
 447 **Figure 3:** The 2000–2020 ozone trends are shown at 7 altitude/pressure levels. The LOTUS model v 0.8.0 is used for trend  
 448 analyses. Umkehr trends (green), COH (orange) and ozonesonde (blue) are shown for 5 ground-based stations:  
 449 Arosa/Davos, OHP, Boulder, MLO and Lauder (panels left to right). Ozonesonde data for the Arosa/Davos panel are  
 450 selected from Hohenpeißenberg, Germany that is in close vicinity to Arosa/Davos. Trends from the zonal-mean COH data  
 451 (orange dashed line) are shown for comparison with the overpass COH data (solid line). The error bars indicate  $\pm 2$  standard  
 452 errors.

453 **4.2 Standard Error of Reference Model**

LOTUS Model Proxy Tests: Standard Error for Reference Model																
Height	Umkehr	Arosa/Davos			OHP			Boulder			MLO			Lauder		
(hPa)	Layer	UMK	COH	SND	UMK	COH	SND	UMK	COH	SND	UMK	COH	SND	UMK	COH	SND
1-2	9		0.92			0.91			0.62			0.43			0.63	
2-4	8	0.85	0.59		1.06	0.68		0.51	0.52		0.52	0.37		0.72	0.57	
4-8	7	0.69	0.59		0.77	0.54		0.41	0.52		0.58	0.62		0.57	0.66	
8-16	6	0.66	0.68		0.75	0.59		0.42	0.43		0.55	0.49		0.61	0.56	
16-32	5	0.66	0.75	0.76	0.89	0.68	1.26	0.54	0.51	0.77	0.82	0.55	0.75	0.73	0.54	0.73
32-63	4	1.05		1.04	1.13		1.95	0.90		1.04	0.90		0.94	0.83		1.16
63-127	3	1.55		1.60	0.15		2.75	1.15		1.63	0.87		1.07	1.11		1.50

454  
 455 **Table 4:** Standard Error (SE) for the Reference model 2000–2020 trend for five ground-based station locations  
 456 (Arosa/Davos, OHP, Boulder, MLO and Lauder). Results are provided for trend analyses of the Cohesive satellite (COH),  
 457 Dobson Umkehr (UMK) and ozonesonde (SND) records and for Umkehr. The layers are selected to represent the best  
 458 quality of data. Values of SE shown are the actual errors in DU.

459 We will use the standard error of the trend fit to the data to evaluate the improvements in the model fit after additional  
 460 proxies are included. We use the standard error as a metric instead of standard deviation to reduce dependence on the



461 number of points in the trends model. The **Table 4** provides the Standard Errors for the Reference Model fit and  
462 represents uncertainty of the trend in **DU** of the mean ozone in each layer at the station. The standard errors of the  
463 trend detected in three co-located ozone records at each station (or in the nearby location as in case of Arosa/Davos  
464 or MLO comparisons) do not significantly differ, although in general ozonesonde errors are slightly larger than  
465 Umkehr errors most likely due to the larger sampling errors in ozonesonde monthly mean record. Also, the errors in  
466 trends detected in COH layers 5–8 are on average smaller than for Umkehr trends (with the exception of layer 7 at  
467 Boulder, MLO and Lauder) which could be explained by an overpass method that averages several satellite profiles  
468 from adjacent orbits and therefore reduces meteorological scale variability in averaged ozone data.

#### 469 **4.3 Adjusted R2**

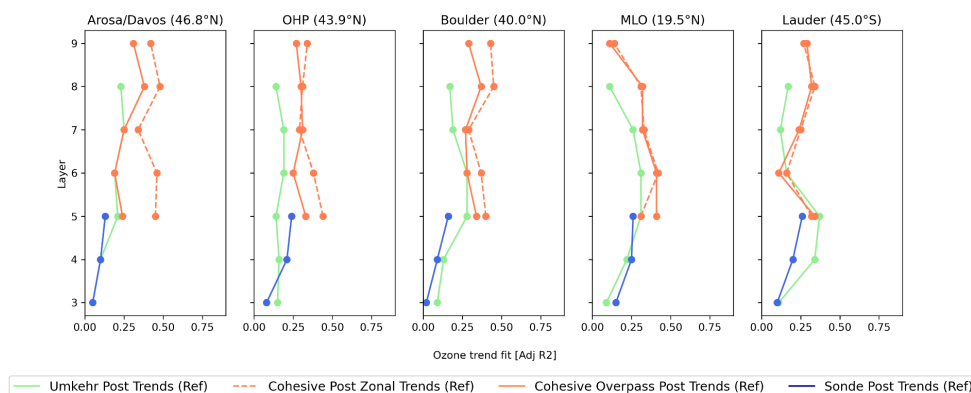
470 The adjusted R2 values of the 2000–2020 trends are shown in Fig. 4 and Table 5 for the data fit using the Reference  
471 model. The adjusted R2 is a modified version of R2 that adjusts for the number of predictors in a regression model  
472 and represents the ‘goodness’ of the model fit to the data. For COH adjusted R2 is shown for both the overpass and  
473 the zonal datasets.

474 Though values are significantly less than the high values usually seen when comparing data that includes the prevalent  
475 seasonal variation, the adjusted R2 values for the COH zonal mean record are similar in magnitude and vertical shape  
476 to the results of the (60°S–60°N) broadband trend analyses published in Godin-Beekmann (2022), Fig. 7 varying  
477 between 0.1 and 0.5. We designate the average values (0.3) as a threshold for satisfactory fit indicating conformance  
478 with prior LOTUS results. We indicate in bold in Table 5 adjusted R2 values of 0.3 or greater to note achievement of  
479 that threshold.

480 The adjusted R2 for the Reference model fit is slightly better for the zonal mean COH data than for the COH overpass  
481 over the Northern middle latitude stations. This is expected as much of the variability of the time series is reduced in  
482 the zonal average as compared to the station overpass data as shown in Fig. 2, and more easily explained by the  
483 typically used predictors. Indeed, the goal of this study is to determine if the additional predictors help to explain the  
484 additional variation as measured at point locations.

485 The model fit to the GB data is similar to the COH overpass results in the middle stratosphere (layers 5 and 6), but the  
486 model explains less ozone variability in the Umkehr records in the upper stratosphere (layers 7 and 8). In the lower  
487 stratosphere (layers 3, 4 and 5), the model fit to the ozonesonde and Umkehr records is similar with the exception of  
488 Lauder (Umkehr has larger adjusted R2 in layers 4 and 5). The adjusted R2 for COH overpass in layer 5 is similar to  
489 Umkehr and sonde with a larger difference at OHP. The adjusted R2 in the lower stratosphere is less than in the middle  
490 stratosphere, which points to other processes (e.g., transport) that drive ozone variability. ~~In this paper we investigate~~  
491 ~~improvement to the trend model fit by introducing additional proxies that can improve representation of the~~  
492 ~~dynamically driven ozone variability in the stratosphere.~~

493



494

495 **Figure 4:** The adjusted R2 is plotted as a function of altitude/pressure for the LOTUS model fit to the Umkehr (green),  
 496 ozonesonde (blue), COH overpass (orange, solid), and COH zonal-mean (orange, dashed). Results are shown in 5 panels  
 497 that represent trend analyses of ozone records over Arosa/Davos (Hohenpeißenberg for sondes), OHP, Boulder, MLO (Hilo  
 498 for sondes) and Lauder ground-based stations.

LOTUS Model Proxy Tests: Adjusted R2 for Reference Model																
Height	Umkehr	Arosa/Davos			OHP			Boulder			MLO			Lauder		
(hPa)	Layer	UMK	COH	SND	UMK	COH	SND	UMK	COH	SND	UMK	COH	SND	UMK	COH	SND
1-2	9		<b>0.31</b>			0.27			0.29			0.11			0.29	
2-4	8	0.23	<b>0.38</b>		0.14	<b>0.30</b>		0.17	<b>0.37</b>		0.11	<b>0.32</b>		0.17	<b>0.32</b>	
4-8	7	0.25	0.25		0.19	<b>0.31</b>		0.19	0.27		0.26	<b>0.32</b>		0.12	0.24	
8-16	6	0.19	0.19		0.19	0.25		0.28	0.28		<b>0.31</b>	<b>0.41</b>		0.16	0.11	
16-32	5	0.21	0.24	0.13	0.14	<b>0.33</b>	0.24	0.28	<b>0.34</b>	0.16	<b>0.31</b>	<b>0.41</b>	0.25	<b>0.37</b>	<b>0.34</b>	0.26
32-63	4	0.10		0.10	0.16		0.21	0.13		0.09	0.22		0.24	<b>0.34</b>		0.20
63-127	3	0.05		0.05	0.15		0.08	0.09		0.02	0.09		0.14	0.11		0.10

499 **Table 5:** Similar to Table 4, but for the adjusted R2. Values of 0.30 and above are indicated in Bold as a threshold to  
 500 indicate a satisfactory fit.

501 **4.4 Reference Model P-Values:**

502 The p-values are often used to evaluate statistical significance of predicted results and results labelled “significant” if  
 503 they remain below a threshold of 0.05. However, Chang et al. (2021) argued as Wasserstein et al. (2019) does that all  
 504 trends should be reported with their associated p-values and a thorough discussion of the certainty of trend detection  
 505 as described by the p-values. Therefore, the p-values can be used for understanding the certainty of the trend. Under  
 506 the IGAC TOAR activity, p-values are scored to define a consistent scale for comparison of the trends between  
 507 different analyses (see Table 3, Chang et al., 2023).

LOTUS Model Proxy Tests: Reference Model P Value																
Height	Umkehr	Arosa/Davos			OHP			Boulder			MLO			Lauder		
(hPa)	Layer	UMK	COH	SND	UMK	COH	SND	UMK	COH	SND	UMK	COH	SND	UMK	COH	SND



1-2	9		0.00			0.00			0.03			0.10			0.00	
2-4	8	0.00	0.00		0.00	0.00		0.05	0.00		0.02	0.00		0.47	0.00	
4-8	7	0.00	0.00		0.02	0.00		0.12	0.00		0.00	0.00		0.43	0.00	
8-16	6	0.00	0.62		0.84	0.98		0.05	0.66		0.01	0.17		0.85	0.50	
16-32	5	0.17	0.08	0.05	0.87	0.15	0.01	0.58	0.00	0.04	0.56	0.00	0.93	0.61	0.62	0.00
32-63	4	0.55		0.57	0.62		0.06	0.21		0.11	0.61		0.11	0.10		0.03
63-127	3	0.23		1.00	0.17		0.15	0.22		0.25	0.47		0.08	0.03		0.49

508 Table 6: Similar to Table 4 but for p-values. Values of less than 0.05 (high certainty of trend detection) are shown in green.  
 509 Values between .05 and 0.1 (yellow) medium certainty, between 0.1 and 0.33 (orange) low certainty of trend detection, and  
 510 above 0.33 (red) very low certainty or no evidence of trend detection.

511 Table 6 provides p-values for the Reference Model. These are further used as a baseline for comparison to model fits  
 512 with additional predictors. P-values of the reference model fit suggest a high certainty ( $p < 0.05$ ) in detected trends in  
 513 the COH data in layers 7, 8 and 9 at almost all stations with the exception of the higher p-value (0.1, medium certainty)  
 514 found at MLO in layer 9. Also, high certainty in derived trends is reached for COH records in layer 5 at Boulder and  
 515 MLO.

516 Umkehr trend analyses also show high confidence in trend detection at Arosa/Davos and MLO stations in layers 6, 7  
 517 and 8, at OHP in layers 6 and 8, and in Boulder in layers 7 and 8. For the ozonesonde data the high confidence (i.e.  
 518 low uncertainty) is found for Hohenpeißenberg, OHP, and Boulder trends detected in layer 5, and at Lauder in layers  
 519 4 and 5.

520 The medium level of the certainty ( $0.05 < p \leq 0.10$ ) is found in trends detected in layer 5 of COH ozone time series at  
 521 Arosa/Davos, layer 4 of ozonesonde records at OHP, layer 9 COH and layer 3 of ozonesonde at MLO, and in layer 4  
 522 of Umkehr at Lauder.

523 Low certainty in detected trends at p-value of 0.10 (not inclusive) to 0.33 is found in Umkehr layer 3 and 5 at  
 524 Arosa/Davos; in COH layer 5, Umkehr and ozonesonde layer 3 at OHP; in Umkehr layers 3, 4 and 7, and ozonesonde  
 525 layers 3 and 4 at Boulder; and in ozonesonde layer 4 and COH layer 6 record at MLO.

526 Highest (lowest certainty) p-values ( $> 0.33$ ) were found in layer 6 of COH overpass records at most stations (except  
 527 for MLO where p-values are medium high). We note that the COH trends are close to zero and the uncertainty envelope  
 528 crosses the zero line. Therefore, these results point to the trend model's inability to detect non-zero trends and account  
 529 for all ozone variability in this layer. Similarly, near-zero Umkehr trends with relatively large SE in layer 6 at OHP  
 530 and Lauder, layer 5 at all (except Arosa/Davos) stations, and in layer 3 and 4 at MLO show the same level of high p-  
 531 values thus suggesting that additional proxies should be added in the trend model to assess the impacts of the natural  
 532 variability and instrumental noise on trend uncertainty.

533 It is also important to note that the reference trend model fit to ozone in Umkehr layers 7 and 8 at Lauder has high p-  
 534 values, which is related to the near-zero trends that shows large disagreement with COH trend. This difference could  
 535 be caused by remaining instrumental step changes that were not fully removed during the record homogenization  
 536 (Petropavlovskikh et al., 2022).

537



538 While near-zero trends and high p-values are found in the fit of the Hilo ozonesonde record in layer 5, the p-values in  
 539 layers 3 and 4 show only medium p-values for near zero trends. It is possible that infrequent launches of ozonesonde  
 540 observations at Hilo could create the temporal sampling bias and appear noisy. The ozonesonde record at  
 541 Hohenpeißenberg has sufficiently frequent sampling (3 times per week) for successful trend analyses (Chang et al.,  
 542 2020; Chang, 2023 preprint), but the p-values remain high in layers 3–4. The p-values for Umkehr fit at Arosa/Davos  
 543 are in the medium to high range for layers 3,4,5, but somewhat smaller which could be due to non-zero trends in layers  
 544 3 and 5. The p-value difference could be also related to the different location of the ozonesonde (HOH) and Umkehr  
 545 (Arosa/Davos) observations, thus the records could contain different atmospheric variability that might impact the  
 546 model fit.  
 547 We will discuss changes to the p-values in the next section after we add more proxies to the trend model in an attempt  
 548 to improve confidence in trend detection.

549 **5 Trends with the Extended Model - testing the addition of single predictors**

550 The LOTUS styled Reference Model is developed and optimized for zonal average datasets. Modeling and trend  
 551 analysis for GB and satellite overpass data may improve by the addition of other proxies not used in the reference  
 552 model to improve capturing processes that impact ozone changes over limited geographical regions. The Extended  
 553 Model tests the addition of single predictors to see if fit statistics can be improved for GB and overpass datasets. We  
 554 judge success of the Extended Model by examination of the reduction in the Standard Error of the trend term, and by  
 555 evaluation of the impact on the adjusted R2 of the model fit. Table 7 displays the change in the Standard Error of the  
 556 post 2000 trend for each proxy tested determined as  $SE_{ref} - SE_{ext}$  as a percent of  $SE_{ref}$ . As such positive values  
 557 correspond to the desired reduction of SE, and are highlighted in the table in green. Low impact changes in the SE  
 558 are highlighted in yellow, and increases in SE (negative values) are highlighted in orange, or red. It may seem unusual  
 559 for the addition of proxies to increase the SE (negative values in the table) which indicates less confidence in the fit.  
 560 But these SE are the uncertainty in the trend term, not in the overall model fit. The new proxies considered each have  
 561 a possible trend and associated error budget for that trend. Whether the additional proxy increases trend uncertainty  
 562 can depend on how well the trend of the new proxy can be characterized. The adjusted R2 is a better indicator of the  
 563 overall model improvement. Table 8 displays the adjusted R2 for the Extended Model for each proxy tested. Values  
 564 of 0.30 and above are indicated in bold as a threshold to indicate a satisfactory fit.

a) LOTUS Model Proxy Tests: Adding Tropopause Pressure (% difference in Std. Error of Model)

Height	Umkehr	Arosa/Davos			OHP			Boulder			MLO			Lauder		
(hPa)	Layer	UMK	COH	SND	UMK	COH	SND	UMK	COH	SND	UMK	COH	SND	UMK	COH	SND
1-2	9		0.33			0.11			0.49			1.39			3.01	
2-4	8	-0.71	-0.51		-0.09	-0.44		-0.19	0.38		-0.58	-0.27		1.26	2.62	
4-8	7	-0.29	0.00		0.26	1.30		0.25	-0.19		2.61	0.33		3.71	1.36	
8-16	6	-1.07	-0.73		0.00	0.34		0.72	-0.23		0.55	0.82		3.11	5.39	
16-32	5	-0.15	2.14	-0.93	1.13	5.34	2.28	-0.37	0.59	0.60	4.54	9.31	2.72	0.00	0.74	2.44



32-63	4	6.60		6.07	5.87		9.81	3.35		7.46	7.02		6.05	8.03		9.44
63-127	3	12.80		10.17	12.80		10.91	6.81		6.01	5.77		4.55	9.76		7.94

565

b) LOTUS Model Proxy Tests: Adding Equivalent Latitude (% difference in Std. Error of Model)																
Height	Umkehr	Arosa/Davos			OHP			Boulder			MLO			Lauder		
(hPa)	Layer	UMK	COH	SND	UMK	COH	SND	UMK	COH	SND	UMK	COH	SND	UMK	COH	SND
1-2	9		8.37			2.85			1.94			-7.18			2.85	
2-4	8	-0.47	0.68		0.09	1.17		-0.39	1.53		-3.48	-5.42		0.98	3.14	
4-8	7	3.75	3.19		2.08	0.56		5.41	4.08		-2.61	-3.90		0.53	1.21	
8-16	6	6.11	8.28		2.54	10.88		2.39	7.75		5.29	7.76		3.44	7.72	
16-32	5	7.93	10.55	5.87	1.92	13.35	7.97	-1.85	0.00	2.84	0.25	0.73	0.65	0.82	3.91	-0.77
32-63	4	-1.44		-1.80	3.20		0.39	-0.22		-0.10	0.33		1.03	-0.24		0.44
63-127	3	1.29		2.02	-1.43		-3.26	-0.79		-0.79	9.57		2.32	1.36		1.88

566

c) LOTUS Model Proxy Tests: Adding QBO CD (% difference in Std. Error of Model)																
Height	Umkehr	Arosa/Davos			OHP			Boulder			MLO			Lauder		
(hPa)	Layer	UMK	COH	SND	UMK	COH	SND	UMK	COH	SND	UMK	COH	SND	UMK	COH	SND
1-2	9		-3.70			1.54			-1.30			-3.70			-4.91	
2-4	8	0.24	5.09		5.65	13.78		0.00	5.74		-4.26	-1.90		0.00	-2.27	
4-8	7	-2.74	-1.34		2.20	0.37		-2.21	-2.33		-2.26	-3.25		-0.18	-0.60	
8-16	6	-3.51	-4.51		-3.07	-3.57		-0.72	0.94		-0.91	0.20		-2.13	-3.95	
16-32	5	-2.59	-1.34	-0.40	-3.84	-1.78	1.14	-1.48	-0.59	-1.94	14.23	9.67	12.55	-1.09	0.74	1.67
32-63	4	-1.44		0.28	-2.22		-1.18	0.00		0.10	9.81		7.38	-0.84		-2.56
63-127	3	-3.04		-1.78	-1.09		-1.00	-0.17		-0.79	-0.58		2.41	0.00		-3.63

567

d) LOTUS Model Proxy Tests: Adding AO/AAO (% difference in Std. Error of Model)																
Height	Umkehr	Arosa/Davos			OHP			Boulder			MLO			Lauder		
(hPa)	Layer	UMK	COH	SND	UMK	COH	SND	UMK	COH	SND	UMK	COH	SND	UMK	COH	SND
1-2	9		1.20			-1.64			0.32			-1.85			-0.48	
2-4	8	-0.83	0.00		-3.77	-1.17		-0.78	-0.38		-2.13	-2.44		0.84	-1.92	
4-8	7	-0.72	1.68		-4.15	-2.60		3.19	4.66		1.22	-3.41		1.24	-1.21	
8-16	6	-0.15	-0.58		-2.41	-3.91		1.20	0.47		1.64	-1.63		-0.33	2.51	
16-32	5	-1.22	-0.40	-1.20	0.45	-2.08	-2.28	0.19	-0.59	-2.09	3.93	1.82	0.65	-1.64	-1.49	1.41
32-63	4	5.84		7.78	0.36		5.47	-1.23		-1.71	7.58		1.74	-0.72		2.47
63-127	3	13.12		12.86	5.45		8.00	-1.40		-3.22	4.38		1.34	-1.08		2.42

568

e) LOTUS Model Proxy Tests: Adding NAO (% difference in Std. Error of Model)																
Height	Umkehr	Arosa/Davos			OHP			Boulder			MLO			Lauder		
(hPa)	Layer	UMK	COH	SND	UMK	COH	SND	UMK	COH	SND	UMK	COH	SND	UMK	COH	SND



1-2	9		0.54			-2.52			-0.16			-3.70			-1.27	
2-4	8	-0.24	0.00			-3.11	-1.91		-0.39	-1.91		-1.74	-3.79		-1.96	-1.75
4-8	7	-0.58	0.67			-1.95	-2.04		0.00	3.88		2.61	-1.14		-2.83	-2.41
8-16	6	0.15	-0.87			-1.74	-3.40		-2.15	-2.82		2.37	-0.41		-1.97	-0.54
16-32	5	-0.46	-1.20	-1.07	0.68	-2.23	-3.98	-0.37	-1.38	-1.20	-1.35	-0.73	-2.98	-2.46	-4.28	-1.54
32-63	4	2.58		3.13	-0.62		-0.39	-0.22		0.40	1.45		-0.82	-2.64		-4.77
63-127	3	10.60		6.74	2.65		1.67	0.44		-2.73	1.73		-0.45	-2.26		-4.91

569

**f) LOTUS Model Proxy Tests: Adding Eddy Heat Flux (% difference in Std. Error of Model)**

Height (hPa)	Umkehr Layer	Arosa/Davos			OHP			Boulder			MLO			Lauder		
		UMK	COH	SND	UMK	COH	SND	UMK	COH	SND	UMK	COH	SND	UMK	COH	SND
1-2	9		4.89			4.61			4.38			-3.24			0.16	
2-4	8	-1.42	4.58		2.64	6.01		3.12	8.80		-1.55	-2.98		0.70	1.92	
4-8	7	-2.74	-3.36		-0.39	-3.90		-2.95	-2.33		5.04	-4.39		1.77	4.52	
8-16	6	-3.21	-3.20		-2.54	-4.76		-2.39	-3.52		-1.09	0.41		-0.16	1.08	
16-32	5	-3.35	-2.80	-3.20	-2.15	-3.71	-2.28	-2.59	-2.37	-2.09	9.33	-0.36	4.14	0.68	2.42	0.90
32-63	4	-1.91		-1.61	-2.04		-1.97	-2.79		-2.82	8.70		2.97	1.92		2.21
63-127	3	1.49		1.35	-0.88		-1.79	-2.53		-2.61	0.92		0.80	2.08		1.68

570 Table 7: Change in Standard Error (SE) of the post-2000 trend estimate, in percent of SE of Reference Model for adding  
 571 single predictors. Panel a: Tropopause Pressure; b: Equivalent Latitude; c: QBO terms C and D; d: AO/AAO; e: NAO; f:  
 572 Eddy Heat Flux.

**a) LOTUS Model Proxy Tests: Adding Tropopause Pressure (Adjusted R2 of Model)**

Height (hPa)	Umkehr Layer	Arosa/Davos			OHP			Boulder			MLO			Lauder		
		UMK	COH	SND	UMK	COH	SND	UMK	COH	SND	UMK	COH	SND	UMK	COH	SND
1-2	9		0.31			0.27			0.29			0.11			0.31	
2-4	8	0.23	0.38		0.15	0.30		0.17	0.38		0.10	0.31		0.18	0.34	
4-8	7	0.24	0.24		0.19	0.32		0.19	0.27		0.28	0.32		0.14	0.24	
8-16	6	0.19	0.19		0.19	0.25		0.29	0.28		0.32	0.42		0.19	0.15	
16-32	5	0.21	0.26	0.13	0.15	0.39	0.27	0.27	0.35	0.16	0.34	0.47	0.28	0.36	0.35	0.30
32-63	4	0.21		0.22	0.29		0.32	0.19		0.18	0.29		0.29	0.42		0.31
63-127	3	0.24		0.23	0.42		0.21	0.22		0.11	0.14		0.18	0.25		0.21

573

**b) LOTUS Model Proxy Tests: Adding Equivalent Latitude (Adjusted R2 of Model)**

Height (hPa)	Umkehr Layer	Arosa/Davos			OHP			Boulder			MLO			Lauder		
		UMK	COH	SND	UMK	COH	SND	UMK	COH	SND	UMK	COH	SND	UMK	COH	SND
1-2	9		0.43			0.37			0.36			0.15			0.32	
2-4	8	0.23	0.39		0.14	0.31		0.17	0.39		0.10	0.30		0.18	0.34	
4-8	7	0.35	0.34		0.31	0.41		0.27	0.33		0.29	0.36		0.17	0.27	
8-16	6	0.31	0.35		0.33	0.45		0.33	0.40		0.40	0.51		0.25	0.23	
16-32	5	0.34	0.39	0.26	0.25	0.51	0.33	0.31	0.40	0.18	0.31	0.42	0.26	0.42	0.41	0.29



32-63	4	0.11		0.09	0.19		0.21	0.12		0.08	0.22		0.25	<b>0.34</b>		0.21
63-127	3	0.08		0.07	0.16		0.08	0.12		0.02	0.18		0.19	0.14		0.12

574

c) LOTUS Model Proxy Tests: Adding QBO CD (Adjusted R2 of Model)																
Height	Umkehr	Arosa/Davos			OHP			Boulder			MLO			Lauder		
(hPa)	Layer	UMK	COH	SND	UMK	COH	SND	UMK	COH	SND	UMK	COH	SND	UMK	COH	SND
1-2	9		<b>0.31</b>			<b>0.30</b>			<b>0.31</b>			0.10			0.28	
2-4	8	0.25	<b>0.44</b>		0.18	<b>0.43</b>		0.19	<b>0.44</b>		0.09	<b>0.32</b>		0.19	<b>0.33</b>	
4-8	7	0.24	0.26		0.22	<b>0.34</b>		0.20	0.28		0.25	<b>0.31</b>		0.13	0.25	
8-16	6	0.19	0.18		0.18	0.24		<b>0.30</b>	<b>0.32</b>		<b>0.32</b>	<b>0.43</b>		0.17	0.10	
16-32	5	0.22	0.24	0.15	0.13	<b>0.34</b>	0.27	0.29	<b>0.36</b>	0.16	<b>0.40</b>	<b>0.48</b>	<b>0.35</b>	<b>0.38</b>	<b>0.37</b>	<b>0.31</b>
32-63	4	0.12		0.13	0.17		0.22	0.14		0.10	0.29		<b>0.32</b>	<b>0.35</b>		0.20
63-127	3	0.05		0.07	0.17		0.09	0.11		0.02	0.10		0.18	0.13		0.10

575

d) LOTUS Model Proxy Tests: Adding AO/AAO (Adjusted R2 of Model)																
Height	Umkehr	Arosa/Davos			OHP			Boulder			MLO			Lauder		
(hPa)	Layer	UMK	COH	SND	UMK	COH	SND	UMK	COH	SND	UMK	COH	SND	UMK	COH	SND
1-2	9		<b>0.33</b>			0.26			<b>0.32</b>			0.11			<b>0.30</b>	
2-4	8	0.23	<b>0.39</b>		0.13	<b>0.30</b>		0.18	<b>0.38</b>		0.11	<b>0.31</b>		0.18	<b>0.31</b>	
4-8	7	0.24	0.26		0.20	<b>0.31</b>		0.23	<b>0.33</b>		0.29	<b>0.32</b>		0.14	0.23	
8-16	6	0.20	0.19		0.18	0.24		<b>0.31</b>	<b>0.30</b>		<b>0.34</b>	<b>0.42</b>		0.19	0.16	
16-32	5	0.22	0.24	0.13	0.15	<b>0.33</b>	0.24	0.29	<b>0.34</b>	0.15	<b>0.34</b>	<b>0.44</b>	0.27	<b>0.37</b>	<b>0.34</b>	0.28
32-63	4	0.17		0.19	0.18		0.28	0.13		0.09	<b>0.30</b>		0.28	<b>0.33</b>		0.22
63-127	3	0.18		0.19	0.24		0.18	0.09		0.02	0.15		0.18	0.11		0.14

576

e) LOTUS Model Proxy Tests: Adding NAO (Adjusted R2 of Model)																
Height	Umkehr	Arosa/Davos			OHP			Boulder			MLO			Lauder		
(hPa)	Layer	UMK	COH	SND	UMK	COH	SND	UMK	COH	SND	UMK	COH	SND	UMK	COH	SND
1-2	9		<b>0.33</b>			0.26			<b>0.31</b>			0.11			<b>0.30</b>	
2-4	8	0.24	<b>0.39</b>		0.13	<b>0.30</b>		0.19	<b>0.37</b>		0.12	<b>0.31</b>		0.17	<b>0.32</b>	
4-8	7	0.25	0.26		0.18	<b>0.31</b>		0.20	<b>0.32</b>		<b>0.30</b>	<b>0.34</b>		0.11	0.23	
8-16	6	0.21	0.20		0.18	0.24		0.28	0.27		<b>0.35</b>	<b>0.44</b>		0.16	0.12	
16-32	5	0.22	0.23	0.14	0.16	<b>0.33</b>	0.23	0.28	<b>0.34</b>	0.17	<b>0.31</b>	<b>0.42</b>	0.24	<b>0.36</b>	<b>0.33</b>	0.28
32-63	4	0.14		0.14	0.17		0.24	0.15		0.13	0.25		0.25	<b>0.33</b>		0.19
63-127	3	0.15		0.13	0.20		0.14	0.12		0.03	0.12		0.16	0.10		0.09

577

f) LOTUS Model Proxy Tests: Adding Eddy Heat Flux (Adjusted R2 of Model)																
Height	Umkehr	Arosa/Davos			OHP			Boulder			MLO			Lauder		
(hPa)	Layer	UMK	COH	SND	UMK	COH	SND	UMK	COH	SND	UMK	COH	SND	UMK	COH	SND



1-2	9		0.39			0.34			0.35			0.11			0.29	
2-4	8	0.25	0.44		0.17	0.38		0.23	0.46		0.12	0.31		0.18	0.33	
4-8	7	0.24	0.24		0.21	0.31		0.20	0.28		0.30	0.31		0.13	0.28	
8-16	6	0.19	0.19		0.18	0.24		0.28	0.28		0.31	0.42		0.16	0.13	
16-32	5	0.21	0.24	0.14	0.15	0.34	0.24	0.28	0.34	0.17	0.36	0.42	0.29	0.37	0.35	0.27
32-63	4	0.11		0.11	0.17		0.20	0.13		0.09	0.28		0.28	0.35		0.21
63-127	3	0.07		0.09	0.18		0.07	0.09		0.01	0.11		0.17	0.12		0.11

578 Table 8: Adjusted R2 after adding single predictors. Panel a: Tropopause Pressure; b: Equivalent Latitude; c: QBO terms  
579 C and D; d: AO/AAO; e: NAO; f: Eddy Heat Flux.

### 580 5.1 Tropopause pressure (TP)

581 Adding the TP proxy to the standard LOTUS model produces the most consistent results between different techniques  
582 (COH, Umkehr and ozonesonde) and also have similar magnitude of standard error changes among different latitudes  
583 (i.e. Arosa/Davos, OHP, Boulder, MLO, Lauder). The most significant impact in improving the SE is found in the  
584 lower stratosphere (layers 3, 4) and in the middle stratosphere (layer 5) at the MLO tropical station. The impact of the  
585 TP proxy on the COH trend uncertainty in the model stratosphere (layer 5) is somewhat larger, likely due to the  
586 satellite AK extending into the lower stratosphere. Similarly, larger reduction of the standard error in the Umkehr  
587 trends in the lowermost stratosphere (layer 3) in comparison to the AK-smoothed ozonesonde record could be due to  
588 sampling biases in the ozonesonde record. Adding the TP proxy to the Reference Model improves the adjusted R2 in  
589 layers 3–5, whereas the SE improvements are also consistent across geo-locations and measurement techniques.  
590 Several improvements resulted in adjusted R2 to exceed the 0.3 threshold (Umkehr at OHP in layer 3, sonde at OHP  
591 in layer 4, and sonde at Lauder in layers 3 and 4) and in many cases the adjusted R2 increased by more than 0.02.

### 592 5.2 Equivalent Latitude (EqLat)

593 In the mid-latitudes, the addition of EqLat as a predictor shows consistent results across measurement techniques and  
594 stations with few exceptions. The reduction in the SE of the model fit is evident in the COH data in the upper  
595 stratosphere (above 4 hPa or ~40 km), but is less pronounced in Umkehr profiles. The impact on MLO SE of the trend  
596 fit in the upper stratosphere is negative (in both COH and Umkehr records) which can be explained by the fact that  
597 the EqLat is much closer to geometric latitude near the equator than at the middle/high latitudes and therefore its use  
598 as a proxy would not provide any additional information in interpretation of the tropical upper stratospheric ozone  
599 variability. It could also suggest that the addition of EqLat will overfit the record.

600 The ozone record trend fits in the middle stratosphere (32–4 hPa or 25–40 km) benefit from adding the EqLat proxy  
601 at most locations. Improvement in the SE of the trends in the lower stratosphere (127–63 hPa or ~15–20 km) is  
602 minimal, limited to some locations and instrumental records (Arosa/Davos Umkehr and HOH sonde, MLO Umkehr  
603 and sonde, and Lauder Umkehr and ozonesonde), which could be related to the location of subtropical jet that  
604 modulates mixing of tropical and subtropical (and occasionally polar) air masses and influences the strat/trop  
605 exchange. Unexpectedly, the addition of the EqLat proxy to the MLR statistical model for trend detection in Boulder  
606 Umkehr and ozonesonde low stratospheric ozone records increases the uncertainties of the fit, while the influence of



607 subtropical jet on Boulder lower stratosphere is well known (Manney et al, 2018). Perhaps, the data analyses also  
608 need to consider the tropopause variability.

609 In terms of the impact on the adjusted R2, the EqLat proxy significantly improves model fit for multiple instruments,  
610 mostly in layers 5–7, and in COH fit in layer 9. The adjusted R2 improvements also often exceeded 0.3 threshold. No  
611 significant improvement is found in the ozonesonde model fit in layer 5 with the exception of the OHP record (0.09  
612 increase).

### 613 **5.3 Extra QBO terms C and D**

614 QBO is an important driver of ozone variability at tropical stations. Based on the results of adding 2 extra terms of the  
615 QBO to the standard model, the recommendation could be to exercise this option only for the tropical station trends.  
616 At the Northern middle latitudes (i.e in Arosa/Davos, OHP and, to a lesser degree, in Boulder) an improvement to the  
617 trend SE uncertainties in layer 8 is noted. There seems to be a similar pattern for the upper stratosphere in trends  
618 derived with Heat Flux. Tweedy et al. (2017) show that the first two EOFs of the QBO did not describe the anomalous  
619 QBO behavior, while Anstey et al. (2021) show that the addition of two more EOFs of the QBO could capture the  
620 effect of the disruptions on the zonal winds. Therefore, including additional QBO EOFs could benefit attribution of  
621 ozone variability in the middle stratosphere (layers 4 and 5) in the tropical latitudes (reduced errors in MLO/Hilo  
622 trends) and in the upper stratosphere (layer 8 in Umkehr and COH trends) in the NH middle latitude stations  
623 (Arosa/Davos, OHP, Boulder) related to the global circulation pattern that are also represented by the Heat Flux proxy.  
624 A slight reduction in the errors at SH middle latitude (COH and sonde at Lauder, New Zealand) could be invoked by  
625 the EqLat variability that has a small correlation with the QBO-D proxy. Reduction of SE in the trend fit of the layer  
626 5 ozonesonde record at OHP (up to 2 %) is not found in the Umkehr or COH results, which suggests overfitting and  
627 sampling bias (see results in Appendix D).  
628 The addition of extra QBO terms improves the adjusted R2 model fit for all COH station overpass records in layer 8  
629 and occasionally improves Umkehr adjusted R2 (except at MLO). The most significant improvement is found at MLO  
630 in layers 3–5 in all three instrument records.

### 631 **5.4 Arctic and Antarctic Oscillations (AO/AAO)**

632 AO/AAO proxies reduce SE (green colored cells) in the lower stratosphere (layers 3 and 4) at Arosa/Davos, OHP, and  
633 MLO, although the reduction somewhat differs between the Umkehr and ozonesonde records. At the same time, at  
634 Boulder and Lauder the SE does not show an improvement after the addition of the AO/AAO proxy (AAO is used  
635 instead of AO at Lauder). In the middle stratosphere (layer 7), a reduction in SE is found over Boulder in both COH  
636 and Umkehr records. The addition of AO/AAO proxies improves the SE of the trend at MLO and Lauder but only in  
637 Umkehr records, while it worsens the COH SE. At Lauder, the COH SE in layer 6 shows an improvement, but not in  
638 Umkehr record. Since results in the middle stratosphere (layers 5–7) are not always consistent among different  
639 techniques (reductions are not in the same layers) it could indicate statistical model overfit into the record's noise, or  
640 vertical smoothing of the Umkehr or COH technique that combines ozone variability in the layer with a portion of  
641 ozone variability in the adjacent layers, thus partially or completely reducing the correlation with the proxy.



642 The addition of the AO predictor increases the adjusted R<sup>2</sup> in the lower stratosphere at Arosa/Davos, OHP and MLO.  
643 Also, a small enhancement of the adjusted R<sup>2</sup> is seen in the middle and upper stratosphere, including in Umkehr layers  
644 6 and 7 and COH layers 6, 7 and 9 over Boulder, as well as in Umkehr fit in layers 5–7 at MLO, and at Lauder (AAO)  
645 for Umkehr and COH records in layer 6. These results are not very consistent across different geolocations, but seem  
646 to be consistent across instrumental records at some stations (Umkehr and ozonesonde in the lower layers, and COH  
647 and Umkehr in the upper layers).

#### 648 **5.5 North Atlantic Oscillation (NAO)**

649 Including the NAO proxy in the trend model appears to have a similar pattern (i.e., in latitude and altitude) of changes  
650 in the standard error as compared to the result of inclusion of the AO/AAO proxy. It is not a surprise, since indices of  
651 the NAO and AO are highly correlated in time due to their common link to the downward propagation of stratospheric  
652 anomalies. Standard errors are somewhat reduced in the lower stratospheric layers at the middle NH latitude and  
653 tropical Umkehr records, but the change is less significant than in AO/AAO cases. The impacts on ozonesonde trend  
654 uncertainties are very minimal and inconclusive at Boulder (layers 3 and 5), OHP (layer 4) and MLO (layer 3) records.  
655 The impacts on Lauder are similar or stronger (SE is increased for both Umkehr and sonde records) to the impacts of  
656 the AO/AAO. In the middle and upper stratosphere the standard errors are typically reduced. The exception is found  
657 in layer 7 of the COH record at Boulder and Arosa/Davos, and in layers 6 and 7 of the Umkehr record at MLO. Similar  
658 negative results are found when AO/AAO proxies are added, which suggests that the observed time series are  
659 overfitted and potentially some instrumental or sampling anomalies are misinterpreted with addition of these proxies.

#### 660 **5.6 Eddy Heat Flux (EHF)**

661 The EHF represents a dynamical proxy for assessment of the impact of the Brewer Dobson Circulation (BDC). It is  
662 expected to have an impact on the upper stratospheric ozone by accelerating the transport in the upper branch that  
663 brings more ozone at higher latitudes (i.e. Arosa/Davos) and middle latitudes (i.e. OHP, Boulder, and Lauder). It could  
664 possibly represent changes in the lower branch of the BDC circulation and the expansion of the tropical band, thus  
665 modulating ozone in the lower stratosphere at tropics (i.e. MLO). In the Southern middle latitudes (i.e. Lauder), the  
666 correlations could be related to the shift in the subtropical wave activities to the higher latitudes in response to the  
667 ozone hole healing.

668 The addition of the EHF predictor leads to the reduced SE uncertainties in the upper stratosphere in COH and Umkehr  
669 trends at OHP and Boulder, and in COH only trends at Arosa/Davos. It has a much smaller reduction of SE for the  
670 Lauder trend and even an increase in uncertainties if used to fit upper stratospheric ozone time series at MLO. At the  
671 same time, the SE in the Umkehr and ozonesonde middle stratosphere (layers 4–5) is substantially reduced, including  
672 smaller improvements at Lauder. In the lower stratospheric (layer 3) ozone trend SE in Umkehr and sonde records at  
673 MLO, Lauder and Arosa/Davos are somewhat reduced when using the EHF proxy.

674 Addition of the EHF predictor seems to have an impact in the upper stratosphere increasing the adjusted R<sup>2</sup> for COH  
675 records in layers 8 and 9 in all but MLO records, which indicates impact of the BDC upper branch on the middle  
676 latitudes. In contrast to the COH, the Umkehr adjusted R<sup>2</sup> has not changed significantly, which possibly suggests a



677 high measurement noise in the station records. There is, however, a small increase in adjusted R2 in the Umkehr  
 678 record in layer 7 at MLO (whereas COH does not show a change).

679 The increase in adjusted R2 is found at MLO in Umkehr and sonde layers 4 and 5, including a small increase in layer  
 680 3, which probably is related to the EHF-driven changes in the middle stratosphere. Ozone variability in Umkehr and  
 681 sonde records at MLO appears to contain information about the circulation changes in the shallow BDC branch.

682 **6 The Full Model - adding multiple predictors**

683 In this paper we seek to develop an improved model and thus trend estimates for point located measurements of ozone  
 684 through modifications of a model optimized for zonal data. Our criteria for model improvement are based on reduction  
 685 of the SE of the trend with either improvement (at best) or moderate impact (at worst) on the model adjusted R2. From  
 686 the results of the previous section, we see several opportunities to improve the model and improve confidence in the  
 687 trend estimates. This section examines if the gains of the above are improved while adding several predictors together.  
 688 As stated above the TP as a predictor exhibits the most consistent results for all stations and measurement techniques.  
 689 The other predictors have successes in SE reduction, but only at some layers, and some stations. Some results are  
 690 instrument dependent.

691 Based on the tests above we expect combining predictors can improve the model fit and trend SE reduction, but it is  
 692 clear that the predictor selection should vary by station and level. Appendix E details the choices made for the Full  
 693 Model which combines 1 to 3 additional proxies beyond the Reference Model.

694 **6.1 Predictors added for the Full Model**

695 Reduction of the SE of the trend while improving (or at least not impacting) model adjusted R2 is the basis of predictor  
 696 choice for the Full Model. To qualify a predictor should exhibit consistent results for all measurement techniques.  
 697 Improvement at multiple stations is preferred to single station improvements. In general, we avoid combining highly  
 698 correlated predictors. Table 9 shows final choices for the Full Model.

699

LOTUS Full Model predictor selection					
	Arosa/Davos	OHP	Boulder	MLO	Lauder
Layer					
9	EqLat	EqLat	EqLat	Reference only	EqLat
8	EqLat	EqLat	EqLat	Reference only	EqLat
7	EqLat	EqLat	EqLat	Reference only	EqLat
6	EqLat	EqLat	EqLat	EqLat	EqLat
5	EqLat	EqLat	EqLat	EqLat, QBO CD, AO	EqLat
4	TP, AO	TP, AO	TP	TP, QBO CD, AO	TP
3	TP, AO	TP, AO	TP	TP, QBO CD, AO	TP

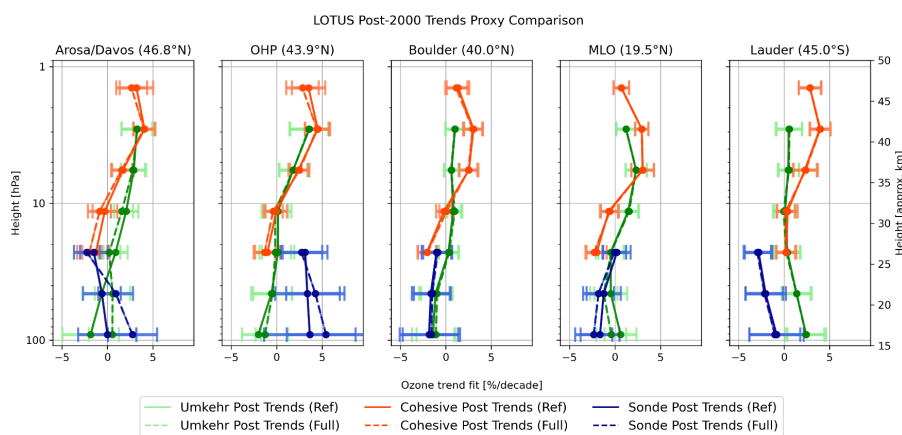
700



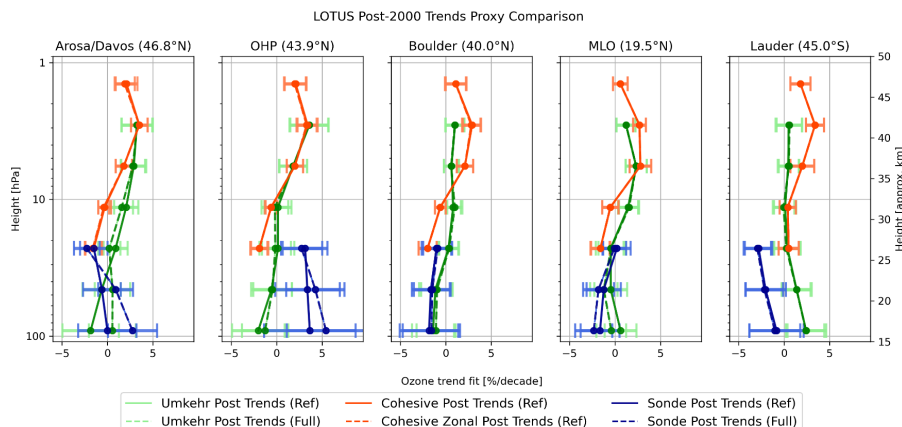
701 **Table 9: Added predictors for the Full model are tuned for each layer and each station. For layers 7 to 9 the SE and**  
 702 **adjusted R2 parameters at MLO are not improved by additional predictors, and the original LOTUS based Reference**  
 703 **Model is used. Appendix E explains the logic of the predictor selection.**

704 **6.2 Impact of the Full Model on trends**

705 Figure 5a shows the trends for the stations (with COH overpass) for the Reference and Full Models. An impact of the  
 706 Full Model on ozone trends derived in the upper stratosphere (above 16 hPa) is neutral. Addition of proxies to the  
 707 LOTUS model does not change trends which remain the same magnitude as those derived using the Reference Model,  
 708 i.e. positive and statistically significant at the SH and MH middle latitudes and over tropics. The largest difference  
 709 (outside of the SE uncertainty) between upper stratospheric Umkehr and COH trends is found over Boulder, MLO  
 710 and Lauder.



711  
 712 **Figure 5a: Post 2000 trends for the Full and Reference Model. In this figure the COH data shown in orange is the overpass**  
 713 **data. Solid lines depict Reference Model values (unchanged from Fig. 3). Dashed lines depict Full Model values for all 3**  
 714 **instrument types.**



715



716 **Figure 5b: Post 2000 trends for the Full and Reference Model. In this case the orange lines are with the zonal data instead**  
 717 **of the COH overpass data. Dashed lines depict Full Model values for all 3 instrument types. The Umkehr and sonde trends**  
 718 **are unchanged from Fig. 5a.**

719 In the middle stratosphere, additional proxies do not change trend values across locations and instrumental records  
 720 (outside of the SE). At OHP, Boulder and Lauder Umkehr trends in layer 6 (8–16 hPa) are barely positive while COH  
 721 trends are negative. At Arosa/Davos and MLO, COH trends in layer 6 are barely negative and Umkehr trends are  
 722 significantly positive. Most COH trends in layer 5 (16–32 hPa) are statistically negative (except at Lauder), while  
 723 Umkehr trends are near zero.

724 In the lower stratosphere, Umkehr and sonde trends Arosa/Davos and MLO change after the Full model is used.  
 725 However, Umkehr and sonde trend changes at MLO are within the SE and therefore can be deemed not significant.  
 726 Ozonesonde trends at Arosa/Davos in layer 3 (125–63 hPa) change from zero to positive. Umkehr trends at  
 727 Arosa/Davos in layer 3 change from negative to near zero. Large differences between ozonesonde and Umkehr trends  
 728 at Lauder and OHP remain unchanged after the Full model is applied although respective SE envelopes overlap.

729 Figure 5b also shows the trends for the Reference and Full Models, but the COH data shown is the associated zonal  
 730 data relevant to each station. Incorporation of the additional proxies does not change the trend values for the zonal  
 731 COH data. Impact on error estimates for the trends are discussed next.

### 732 6.2 Impact of the Full Model on the Trend SE

733 Table 10 summarizes the reduction in the SE for the Full model. Selection of the EqLat predictor for the Full model  
 734 in the layers 5–9 and for all stations (except MLO/Hilo, to be discussed later) shows the improvement in the SE (as  
 735 discussed in the previous section). Also, the TP predictor is selected for inclusion to the Full model for trend analyses  
 736 at Boulder and Lauder stations in layers 3 and 4. The combination of several predictors are used for individual stations  
 737 based on the additional reduction in the SE. For the Arosa/Davos and OHP stations we select a combination of the TP  
 738 and AO to reduce the SE almost twice as much in some layers. Inclusion of AO proxy is in support of the interpretation  
 739 of seasonal and interannual ozone variability recorded over stations in Europe that are north of 40 degrees latitudes  
 740 and are exposed to the seasonal events of ozone depleted air masses transported from the Polar region during the  
 741 spring season (Steinbrecht et al., 2011; Manney et al., 2011; Knudsen and Grooss, 2000; Fioletov and Shepherd, 2003;  
 742 Zhang et al., 2017; Weber et al., 2022a). The strong impact of AO/AAO on the lower stratosphere ozone variability  
 743 are not detected in Boulder or Lauder and we choose not to include it in the Full model for trend analyses at these  
 744 stations.

LOTUS Model Proxy Tests: (% Difference in Std. Error of Model)																
Height	Umkehr	Arosa/Davos			OHP			Boulder			MLO			Lauder		
(hPa)	Layer	UMK	COH	SND	UMK	COH	SND	UMK	COH	SND	UMK	COH	SND	UMK	COH	SND
1-2	9		8.35			2.74			1.94			0.00			2.85	
2-4	8	-0.47	0.68		0.09	1.03		-0.39	1.53		0.00	0.00		0.98	3.14	
4-8	7	3.75	3.04		2.08	1.86		5.41	4.08		0.00	0.00		0.53	1.21	
8-16	6	6.11	8.36		2.54	10.88		2.39	7.75		0.55	0.82		3.44	7.72	
16-32	5	7.93	10.72	5.87	1.92	13.33	7.97	-1.85	0.00	2.84	19.39	13.32	15.27	0.82	3.91	-0.77



32-63	4	8.71		9.96	6.13		9.92	3.35		7.46	20.51		9.64	8.03		9.44
63-127	3	20.30		18.49	13.48		14.01	6.81		6.01	6.00		4.73	9.76		7.94

745 **Table 10: Change in post 2000 trend SE in the Full Model as a % difference of the Reference Model. Color coding is the**  
 746 **same as introduced in Table 7.**

747 The MLO/Hilo location is close to the Tropical belt and therefore has different processes impacting stratospheric  
 748 ozone variability as discussed in the previous section. We find that EqLat proxy can be added to the Full model in  
 749 layer 6 and 5 (similar to other stations); however, above layer 6, EqLat or TP is not useful for interpretation of tropical  
 750 ozone variability and therefore we believe the trend model in these layers should remain as it currently is used in  
 751 Godin-Beekmann et al. (2022) analyses. The EqLat and TP are mildly correlated (-0.4) in the stratosphere, and  
 752 therefore we decided against combining both of these proxies in the Full model. However, we also found that adding  
 753 AO and QBO C/D proxies in layers 3, 4 and 5 improved the model fit and reduced the SE. These combined additional  
 754 proxies are not correlated and reduce SE more than when using them separately.

755 The Full Model showed impacts on the SE in the upper stratosphere (above 8 hPa). The trend errors were reduced  
 756 with the exception of Umkehr trends at 4–2 hPa over Boulder and Arosa/Davos where errors did not change. No  
 757 changes in SE are found at MLO with additional proxies, thus the Full Model is kept the same as the Reference Model  
 758 for this station in the upper stratosphere.

759 Similarly, in the middle stratosphere SE were mostly reduced after the Full Model was applied (except for slightly  
 760 larger SE in trends derived from ozonesonde at OHP and from Umkehr at Boulder).

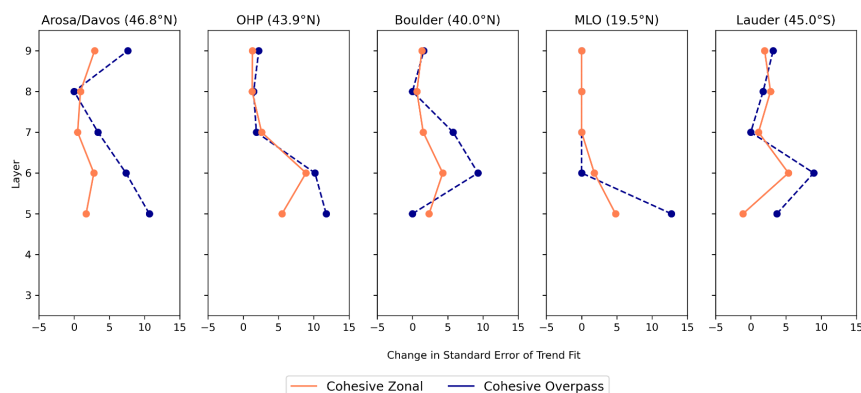
761 After applying the Full Model in the lower stratosphere, we still found high uncertainty due to higher ozone variability  
 762 (natural variability), but SE were reduced. Arosa/Davos and MLO Umkehr and sonde trends changed after Full Model  
 763 was used. Change in ozonesonde trends at HOH in layer 3 (125–63 hPa) goes from zero to positive and trend detection  
 764 becomes highly confident (p-value <0.05). Umkehr trends at Arosa/Davos in layer 3 changed from negative to near  
 765 zero but results have low certainty (p-value >0.1). Larger trend differences remain between ozonesonde and Umkehr  
 766 at Lauder and OHP after the Full Model is applied.

767

LOTUS Model Proxy Tests: (% difference of SE of Trend): overpass and zonal COH											
Height	Umkehr	Arosa/Davos		OHP		Boulder		MLO		Lauder	
(hPa)	Layer	Overpass	Zonal	Overpass	Zonal	Overpass	Zonal	Overpass	Zonal	Overpass	Zonal
1-2	9	7.61	2.89	2.20	1.30	1.61	1.34	NA	NA	3.17	1.97
2-4	8	0.00	0.90	1.47	1.26	0.00	0.63	NA	NA	1.75	2.76
4-8	7	3.39	0.47	1.85	2.55	5.77	1.53	NA	NA	0.00	1.11
8-16	6	7.35	2.75	10.17	8.98	9.30	4.30	0.00	1.79	8.93	5.34
16-32	5	10.67	1.74	11.76	5.54	0.00	2.36	12.73	4.81	3.70	-1.11

768 **Table 11: Change in Standard Error of Trend, as percent of Reference Model SE, for the COH overpass data and zonal**  
 769 **data at the 5 ground stations. MLO Full Model in layers 9-7 is the same as the Reference Model (change is marked as NA).**

770



771

772 **Figure 6: Change in Standard Error of Trend, as percent of Reference Model SE, for the COH overpass data (blue) and**  
 773 **COH zonal data (red) at the 5 ground stations.**

774 It is instructive to ponder if the addition of proxies that yield improvements via reduction of the standard error in the  
 775 localized GB or overpass measurements also have the potential to improve uncertainties in the zonal data. To explore  
 776 this Table 11 and Fig. 6 show the percent change in SE of the trend when adding the proxies for the Full model.  
 777 Values are shown for both the COH overpass and the COH zonal data. In general, except when the improvement in  
 778 the SE for the overpass COH is small (3% or less), addition of proxies has much less impact on the zonal results than  
 779 on overpass results. This suggests that indeed the Reference LOTUS model is well tuned for zonal datasets, but can  
 780 be improved with select addition of proxies for overpass or localized GB data.

781 **6.3 Impact of the Full Model on adjusted R2**

782 Table 12 shows the adjusted R2 for the Full Model. In the upper stratosphere, the Full Model increases the adjusted  
 783 R2 above 8 hPa (except in Umkehr at 4–2 hPa). Over MLO there is no change because the Full Model is kept the  
 784 same as the Reference Model for layers 7, 8 and 9.

LOTUS Model Proxy Tests: (Adjusted of Model)																
Height	Umkehr	Arosa/Davos			OHP			Boulder			MLO			Lauder		
(hPa)	Layer	UMK	COH	SND	UMK	COH	SND	UMK	COH	SND	UMK	COH	SND	UMK	COH	SND
1-2	9		<b>0.42</b>			<b>0.37</b>			<b>0.36</b>			0.11			<b>0.32</b>	
2-4	8	0.23	<b>0.39</b>		0.14	<b>0.31</b>		0.17	<b>0.39</b>		0.11	<b>0.32</b>		0.18	<b>0.34</b>	
4-8	7	<b>0.35</b>	<b>0.35</b>		<b>0.31</b>	<b>0.41</b>		0.27	<b>0.33</b>		0.26	<b>0.32</b>		0.17	0.27	
8-16	6	<b>0.31</b>	<b>0.35</b>		<b>0.33</b>	<b>0.45</b>		<b>0.33</b>	<b>0.40</b>		<b>0.40</b>	<b>0.51</b>		0.25	0.23	
16-32	5	<b>0.34</b>	<b>0.38</b>	0.26	0.25	<b>0.51</b>	<b>0.34</b>	<b>0.31</b>	<b>0.40</b>	0.18	<b>0.44</b>	<b>0.53</b>	<b>0.39</b>	<b>0.42</b>	<b>0.41</b>	0.29
32-63	4	0.23		0.25	0.29		<b>0.34</b>	0.19		0.18	<b>0.42</b>		<b>0.38</b>	<b>0.42</b>		<b>0.31</b>
63-127	3	<b>0.31</b>		<b>0.31</b>	<b>0.44</b>		0.26	0.22		0.11	0.19		0.24	0.25		0.21

785 **Table 12: Adjusted R2 of the Full Model. Values of 0.30 and above are indicated in Bold as a threshold to indicate a**  
 786 **satisfactory fit. Compare to Table 4 containing values for the Reference Model.**

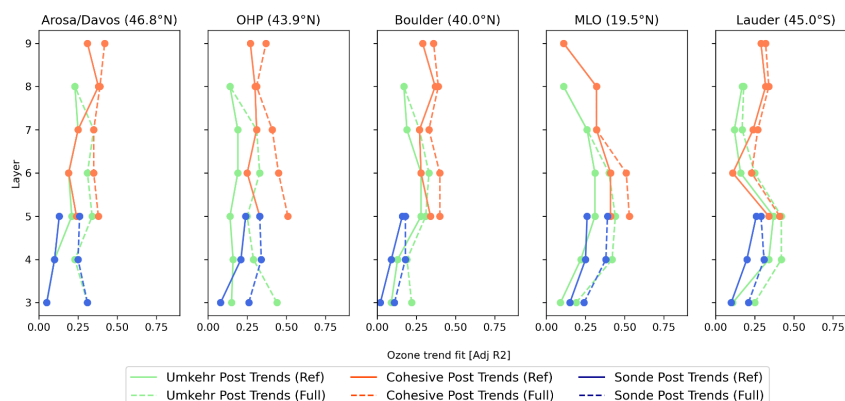


787 In the middle stratosphere (32–8 hPa) adjusted R2 increases are found in all records (although smaller increases are  
788 found in ozonesonde and Umkehr records at OHP, Boulder and Lauder at 32–64 hPa). At Arosa/Davos, Boulder and  
789 Lauder the adjusted R2 in the COH and Umkehr trend models increase and continue to be very close in value. The  
790 COH adjusted R2 is larger at OHP and MLO than in Umkehr and sonde records thus suggesting that overpass  
791 conditions might have smoothed some natural variability observed in the GB records. In general, the adjusted R2 is  
792 the largest at the 32–64 hPa level. This suggests that the Full Model shows an improvement for regional trend analyses  
793 in the middle stratosphere.

794 Although Umkehr and sonde trend changes at MLO in the low stratosphere are within the SE and therefore can be  
795 deemed not significant, the adjusted R2 is increased which suggests a better model fit in the Full Model. The adjusted  
796 R2 increases in both Umkehr and ozonesonde data, while the largest increases are found in the Arosa/Davos, OHP  
797 and MLO records.

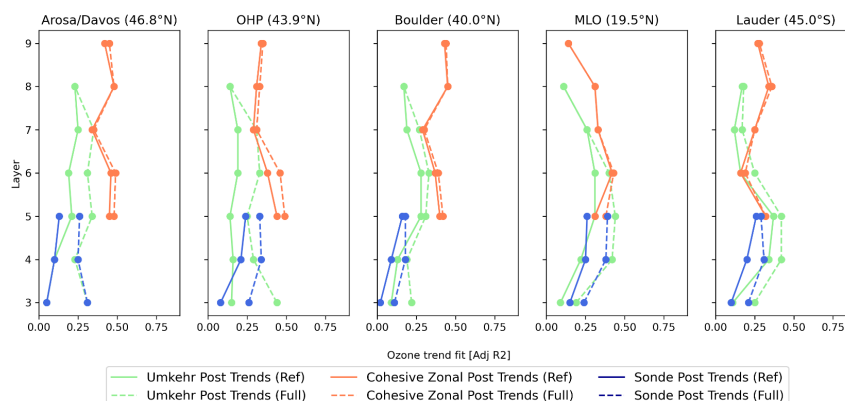
798 In the lower stratosphere, the adjusted R2 remains low in both Umkehr and sonde records at Boulder (only TP is added  
799 for the Full model). While the p-values at 63–32 hPa are significantly reduced (see discussion in the next section),  
800 they still remain relatively high. These results suggest that additional research is needed to identify the best set of  
801 proxies for Boulder records in the lower stratosphere. At Lauder, the ozonesonde record shows smaller adjusted R2  
802 as compared to Umkehr partially due to low sampling biases.

803 It is valuable to further explore the impact of the Full Model on the adjusted R2 for the zonal and overpass COH data.  
804 Fig. 7a shows the adjusted R2 for the Reference and Full Models at each of the 5 stations using the COH overpass  
805 data. In all cases the Full Model improves the adjusted R2 except for MLO layers 7, 8 and 9 where the Full and  
806 Reference Model are identical. The most significant improvements are seen by Umkehr at layers 3 to 7, COH overpass  
807 at Layers 5, 6 and 7, and sonde layers 3–5. Figure 7b shows similar results using COH zonal data instead of overpass.  
808 There is practically no further improvement in the adjusted R2 for the zonally averaged COH results (except for a  
809 small increase for MLO layer 5). Comparison of results reveals that for OHP the implementation of the Full model  
810 for the COH overpass data (Fig. 7a, dashed line) improves the adjusted R2 to values nearing that of the Reference  
811 Model zonal data in layer 7 and below (Fig. 7b, solid line). For MLO and Lauder the use of the Full Model on the  
812 COH overpass data improves the adjusted R2 over the Reference Model beyond the improvement seen in the COH  
813 zonal results for layers 5 and 6. At Arosa/Davos and Boulder the implementation of the Full Model does not fully  
814 reach the magnitude of the COH zonal adjusted R2.



815  
816  
817

**Figure 7a: Adjusted R2 for the Full Model (dashed lines) and Reference Model (solid lines) at 5 stations. The COH data in this figure is the overpass data at each station.**



818  
819  
820

**Figure 7b: Adjusted R2 for the Full Model (dashed lines) and Reference Model (solid lines) at 5 stations. The COH data in this figure is the zonal data for each station. The Umkehr and sonde lines are identical to those in Fig. 7a.**

821 **6.3 Examination of the p-values of the Full Model**

822 In the upper stratosphere (above 8 hPa), the confidence in Umkehr trends remained high (see Table 13) for most  
823 stations except at Boulder (medium to low) and Lauder (very low, although some improvement was found). COH  
824 trends confidence was very slightly degraded over Boulder at 1–2 hPa, but mostly has not changed.

825 In the middle stratosphere (between 32 and 8 hPa), p-values were significantly reduced in COH records. At 8–16 hPa  
826 remained high, but at 16–32 hPa the confidence improved (continued) to high over Arosa/Davos and OHP (Boulder  
827 and MLO). In case of Umkehr analyses in layer 8–16 hPa at Arosa/Davos, Boulder and MLO the confidence remained  
828 high. However, at 16–32 hPa the Umkehr trend detection confidence was degraded over Arosa/Davos and Lauder.

829 For the ozonesonde record, the p-values remained low (<0.05) except at MLO where some improvement was found  
830 after the Full Model was used, but the p-value remained high. It suggests that some instrumental records have either



831 high atmospheric or instrumental noise and therefore perhaps high certainty in trend detection cannot be achieved with  
 832 linear trend models. For near zero trends with high variability, the p-values are not a good criterion for trend  
 833 detectability.

834 In the lower stratosphere (between 125 and 32 hPa), analyses of p-values for the Full Model fit show significant  
 835 improvement for Umkehr trends at MLO between 63–32 hPa (while the p-value was increased at other stations at this  
 836 level). In addition, improvement in p-values was found for ozonesonde trends at all stations. Specifically, very low p-  
 837 values for the Full model were reached at Arosa/Davos (125–63 hPa), OHP (125–63 and 63–32 hPa), MLO (125–63  
 838 and 63–32 hPa), and Lauder (63–31 hPa).

LOTUS Model Proxy Tests: (P Value of Model)																
Height	Umkehr	Arosa/Davos			OHP			Boulder			MLO			Lauder		
(hPa)	Layer	UMK	COH	SND	UMK	COH	SND	UMK	COH	SND	UMK	COH	SND	UMK	COH	SND
1-2	9		0.00			0.00			0.06			0.10			0.00	
2-4	8	0.00	0.00		0.00	0.00		0.06	0.00		0.02	0.00		0.41	0.00	
4-8	7	0.00	0.01		0.02	0.00		0.13	0.00		0.00	0.00		0.34	0.00	
8-16	6	0.01	0.17		0.81	0.47		0.02	0.83		0.00	0.21		0.92	0.71	
16-32	5	0.74	0.00	0.00	0.86	0.03	0.02	0.50	0.00	0.05	0.51	0.00	0.57	0.74	0.73	0.00
32-63	4	0.56		0.34	0.67		0.01	0.27		0.15	0.09		0.02	0.08		0.01
63-127	3	0.66		0.04	0.32		0.01	0.31		0.35	0.63		0.02	0.02		0.30

839 **Table 13: P Value of the Full Model. High certainty of trend detection is seen for values below .05 (green). Values between**  
 840 **.05 and 0.1 (yellow) medium certainty, between 0.1 and 0.33 (orange) low certainty of trend detection, and above 0.33 (red)**  
 841 **very low certainty or no evidence of trend detection.**

842 **7 Summary of the Full Model findings.**

843 We find that upper stratospheric trends in COH overpass and Umkehr records detect ozone recovery with high  
 844 confidence ( $p < 0.05$ ) above 8 hPa (with the exception of near-zero positive Umkehr trends over Lauder and Boulder).  
 845 We note the largest difference between Umkehr and COH trends (outside of the SE uncertainty) at Boulder, Mauna  
 846 Loa and Lauder.

847 Confidence for the middle stratosphere (between 32 and 8 hPa) trends vary between high, medium and low. Although  
 848 most of the trends are narrowly different from zero (especially when error bars are considered), there are some  
 849 differences in results across instrumental groups: trends in COH and sonde (except at OHP) between 32 and 16 hPa  
 850 tend to be small negative, while Umkehr trends are slightly positive. Some trends are statistically different from zero.  
 851 However, instrument-specific error bars often overlap and thus making differences in trends not significant.

852 Confidence in lower stratosphere trends is highly variable and even lower than in the middle stratosphere due to higher  
 853 ozone variability unaccounted for by Solar, QBO and ENSO proxies used in the Reference Model. However, high  
 854 confidence ( $p < 0.05$ ) is still found in ozonesonde trends at Arosa/Davos, OHP, MLO and Lauder (although not at all  
 855 layers). Umkehr trends in the lower stratosphere show lower confidence than ozonesonde trends (except at Lauder  
 856 and Arosa/Davos in the lowermost altitudes). The low confidence levels could be related to the near-zero trends  
 857 derived from Umkehr data, whereas ozonesonde trends are often different from zero lines. Also, we apply AK-



858 smoothing to the sondes to account for the wide AKs in the Umkehr retrieval. We tested the impacts of the AK on  
859 ozonesonde trends (see Appendix A) and did not find any significant impacts. Most notably, ozonesonde and Umkehr  
860 trends significantly disagree in the lower stratosphere at OHP and Lauder and therefore require further investigation.  
861 The instrumental drifts and differences in Lauder trends are also discussed in Bjorkland et al. (2023 preprint) and are  
862 consistent with our findings.

## 863 **8 Conclusions**

864 This paper is a follow up to Godin-Beekmann et al. (2022) with a focus on the GB record trend assessment. Therefore,  
865 our trend analyses focus on the questions:

- 866 1) Do proxies for evaluating trends of GB stations need to be different from those of the optimized set for zonal  
867 data?
- 868 2) Are station records representative of the small geophysical region or semi-global changes?
- 869 3) Do uncertainties of the zonal averaged trends improve with additional proxies?

870

871 The Full Model developed in this paper for station and overpass data adds proxies to the LOTUS models of Godin-  
872 Beekmann (2022). Our trend analysis of stratospheric ozone records from the Umkehr, ozonesonde and COH station  
873 overpass data at 5 geographical regions using the Full Model (LOTUS v 0.8.0) show similar trends to those published  
874 in Godin-Beekmann et al. (2022) paper. We analyze trends for instrumental records converted to 7 Umkehr layers that  
875 represent ozone changes in the upper, middle and lower stratosphere over NH and SH middle latitudes and over high  
876 tropics of the NH. We also analyze GB station records at Arosa/Davos, Hohenpeißenberg and OHP separately in  
877 contrast to the “European regional” trend analyses presented in Godin-Beekmann et al. (2022) and included COH  
878 overpass records for comparisons with the GB records. Our analyses include evaluation of the adjusted R<sup>2</sup> (aka  
879 goodness of the model fit), standard error and p-values.

880 We also investigate differences between satellite trends as detected in the records sampled for individual geographical  
881 locations (spatial and temporal overpass criteria) versus zonal average datasets. We find that COH overpass ozone  
882 records capture ozone variability of the ground-based station records (Umkehr and sonde) better than COH zonal data.  
883 We do not find that the COH zonal record is improved by using EqLat instead of geometric latitude to construct the  
884 dataset (see Appendix C), but EqLat can be an important additional proxy at some levels for GB data. To determine  
885 the improvement to the model fit we use the Standard Error and adjusted R<sup>2</sup> for the Full and Reference model fit.  
886 Using the Reference model for the zonal mean COH data we find slightly better adjusted R<sup>2</sup> than for the COH overpass  
887 data fit over the Northern middle latitude stations. This is expected as much of the variability of the overpass time  
888 series is reduced in the zonal average data. Therefore, we also explore the impact of additional predictors in the trend  
889 model fit applied to the more variable GB and satellite COH overpass data to determine if that will reduce the SE and  
890 improve the adjusted R<sup>2</sup>. We also apply the Full model to the zonally averaged data to assess the benefits of additional  
891 proxies to further reduce trend uncertainties.

892 We find that adding predictors (with few exceptions) does not change the trends but often reduces SEs and increases  
893 the adjusted R<sup>2</sup> (with the exception of the upper stratospheric ozone trends at MLO). We also find that the p-values



894 are useful for interpretation of improvements of the model fit in the data, although improvements in the SE do not  
895 always result in improved confidence in derived trends, especially when the trends are close to zero. In these cases we  
896 conclude that either longer records are needed to discern trend information outside of the atmospheric noise or further  
897 research into the inconsistencies between instrumental records and homogenization procedures is required. We also  
898 find the small changes in trends in the lower stratosphere and improvements in the model fit after additional proxies  
899 are used. However, the sampling tests indicate that trends can depend on the temporal selection of the records when  
900 AK are used to smooth ozonesonde high resolution profiles (see discussion in Appendix D).

901 This paper concludes that additional proxies bring improvements to trend detectability in case of GB and gridded  
902 satellite data analyses and better agreement is achieved between satellite overpass and GB trends. We also find that  
903 zonally averaged and gridded satellite records produce comparable trends over the studied middle latitudes and  
904 subtropical regions. Therefore, the GB trends are representative of the stratospheric ozone changes over the semi-  
905 global area. Finally, zonally averaged data do not benefit from addition of proxies beyond what LOTUS model uses  
906 for global trend detection whereas the uncertainties in GB and gridded trends are significantly reduced and sometimes  
907 (Boulder, MLO, Lauder) become comparable to the uncertainties of the zonally averaged trends in the upper and  
908 middle stratosphere. Based on analyses presented in this paper we strongly recommend using additional proxies for  
909 trend analyses of GB and gridded satellite stratospheric ozone records. Additional proxies should be selected based  
910 on the latitude and altitude of the observational ozone record to adequately represent stratospheric transport and mixing  
911 processes impacting interannual and seasonal ozone variability.

## 912 **Appendices**

### 913 **Appendix A: AK Smoothing for ozonesondes**

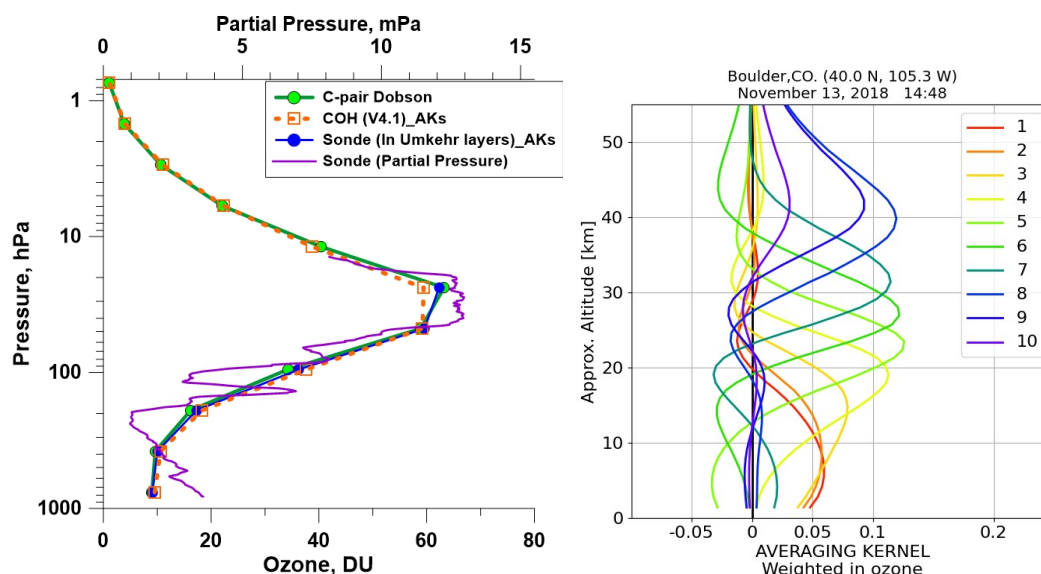
914 Ozonesonde profiles have high vertical resolution (purple line in Fig. A1) in comparison to the Umkehr (green solid  
915 line) or COH (orange dashed line) ozone profiles. Each Umkehr layer is referenced to the atmospheric pressure at the  
916 bottom of the layer, which is constructed using half of the pressure in the layer below. Averaging Kernels (AK) as  
917 shown in Fig. A1, panel b, define the granularity of the Umkehr vertical grid. In order to compare trends from three  
918 instrumental records in the same vertical system, we convert the ozonesonde and COH profiles to the Umkehr layers  
919 and DU. The COH overpass data is in units of DU, but on different layers than the defined Umkehr layers, so only  
920 vertical grid modification is required. The sonde profiles (purple thin line) are in units of partial pressure and are first  
921 converted to DU, then converted to the Umkehr grid (blue solid line in panel a). Conversion to the Umkehr grid can  
922 be done either by interpolation, or by AK smoothing. The equation describing the process of applying AK smoothing  
923 is

$$924 \quad Ozone_{smoothed}(i) = \sum_j \{AK_{i,j} * Ozone_{true}(j) - Ozone_{apriori}(j)\} + Ozone_{apriori}(i)$$

925 where AK is the Averaging Kernel for layer i,  $Ozone_{smoothed}$  is the smoothed ozone result,  $Ozone_{true}$  is the  
926 ozonesonde profile, and  $Ozone_{apriori}$  is the Umkehr a priori (climatological) profile. The AK for each Umkehr layer



927 is used as a weighting function applied to the ozonesonde profile (*Ozone<sub>true</sub>*) prior to the integration which simulates  
 928 the Umkehr optimal estimation method used for estimating the ozone content in the targeted layer (Rodgers, 2000).  
 929



930  
 931 **Figure A1:** a) An example of ozone observations over the Boulder, CO station. The purple line is 100-m averaged ozone  
 932 partial pressure (hPa) vertical profile measured by sonde on 13 November, 2018. The green line with solid circles is the  
 933 ozone profile derived from Dobson Umkehr observations on the same day. The blue line with blue dots is the ozonesonde  
 934 profile converted to the Umkehr layers and smoothed with the Umkehr AK. The orange dashed line with open squares is the  
 935 COH ozone profile observed over Boulder on the same day and interpolated to the Umkehr layer vertical grid. b) The  
 936 Umkehr AK for the ozone profile derived from observations in Boulder on 13 November, 2018. Each line represents the  
 937 smoothing function for one of 10 Umkehr layers (see color legend).

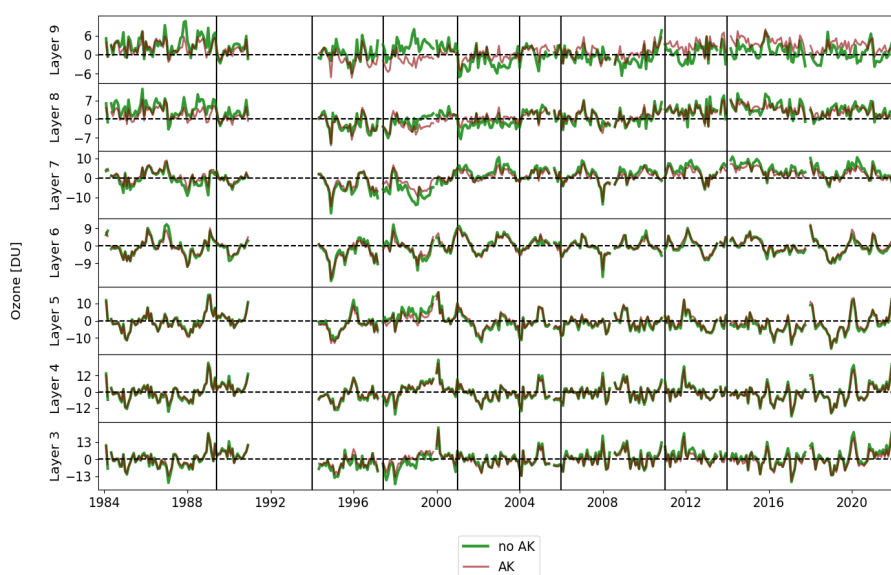
938 Although the ozonesonde measurement typically reaches altitudes between 32 and 10 hPa, the balloon often bursts  
 939 before reaching the top of layer 6 (16 hPa), therefore only partially covering the ozone content in that layer. We also  
 940 note that Umkehr AKs are relatively wide and therefore will incorporate (weight in) ozone variability from the layer  
 941 above and layer below of the targeted Umkehr layer. (See layer 6, green line in Fig. A1, panel b.) Therefore, there  
 942 are two sources of error in ozonesonde comparisons with Umkehr ozone in layer 6: a) burst level for ozonesonde does  
 943 not reach the top of the layer 6, thus the integrated ozone is smaller than expected. b) the Umkehr AK for layer 6 is  
 944 relatively wide and therefore the Umkehr layer partially contains information from above the burst altitude of the  
 945 ozonesonde, thus making smoothed ozonesonde concentration lower than expected. In order to avoid these errors, we  
 946 only show ozonesonde results up to layer 5.

947 Similarly, we explored smoothing COH profiles with Umkehr AKs. Figure A2 demonstrates the time series of the  
 948 COH ozone over the Mauna Loa station. The trend model was fitted to the COH record with and without AK applied.  
 949 The reference trend model included proxies and trends. To focus on ozone variability that contributes to the trends we  
 950 subtracted the modeled ozone variability from the COH data and then added the trend component back. The COH  
 951 record residuals in Fig. A2 are shown in Umkehr layers where COH is either smoothed with AK (red lines) or not  
 952 (green lines). We notice that the AK-smoothing of the COH profile in layer 9 does not have a lot of independent



953 information from layer 8. In this example it clearly shows that the trends in layer 8 are embedded in the COH layer 9  
 954 ozone time series, which was confirmed when we compared trends derived from the AK-smoothed COH in layers 8  
 955 and 9. In case of the integrated COH ozone record, the trends in layers 8 and 9 differed. In order to avoid biasing the  
 956 COH trends at layer 9 we decided to not apply Umkehr AKs for COH smoothing and only use COH profiles  
 957 interpolated into the Umkehr layers. This result makes sense since COH overpass data are derived from UV  
 958 backscatter radiances also using an Optimal Estimation technique. COH overpass data has a comparable vertical  
 959 resolution to Umkehr, simply with different layer definitions. Interpolation makes the most sense for rendering COH  
 960 data in the Umkehr vertical coordinate system.

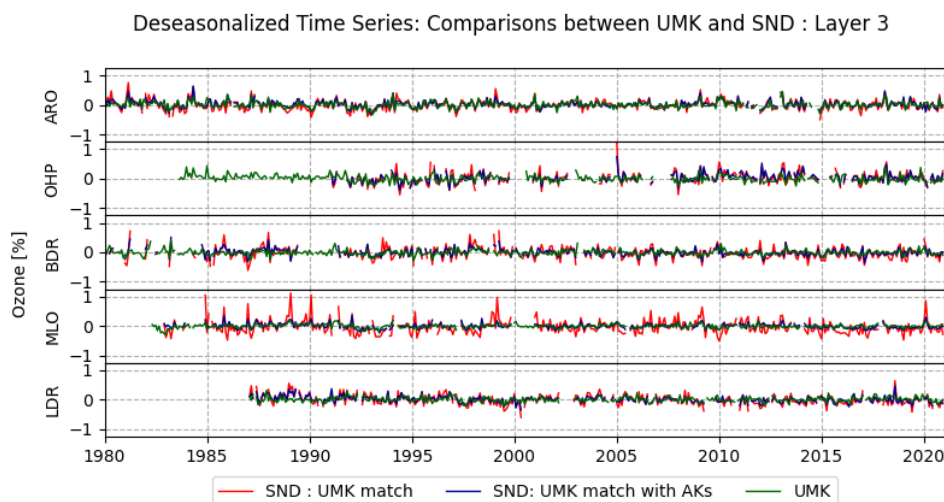
COH Time Series at Mauna Loa, Proxy Tested: AKs



961

962 **Figure A2: Modified residuals (seasonal cycle, Solar, QBO, and ENSO are removed, but trend is retained) of COH overpass**  
 963 **data at Mauna Loa (20N, 156W). Red: AK smoothed to Umkehr layers; Green: Interpolated to Umkehr layers. Vertical**  
 964 **lines show the dates of satellite records in COH. The largest impact of the AK is seen between 1997 and 2001 where two**  
 965 **curves separate in layers 7, 8 and 9, and also after 2001 in layer 9.**

966 Figure A3 demonstrates time series of monthly mean ground-based records the lower stratosphere at 5 stations. The  
 967 Umkehr data (blue) are compared with the ozonesonde anomalies either interpolated to the Umkehr layer 3 (green),  
 968 or ozonesonde profiles matched with Umkehr profiles in time and smoothed using the Umkehr averaging kernels  
 969 (crimson). All three datasets have been deseasonalized using their respective climatological (using 1998-2008  
 970 climatology) average monthly mean ozone. The application of the Averaging Kernels has the effect of smoothing the  
 971 temporal variability.



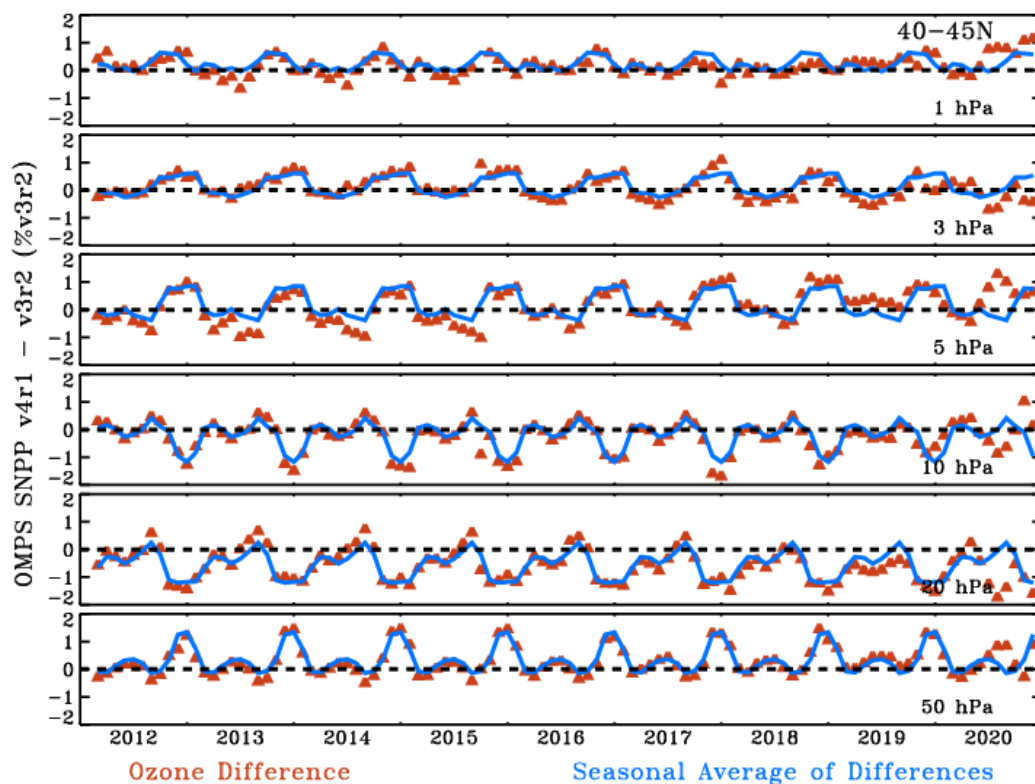
972

973 **Figure A3:** Time series of monthly averaged and de-seasonalized (in %) ozone anomalies of Umkehr (green) and  
974 ozonesonde records are compared at 5 ground-based stations. Ozonesonde data are either calculated using only profiles  
975 that are interpolated in Umkehr layer 3 (blue) or matched with Umkehr profile in time and smoothed with the Umkehr  
976 averaging kernels (crimson).

#### 977 **Appendix B: COH using OMPS v3r2 vs OMPS v4r1**

978 OMPS SNPP v4r1 uses updated SDRs as input which incorporate unified and consistent calibration algorithms  
979 removing artificial jumps caused by operational changes, instrument anomalies, or contamination for anomaly views  
980 of the environment or spacecraft. Also included are new interpolated band-passes, and updated soft calibration based  
981 on the new input SDR's.

982 Differences between the v3r2 and v4r1 versions of the resulting COH dataset are typically less than 1 percent (Fig.  
983 A4 and A5). Small seasonal variation is apparent at all levels. Larger differences are visible in 2020 when the soft  
984 calibration for v3r2 is extended beyond its period of relevance. Figure A6 shows the drift between the two versions.  
985 Drift between the datasets is less than +/- 1% at all levels. This is a reasonable estimate of the resulting expected trend  
986 difference in using the newest COH version as compared to the v3r2 results used in Godin-Beckmann (2022).



987

988

989

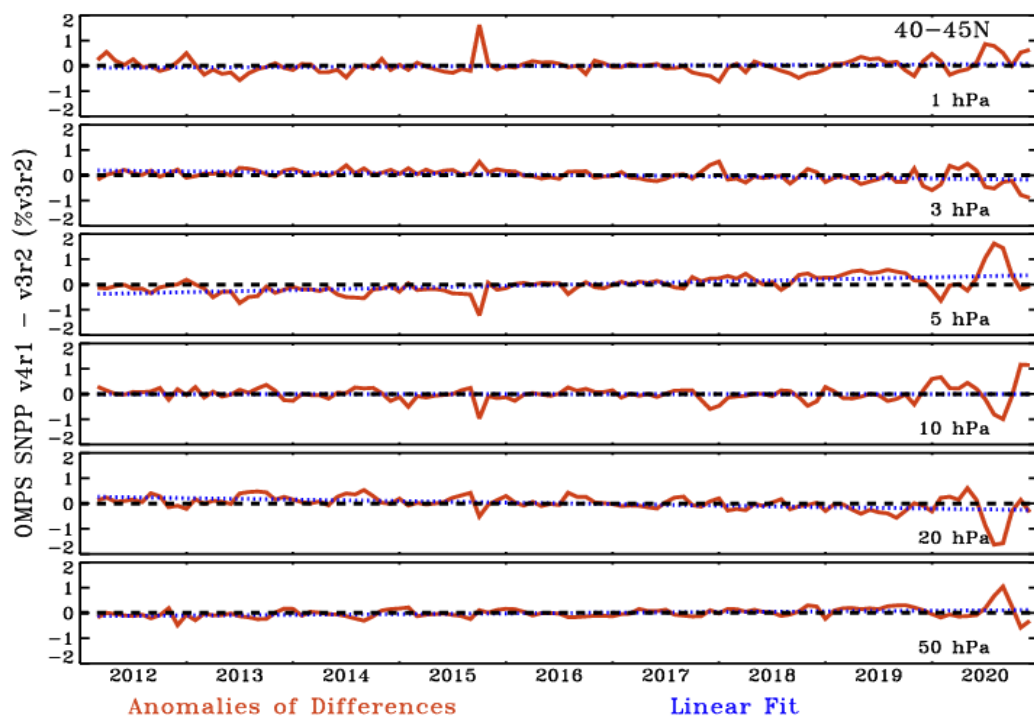
990

991

992

993

Figure A4: Differences in the COH monthly average zonal product as generated from SNPP v4r1 and v3r2 processing. Also shown is the annual cycle in this difference as depicted by the average over all years for each month. Exhibited at 40-45N is a less than 2% difference with an annual cycle. A somewhat different pattern is seen in 2020 where the soft calibration for v3r2 is extended beyond its period of relevance.



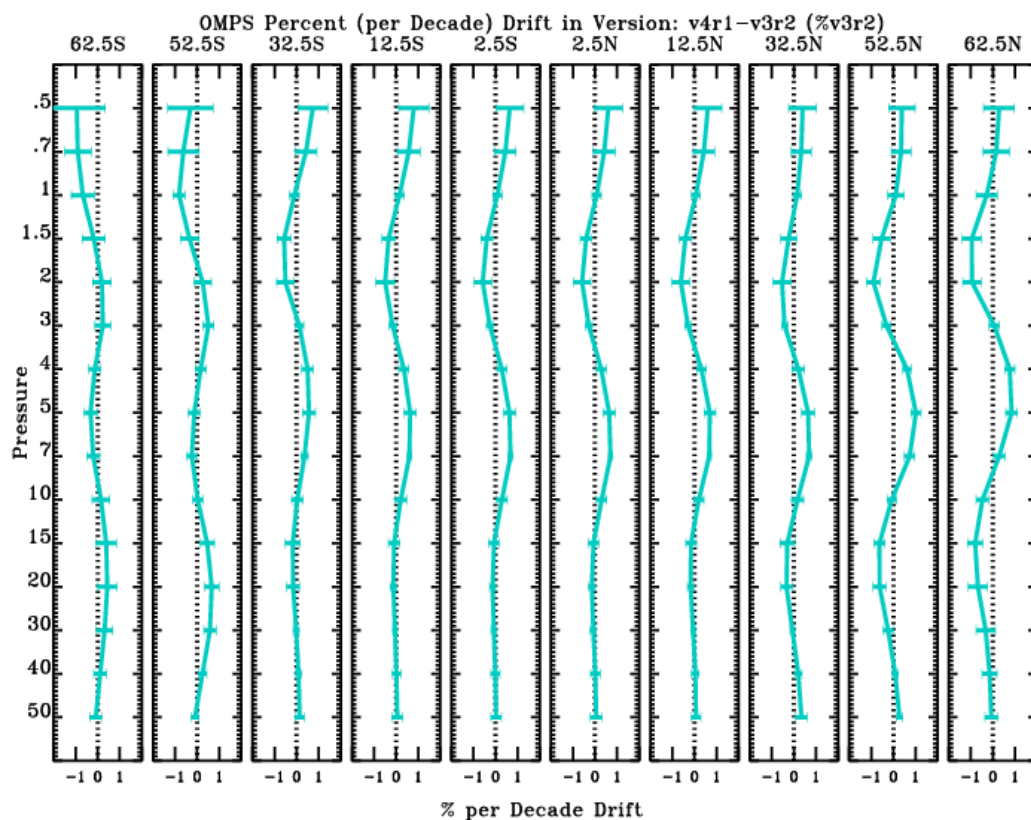
994

995

996

997

Figure A5: Anomalies of the differences in version (v4r1 vs v3r2) in the COH monthly average zonal product at 40-45N. Anomalies are enhanced in 2020. Also shown as a blue dotted line is a linear least square fit to the anomalies representing the drift between the two versions.



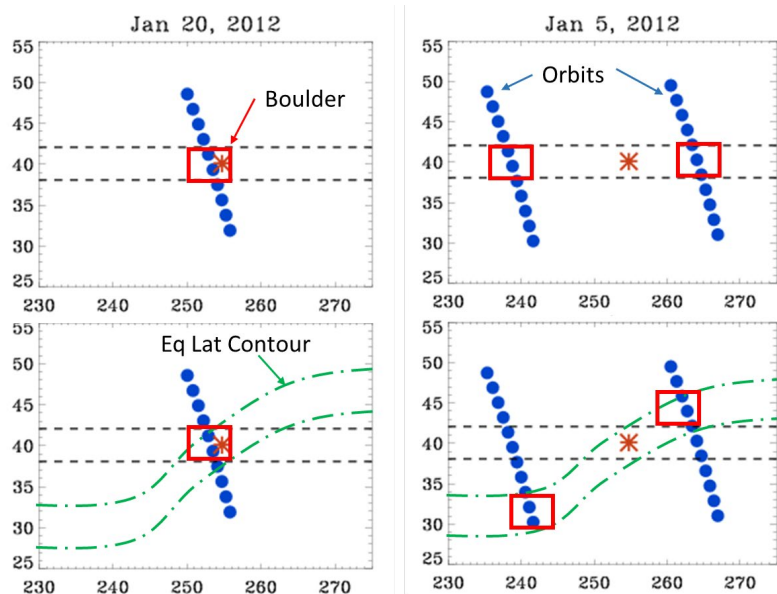
998

999 Figure A6 shows the drift between the two versions (v4r1 vs v3r2) as function of pressure level at 10 latitudes.

1000 **Appendix C: Impact of using equivalent latitude in generation of the COH product**

1001 The COH overpass data used in this paper collects all profiles during the day within a latitude and longitude box of  
 1002 +/- 2 degrees by +/- 20 degrees, then generates a 1/distance averaged value for the station. The box is based on  
 1003 geometric latitude and longitude. With 15 orbits per day, the chosen box size guarantees 2 to 4 possible profiles within  
 1004 the box depending on whether the orbit overpasses or straddles the site as shown in Fig. A7. Also shown is a scenario  
 1005 when the equivalent latitude (EqLat) near the site is particularly non-zonal. In such cases the profiles selected using  
 1006 a geometric coordinate box will select SBUV profiles from an Eq Lat that is different from that of the measurement  
 1007 station.

1008



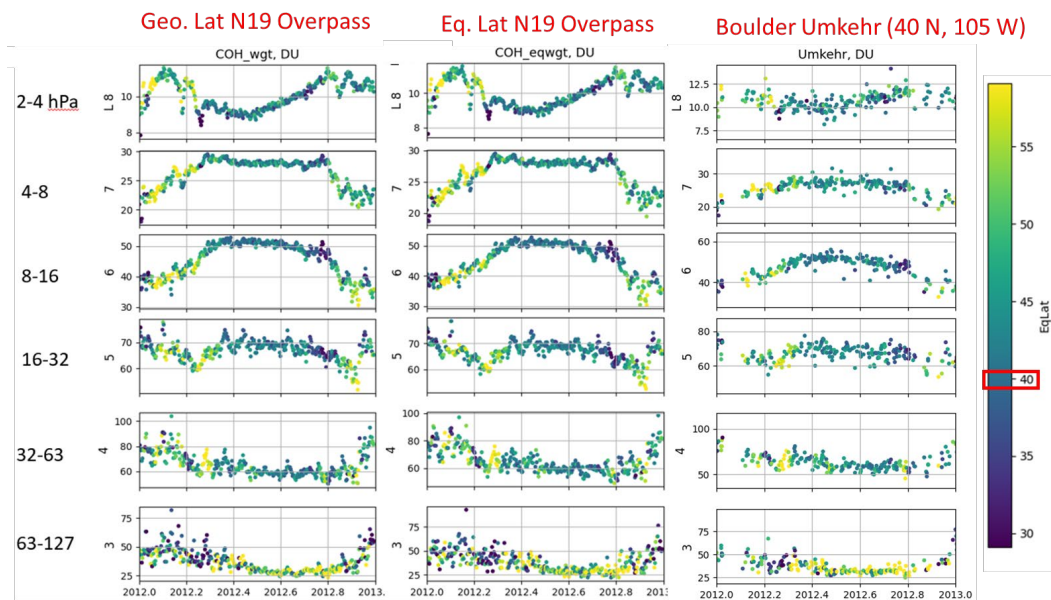
1009

1010 **Figure A7: Shows orbits of SNPP and positions of OMPS NP ozone profiles on January 20, 2012 and January 5, 2012. The**  
1011 **second row displays a possible EqLat contour overlaid.**

1012 It is informative to create an overpass product using boxes based on EqLat and determine the impact on the data.  
1013 Since EqLat is layer dependent, the included profiles must be selected independently for each layer. Figure A8 shows  
1014 COH overpass data for Boulder using geometric coordinates, EqLat based coordinates, and the associated Umkehr  
1015 data. Color coding shows the EqLat at Boulder for each measurement day with dark blue and yellow indicating days  
1016 with extreme variation from 40N.

1017

1018



1019

1020

1021

**Figure A8: COH overpass data generated with geometric coordinates, EqLat based coordinates, and the associated Umkehr dataset at Boulder for 2012. Data points are color coded for the EqLat at the measurement site. Boulder is at 40 N.**

1022

1023

1024

1025

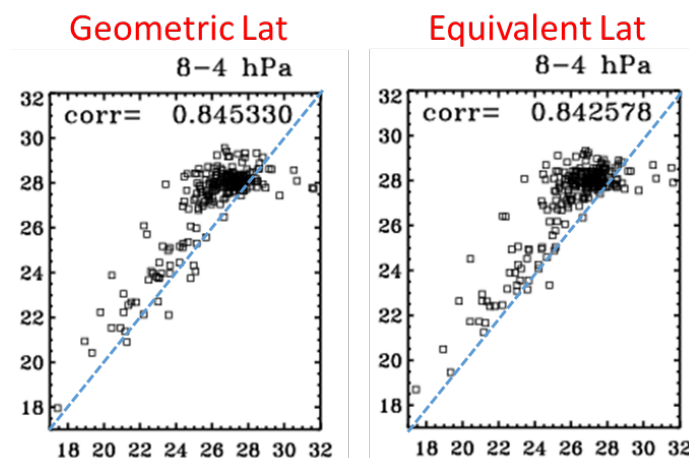
1026

1027

1028

Variation in EqLat is most apparent in Winter months and transitional Fall and Spring, less so in Summer. Yet the value of the COH ozone is not dramatically altered in the time series. Figure A9 shows correlation plots of the COH overpass to Umkehr for the data at layer 7 (4-8 hPa). The pattern of the scatter and the value of the correlation coefficient are not substantially altered for overpass determination using geometric latitude (left) and EqLat (right). Figure A10 shows the vertical distribution of the Correlation coefficient and the RMS Difference for the two COH datasets vs Umkehr. These two metrics are minimally impacted for this sample year in the layers where COH is valid.

1029

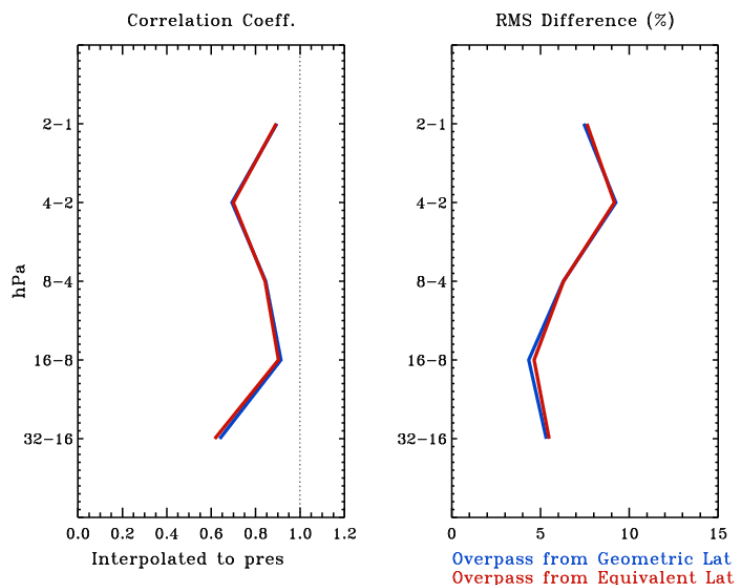


1029



1030 **Figure A9: Correlation between Umkehr and COH overpass using Geometric Latitude (left) and EqLat (right) to select**  
 1031 **included profiles for layer 7 (4-8 hPa).**

1032



1033

1034 **Figure A10: Profiles of Correlation coefficients and RMS differences between COH overpass data at Boulder for 2012 using**  
 1035 **Geometric Latitude (blue) and EqLat (red) to select data points included in the average.**

1036

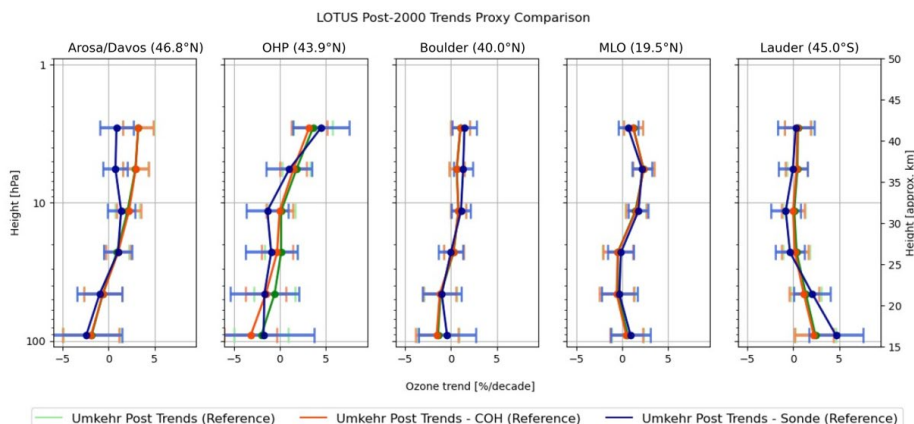
1037 The use of geometric latitude appears to be sufficient in the choice of included data points in the overpass COH product  
 1038 at the layers used in this paper. Likely this is a ramification of the smooth horizontal resolution of the satellite product.

1039 **Appendix D: Temporal Sampling and Impact on Trends**

1040 This paper compares trends for three instrument types each with differing measurement frequency. From each set of  
 1041 measurements a monthly average is constructed. See the data files at  
 1042 [https://gml.noaa.gov/aftp/ozwv/Publications/2023\\_Umkehr\\_Ozone\\_Trends\\_Paper/](https://gml.noaa.gov/aftp/ozwv/Publications/2023_Umkehr_Ozone_Trends_Paper/) for the data and the number of  
 1043 data points in each monthly average with the sampling variations. Umkehr measures once or twice per day depending  
 1044 on cloud interference with the measurement. At Arosa/Davos and Lauder, Umkehr measurements are sparser than  
 1045 the other GB stations, often less than 10 per month. At Boulder beginning in 1983 measurements number 20 or more  
 1046 per month. At OHP the Umkehr record begins in 1983 with a strong 20 or more measurements per month. From  
 1047 1999 to 2016, however, measurements per month are often less than 15 per month. The most Umkehr measurements  
 1048 at MLO are the most abundant, especially after 1985 measuring multiple times in a day, resulting in 50-70 data points  
 1049 contributing to the monthly average. The COH overpass dataset is typically available once per day at each station with  
 1050 occasional misses, contributing usually 27-30 data points per month. Since Umkehr can measure multiple times per  
 1051 day, the COH data matched to Umkehr can contain more profiles in the monthly average than the original full COH  
 1052 data, since the COH overpass data will appear twice in the monthly average, once per each Umkehr measurement.



1053 This occurs often at MLO. Ozonesonde launches are typically one to three times per week depending on the station.  
1054 At Arosa/Davos, sonde measurements are typically about 15 per month. Sonde measurements at the other stations  
1055 usually have approximately 5 measurements per month, with some periods of up to 10 per month. As with COH  
1056 overpass measurements, the sonde dataset matched to Umkehr can have more contributions to the monthly average  
1057 resulting from dates with more than one Umkehr measurement, resulting in multiple sonde matches.  
1058 The trend results in this paper use all available Umkehr data to generate the monthly means. The COH and sonde data  
1059 are matched to Umkehr to use the Umkehr temporal sampling for COH, and to be able to use the Umkehr averaging  
1060 kernels for sonde. It is important to determine how the temporal sampling within the monthly mean data may impact  
1061 trend results. To aid this understanding, we create three subsets of Umkehr data each with different temporal sampling  
1062 and create the corresponding monthly mean: 1) all observations in Umkehr record; 2) Umkehr matched to the COH  
1063 dataset; and 3) Umkehr matched to the sonde dataset. In this way we use the same data, but only vary the temporal  
1064 sampling. Since the COH is measured every day, except in the rare case that the satellite data is missing due to  
1065 instrument issues, sampling 1 and 2 should provide nearly identical results. We expect a strong change in the monthly  
1066 mean and resulting trends for Umkehr record when it is matched with infrequent sampling of ozonesonde profiles  
1067 (especially in Boulder, Hilo and Lauder).  
1068 Figure A11 summarizes the results. Each line in Fig. A11 is trend derived from Umkehr data, but with sampling of all  
1069 data, data matched to COH dates, and data matched to sonde dates. In general, the differences are within the envelope  
1070 of trend uncertainty ( $\pm 2$  std errors). As expected, the trends and standard errors for all (green) and COH-matched  
1071 subsampled (orange) Umkehr records are nearly the same. The largest differences in all Umkehr and COH matched  
1072 Umkehr lines are apparent at OHP. We have determined that this arises from occasional months when there is a short  
1073 satellite outage coupled with sparse Umkehr observations at the station. However, trends derived from sonde-matched  
1074 Umkehr data (blue) show deviations from other observations. This is especially clear at Arosa/Davos in the upper  
1075 stratosphere ( $\sim 2$ -3 % above 10 hPa). But since this is above the measurement capability of the ozonesonde, this will  
1076 not impact the ozonesonde trend results at Arosa/Davos. At Lauder the most significant differences are seen in layer  
1077 3 (2.5%), but unfortunately not in the direction to explain sonde differences in the Lauder trend curves as compared to  
1078 Umkehr. Smaller differences are seen at other layers (very small, less than 1 %, differences in layers 6 and 4). At  
1079 OHP small differences of less than 1 % are seen between 50 and 10 hPa, well within error estimates.

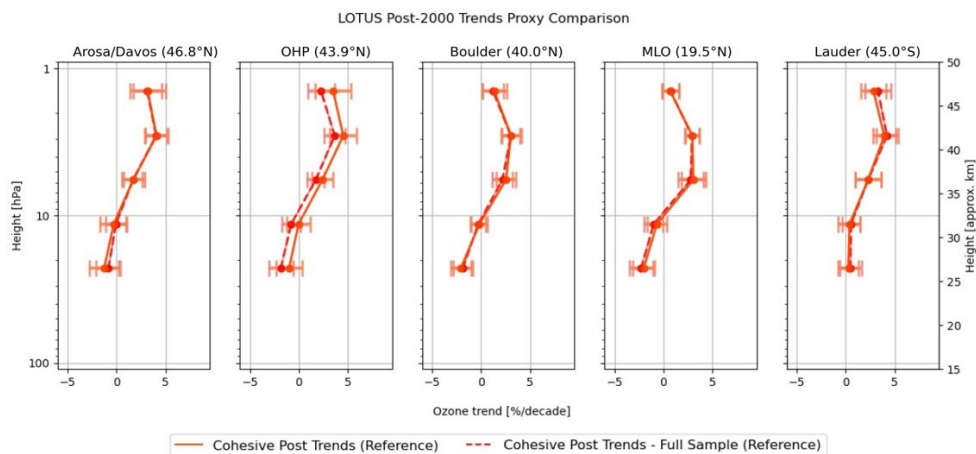


1080

1081 **Figure A11: Trend results for the Reference Model using Umkehr data mimicking the temporal sampling of COH and**  
 1082 **sonde. Green is all available Umkehr data; orange is Umkehr data matched to COH measurements dates; blue is Umkehr**  
 1083 **data matched to sonde measurement dates.**

1084 Figure A12 further explores sampling differences by examination of trends of COH data using the full COH dataset,  
 1085 and data sampled to the Umkehr dates in generation of the monthly mean datasets. As with Fig A11, the trend lines  
 1086 are nearly identical at all stations except OHP. At OHP in the early 2000's there are significantly fewer COH points  
 1087 matched to Umkehr because of the drop in Umkehr measurements. This likely impacts the post-2000 trend estimate.  
 1088 The differences remain below 2%, and are within the error estimate of the trends. In summary, the sampling biases  
 1089 between COH overpass and Umkehr data cannot explain the difference in the derived trends (see Fig. 3, most notable  
 1090 in layers 7 and 8 at Boulder and Lauder).

1091

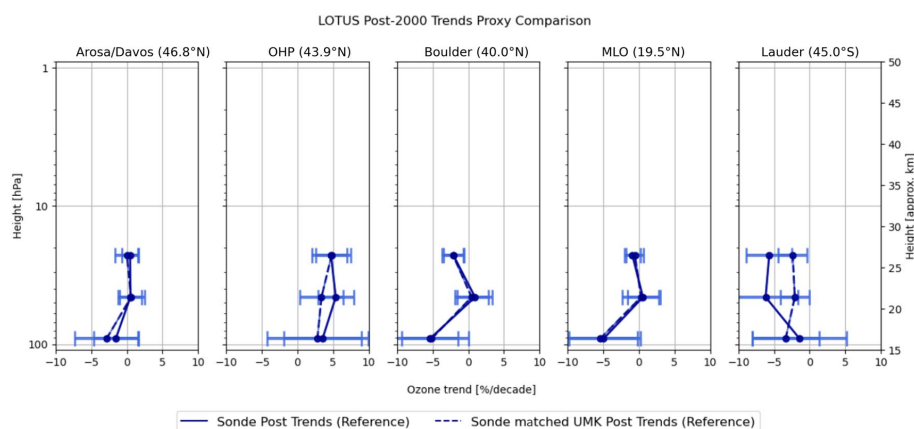


1092

1093 **Figure A12: Trend results for the Reference Model exploring variations in sampling of the COH data. Solid orange is COH**  
 1094 **data matching Umkehr sampling; dotted orange is all available COH data.**



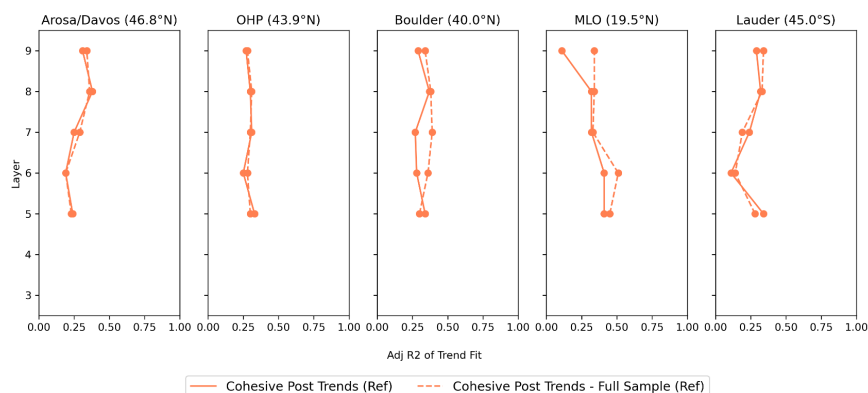
1095 Figure A13 explores the impact on trends from sampling differences of the sonde data. Shown are trends with all  
 1096 sonde data, and trends with Umkehr matched data. In this figure only, the sonde data is not AK smoothed since the  
 1097 Umkehr AK are only available on dates when there is an Umkehr measurement. So shown here are trends from sonde  
 1098 data integrated to the Umkehr levels. As with Fig. A11 the only visible impact is seen at OHP and Lauder, though  
 1099 both are within error estimates. At Lauder the trends remain negative for both samplings, but sonde sampled to  
 1100 Umkehr moves closer to the zero line. At OHP the sonde trends are positive, but sonde sampled to Umkehr moves  
 1101 slightly closer to zero. The sampling impact on trends for both OHP and Lauder are likely due to the reduced number  
 1102 of Umkehr data at these sites.



1103

1104 **Figure A13: Trend results for Reference model exploring sampline of the sonde data. Solid blue is all sonde data; dashed**  
 1105 **is Umkehr matched sonde data.**

1106 Figure A14 explores the impact of sampling on the adjusted R2 using the COH overpass data. Shown are the adjusted  
 1107 R2 for all available COH overpass data, and the same using only COH overpass with matches to the Umkehr data.  
 1108 For Arosa/Davos, OHP and Lauder the differences are small. For Boulder and MLO at some layers (Boulder, layers  
 1109 6,7; MLO layers 6,9), the impact is more apparent with the Full COH exhibiting higher adjusted R2 at these stations.



1110

1111 **Figure A14: Adjusted R2 for the Reference Model exploring variations in sampling of the COH data. Solid orange is COH**  
 1112 **data matching Umkehr sampling; dotted orange is all available COH data.**

1113 **Appendix E: Decision process for the Full Model**

1114 The LOTUS styled Reference Model is developed and optimized for zonal average datasets. The Extended Model  
 1115 tests the addition of single predictors to see if fit statistics can be improved for GB and overpass datasets. For  
 1116 Tropospheric Pressure (TP), improvements are consistent among layers and among instrument types. The addition of  
 1117 EqLat also yields consistent results for instrument types and at most stations, though not Mauna Loa. Addition of  
 1118 other predictors gives mixed results depending on level and station. The potential for improving confidence in trend  
 1119 results exists by combining predictors using different choices depending on layer and station. We choose additional  
 1120 predictor combinations with consideration of three criteria: 1) combined predictors should not have a high correlation  
 1121 with each other (usually .2 or less); 2) predictors should reduce the SE of the trend consistently for all instrument  
 1122 types; 3) addition of the predictor should not greatly reduce the adjusted R2 of the model fit, but preferentially increase  
 1123 it. As seen in Tables 7e and 7f the NAO and the EHF predictors do not make a significant improvement when added  
 1124 to the Reference Model, so we do not include either in the Full Model.

1125 **Mixed Model:**

1126 We have noted a high correlation between the TP and EqLat predictors at all levels especially for Boulder, Mauna  
 1127 Loa and Lauder with correlation adjusted R2 of .4 to .7, and somewhat less correlated at Arosa/Davos and OHP with  
 1128 adjusted R2 of .2 and .3. Subsequently, we choose to not use these two predictors together (at the same station/layer  
 1129 combination). The addition of TP at all stations for layers 3 and 4 uniformly decreases the standard errors at all  
 1130 stations for both Umkehr and sonde. The addition of EqLat (with the exception of Umkehr at Boulder, level 5) almost  
 1131 uniformly decreases the standard errors at all stations for layers 5 and 6. There is additional reduction in the SE for  
 1132 layers 7 to 9 for all stations except at Mauna Loa. Thus, we choose TP and EqLat as additional predictors at these  
 1133 layers. QBO C and D, have significant impact in decreasing the SE in layers 4 and 5 for both Umkehr and sonde, and  
 1134 layer 3 for sonde with only a small degradation for Umkehr. QBO-CD shows an improvement in layer 8 at OHP, both



1135 COH and Umkehr, and Arosa/Davos and Boulder for COH only. We have tested adding both QBO and EqLat for  
 1136 layer 8 at these 3 stations. For Umkehr measurements, there is no improvement beyond EqLat only with QBO-CD  
 1137 also included. For COH there is additional improvement, but not to the extent of QBO-CD alone. Since the  
 1138 improvement is limited to one layer, and for only COH, we choose to only add the additional QBO-CD for the tropical  
 1139 MLO. Table A1 shows the resulting combination of additional predictors for this Mixed Model.  
 1140

LOTUS Mixed Model					
Layer	Arosa/Davos	OHP	Boulder	MLO	Lauder
9	EqLat	EqLat	EqLat	Ref	EqLat
8	EqLat	EqLat	EqLat	Ref	EqLat
7	EqLat	EqLat	EqLat	Ref	EqLat
6	EqLat	EqLat	EqLat	EqLat	EqLat
5	EqLat	EqLat	EqLat	EqLat, QBO CD	EqLat
4	TP	TP	TP	TP, QBO CD	TP
3	TP	TP	TP	TP, QBO CD	TP

1141

1142 **Table A1: Details of additional predictor combinations for each level and station in the Mixed Model**

1143 The resulting change in SE from the Reference Model is shown in Table A2. For most stations/layers this is simply a  
 1144 composite of the values from the single EqLat or TP Extended Model results. There remain a few  
 1145 instrument/station/layers where the SE is slightly increased - OHP sonde Layer 5, Arosa/Davos Umkehr layer 8 and  
 1146 Boulder Umkehr layer 8, but these are negligible. At Boulder Layer 5 Umkehr the increase in SE is somewhat more  
 1147 at 1.85% difference, but this is still small enough to not be of great concern. For Mauna Loa at layers 3,4 and 5 the  
 1148 model is rerun adding two predictors together and the results are new. Indeed in these cases the SE is improved  
 1149 beyond the single predictor results of either QBO alone, or TP or EqLat alone with the exception of Sonde layer 5  
 1150 where the change in SE is just slightly degraded from QBO alone (13.42% vs 13.69% reduction in SE).

LOTUS Model Proxy Tests: (% Difference in Std. Error of Model)																
Height	Umkehr	Arosa/Davos			OHP			Boulder			MLO			Lauder		
(hPa)	Layer	UMK	COH	SND	UMK	COH	SND	UMK	COH	SND	UMK	COH	SND	UMK	COH	SND
1-2	9		8.35			2.74			1.94			0.00				2.85
2-4	8	-0.47	0.68		0.09	1.03		-0.39	1.53		0.00	0.00		0.98	3.14	
4-8	7	3.75	3.04		2.08	1.86		5.41	4.08		0.00	0.00		0.53	1.21	
8-16	6	6.11	8.36		2.54	10.88		2.39	7.75		0.55	0.82		3.44	7.72	
16-32	5	7.93	10.72	5.87	1.92	13.33	-0.56	-1.85	0.00	0.90	15.21	11.13	13.42	0.82	3.91	0.00
32-63	4	6.60		6.07	5.87		7.04	3.35		2.97	13.15		9.70	8.03		4.13



63-127	3	12.80		10.17	12.80		6.91	6.81		2.46	3.81		4.19	9.76		4.41
--------	---	-------	--	-------	-------	--	------	------	--	------	------	--	------	------	--	------

1151 **Table A2: Change in the SE of the trend using the Mixed Model.**

1152 Table A3 shows the associated adjusted R2 for the proposed Mixed Model. Similarly to the change in SE the adjusted  
 1153 R2 is a composite of the individual EqLat or TP results from the extended model with the exception of the results for  
 1154 layers 3,4, and 5 at Mauna Loa where both predictors are included concurrently. At these layers the adjusted R2 in  
 1155 some cases matches the higher Adj R2 values of the two predictors, and in others improves with the combination of  
 1156 QBO and TP or EqLat.

1157

LOTUS Model Proxy Tests: (Adjusted R2 of Model)																
Height	Umkehr	Arosa/Davos			OHP			Boulder			MLO			Lauder		
(hPa)	Layer	UMK	COH	SND	UMK	COH	SND	UMK	COH	SND	UMK	COH	SND	UMK	COH	SND
1-2	9		0.42			0.37			0.36			0.11			0.32	
2-4	8	0.23	0.39		0.14	0.31		0.17	0.39		0.11	0.32		0.18	0.34	
4-8	7	0.35	0.35		0.31	0.41		0.27	0.33		0.26	0.32		0.17	0.27	
8-16	6	0.31	0.35		0.33	0.45		0.33	0.40		0.40	0.51		0.25	0.23	
16-32	5	0.34	0.38	0.26	0.25	0.51	0.21	0.31	0.40	0.19	0.40	0.35	0.37	0.42	0.41	0.24
32-63	4	0.21		0.22	0.29		0.32	0.19		0.13	0.34		0.35	0.42		0.25
63-127	3	0.24		0.23	0.42		0.26	0.22		0.13	0.14		0.21	0.25		0.19

1158 **Table A3: Adjusted R2 for the Mixed Model**

1159 **Augmented Mixed Model**

1160 It is hard to ignore the substantial reduction of SE when adding the AO/AAO predictor especially for layers 3,4 and 5  
 1161 at Mauna Loa, and for layers 3 and 4 at Arosa/Davos. The results for OHP layers 3 and 4 are still compelling, though  
 1162 somewhat less so. So we explore the addition of AO/AAO at these three stations only, for the layers specified. **Table**  
 1163 **A4** summarizes the predictor choices for this Augmented Mixed Model.

1164

1165

LOTUS Augmented Mixed Model					
	Arosa/Davos	OHP	Boulder	MLO	Lauder
Layer					
9	EqLat	EqLat	EqLat	Ref	EqLat
8	EqLat	EqLat	EqLat	Ref	EqLat
7	EqLat	EqLat	EqLat	Ref	EqLat
6	EqLat	EqLat	EqLat	EqLat	EqLat
5	EqLat	EqLat	EqLat	EqLat, QBO, AO/AAO	EqLat
4	TP, AO/AAO	TP, AO/AAO	TP	TP, QBO CD, AO/AAO	TP
3	TP, AO/AAO	TP, AO/AAO	TP	TP, QBO CD, AO/AAO	TP



1166 **Table A4: Details of additional predictor choices for each level and station in the Augmented Mixed Model . This differs**  
 1167 **from Table A1 by adding AO/AAO at some levels for Arosa/Davos, OHP and Mauna Loa.**

LOTUS Model Proxy Tests: (% Difference in Std. Error of Model)																
Height	Umkehr	Arosa/Davos			OHP			Boulder			MLO			Lauder		
(hPa)	Layer	UMK	COH	SND	UMK	COH	SND	UMK	COH	SND	UMK	COH	SND	UMK	COH	SND
1-2	9		8.35			2.74			1.94			0.00			2.85	
2-4	8	-0.47	0.68		0.09	1.03		-0.39	1.53		0.00	0.00		0.98	3.14	
4-8	7	3.75	3.04		2.08	1.86		5.41	4.08		0.00	0.00		0.53	1.21	
8-16	6	6.11	8.36		2.54	10.88		2.39	7.75		0.55	0.82		3.44	7.72	
16-32	5	7.93	10.72	5.87	1.92	13.33	-0.56	-1.85	0.00	0.90	19.39	13.32	15.70	0.82	3.91	0.00
32-63	4	8.71		9.96	6.13		7.04	3.35		2.97	20.51		10.45	8.03		4.13
63-127	3	20.30		18.49	13.48		5.46	6.81		2.46	6.00		4.85	9.76		4.41

1168

1169 **Table A5: Change in the SE of the trend using the Mixed Model.**

1170

1171 **Table A5** displays the change in the SE from the Reference Model now for the Augmented Mixed Model. Adding  
 1172 AO/AAO at Arosa/Davos (layers 3 and 4) and Mauna Loa (layers 3 to 5) greatly reduces the SE beyond that of the  
 1173 Mixed Model results in **Table A2**. For OHP (layers 3 and 4) the impact is less dramatic for Umkehr. For sonde  
 1174 measurements at layer 4 the AO/AAO addition has no impact beyond the Mixed Model; for layer 3 the addition of  
 1175 AO/AAO results in less reduction of the SE.

1176

LOTUS Model Proxy Tests: (Adjusted R2 of Model)																
Height	Umkehr	Arosa/Davos			OHP			Boulder			MLO			Lauder		
(hPa)	Layer	UMK	COH	SND	UMK	COH	SND	UMK	COH	SND	UMK	COH	SND	UMK	COH	SND
1-2	9		0.42			0.37			0.36			0.11			0.32	
2-4	8	0.23	0.39		0.14	0.31		0.17	0.39		0.11	0.32		0.18	0.34	
4-8	7	0.35	0.35		0.31	0.41		0.27	0.33		0.26	0.32		0.17	0.27	
8-16	6	0.31	0.35		0.33	0.45		0.33	0.40		0.40	0.51		0.25	0.23	
16-32	5	0.34	0.38	0.26	0.25	0.51	0.21	0.31	0.40	0.19	0.44	0.53	0.40	0.42	0.41	0.24
32-63	4	0.23		0.25	0.29		0.34	0.19		0.13	0.42		0.39	0.42		0.25
63-127	3	0.31		0.31	0.44		0.26	0.22		0.13	0.19		0.26	0.25		0.19

1177 **Table A6: Adjusted R2 for the Augmented Mixed Model**

1178 Table A6 displays the Adj R2 for the Augmented Mixed Model. Adding AO/AAO improves the Adj R2 results for  
 1179 Arosa/Davos and MLO and has little to no impact at OHP. Based on the criteria outlined at the beginning of this  
 1180 appendix, we assign the Augmented Mixed Model as the ‘Full Model’ in the body of this paper.

1181

1182 **Code/Data availability:** All dataset used in this study are publicly available at the website



1183 [https://gml.noaa.gov/aftp/ozwv/Publications/2023\\_Umkehr\\_Ozone\\_Trends\\_Paper/](https://gml.noaa.gov/aftp/ozwv/Publications/2023_Umkehr_Ozone_Trends_Paper/).

1184 **Competing interests:** The authors declare that they have no conflict of interest.

1185 **Author contributions:** IP and JW conceptualized the paper, and IP led the paper preparation. PE, KA, and JW  
1186 performed the data analysis. KM is responsible for the production of the spatial and temporally matched ground-based  
1187 and satellite ozone profile data. JW is responsible for producing COH zonally averaged and station overpass ozone  
1188 profile records. LF is responsible for the retrieval and calibration of the OMPS data. GM, PE, KM and KA are  
1189 responsible for NOAA Umkehr measurements. EMB is responsible for measurements in Arosa/Davos. RQ is  
1190 responsible for Umkehr and ozonesonde observations in Lauder, New Zealand. BJ and PC are responsible for  
1191 ozonesonde observations in Boulder and Hilo. GA is responsible for the ozonesonde observations in OHP. RVM is  
1192 responsible for HEGIFTOM ozonesonde records and data analyses. RD, SGB, DZ provided context of the LOTUS  
1193 model use and interpretation of trend analyses. All authors contributed to the writing of the paper.

1194 **Acknowledgements:**

1195 This study was supported in part by NOAA grant NA19NES4320002 (Cooperative Institute for Satellite Earth System  
1196 Studies - CISESS) at the University of Maryland/ESSIC and NOAA grant NA22OAR4320151, for the Cooperative  
1197 Institute for Earth System Research and Data Science (CIESRDS). Additional funding is from NOAA Climate  
1198 Program Office's Atmospheric Chemistry, Carbon Cycle, and Climate program (AC4), grant numbers  
1199 NA19OAR4310169 (CU)/ NA19OAR4310171 (UMD). The statements, findings, conclusions, and recommendations  
1200 are those of the author(s) and do not necessarily reflect the views of NOAA or the U.S. Department of Commerce.

1201 The authors would like to thank the NASA/GSFC Atmospheric Chemistry and Dynamics team for the SBUV/2 v8.6  
1202 profile data, Eric Beach from the NESDIS/STAR for his help with the S-NPP OMPS data, the NOAA GML  
1203 observatory team (Boulder, MLO and Fairbanks observatories), LATMOS (OHP), and NIWA (Lauder) for Umkehr  
1204 and ozonesonde data, Wolfgang Steinbrecht of the DWD for help with interpretation of the Hohenpeißenberg  
1205 ozonesonde data, the MeteoSwiss and PMOD/WRC teams (Arosa/Davos) for Dobson Umkehr data. Some data are  
1206 associated with the Network for the Detection of Atmospheric Composition Change (NDACC) and are available  
1207 through the NDACC website ([www.ndacc.org](http://www.ndacc.org)). Additional thanks are due to Susan Strahan for Equivalent Latitude  
1208 data at each station, to Kai-Lan Chang of CIRES for discussion of statistical interpretation of the thresholds, and to  
1209 Justin Alsing for development of the LOTUS code. North American Regional Reanalysis (NARR) data provided by  
1210 the NOAA PSL, Boulder, Colorado, USA, from their website at <https://psl.noaa.gov>.

1211 **References**

1212 Anstey, J.A., T.P. Banyard, N. Butchart, L. Coy, P.A. Newman, S. Osprey, and C.J. Wright, Prospect of increased  
1213 disruption to the QBO in a changing climate, *Geophys. Res. Lett.*, 48 (15), <https://doi.org/10.1029/2021gl093058>,  
1214 2021.



- 1215
- 1216 Ancellet, G., Godin-Beekmann, S., Smit, H. G. J., Stauffer, R. M., Van Malderen, R., Bodichon, R., Pazmino, A.:
- 1217 Homogenization of the Observatoire de Haute Provence electrochemical concentration cell (ECC) ozonesonde data
- 1218 record: comparison with lidar and satellite observations, *Atmos. Meas. Tech.*, 15, 3105–3120,
- 1219 <https://doi.org/10.5194/amt-15-3105-2022>, 2022.
- 1220
- 1221 Bai, K., Liu, C., Shi, R. et al. Comparison of Suomi-NPP OMPS total column ozone with Brewer and Dobson
- 1222 spectrophotometers measurements. *Front. Earth Sci.* 9, 369–380 (2015). <https://doi.org/10.1007/s11707-014-0480-5>.
- 1223
- 1224 Ball, W. T., Chiodo, G., Abalos, M., Alsing, J., and Stenke, A., Inconsistencies between chemistry–climate models
- 1225 and observed lower stratospheric ozone trends since 1998, *Atmos. Chem. Phys.*, 20, 9737–9752,
- 1226 <https://doi.org/10.5194/acp-20-9737-2020>, 2020.
- 1227
- 1228 Bernet, L., Svendby, T., Hansen, G., Orsolini, Y., Dahlback, A., Goutail, F., Pazmiño, A., Petkov, B.,
- 1229 and Kylling, A.: Total ozone trends at three northern high-latitude stations, *Atmos. Chem. Phys.*, 23,
- 1230 4165–4184, <https://doi.org/10.5194/acp-23-4165-2023>, 2023.
- 1231
- 1232 Bhartia, P. K., Herman, J. R., McPeters, R. D., Torres, O.: Effect of Mount Pinatubo aerosols on total ozone
- 1233 measurements from backscatter ultraviolet (BUV) experiments, *J. Geophys. Res.*, 98, 18,547– 18,554,
- <https://doi.org/10.1029/93JD01739>, 1993.
- 1234
- 1235 Bhartia, P. K., McPeters, R. D., Flynn, L. E., Taylor, S., Kramarova, N. A., Frith, S., Fisher, B., and DeLand, M.:
- 1236 Solar Backscatter UV (SBUV) total ozone and profile algorithm, *Atmos. Meas. Tech.*, 6, 2533–2548,
- <https://doi.org/10.5194/amt-6-2533-2013>, 2013.
- 1237
- 1238 Björklund, R., Vigouroux, C., Effertz, P., Garcia, O., Geddes, A., Hannigan, J., Miyagawa, K., Kotkamp, M.,
- 1239 Langerock, B., Nedoluha, G., Ortega, I., Petropavlovskikh, I., Poyraz, D., Querel, R., Robinson, J., Shiona, H., Smale,
- 1240 D., Smale, P., Van Malderen, R., and De Mazière, M.: Intercomparison of long-term ground-based measurements of
- 1241 tropospheric and stratospheric ozone at Lauder, New Zealand (45S), *EGUsphere* [preprint],
- <https://doi.org/10.5194/egusphere-2023-2668>, 2023.
- 1242
- 1243 Boynard, A., Hurtmans, D., Garane, K., Goutail, F., Hadji-Lazaro, J., Koukouli, M. E., Wespes, C., Vigouroux, C.,
- 1244 Keppens, A., Pommereau, J.-P., Pazmino, A., Balis, D., Loyola, D., Valks, P., Sussmann, R., Smale, D., Coheur, P.-
- 1245 F., and Clerbaux, C.: Validation of the IASI FORLI/EUMETSAT ozone products using satellite (GOME-2), ground-
- 1246 based (Brewer–Dobson, SAOZ, FTIR) and ozonesonde measurements, *Atmos. Meas. Tech.*, 11, 5125–5152,
- <https://doi.org/10.5194/amt-11-5125-2018>, 2018.



- 1247 Chang, K.-L., Cooper, O. R., Gaudel, A., Petropavlovskikh, I., and Thouret, V., Statistical regularization for trend  
1248 detection: an integrated approach for detecting long-term trends from sparse tropospheric ozone profiles, *Atmos.*  
1249 *Chem. Phys.*, 20, 9915–9938, <https://doi.org/10.5194/acp-20-9915-2020>, 2020.
- 1250 Chang, K. L., Schultz, M. G., Lan, X., McClure-Begley, A., Petropavlovskikh, I., Xu, X., & Ziemke, J. R., Trend  
1251 detection of atmospheric time series: Incorporating appropriate uncertainty estimates and handling extreme events,  
1252 *Elem Sci Anth*, 9(1), 00035, <https://doi.org/10.1525/elementa.2021.00035>, 2021.
- 1253 Chang, K.-L., Schultz, M.G., Koren, G., Selke, N., Guidance note on best statistical practices for TOAR analyses, in  
1254 TOAR tropospheric ozone assessment report, 2023, available at [https://igacproject.org/sites/default/files/2023-](https://igacproject.org/sites/default/files/2023-04/STAT_recommendations_TOAR_analyses_0.pdf)  
1255 [04/STAT\\_recommendations\\_TOAR\\_analyses\\_0.pdf](https://igacproject.org/sites/default/files/2023-04/STAT_recommendations_TOAR_analyses_0.pdf), last access 12/07/2023.
- 1256 Chang, K.-L., Cooper, O.R., Gaudel, A., Petropavlovskikh, I., Effertz, P., Morris, G., McDonald, B.C., Challenges of  
1257 detecting free tropospheric ozone trends in a sparsely sampled environment, in Special issue: Tropospheric Ozone  
1258 Assessment Report Phase II (TOAR-II) Community Special Issue (ACP/AMT/BG/GMD inter-journal SI), 2023  
1259 preprint.
- 1260 Cochran, D., Orcutt, G. H.: Application of least squares regression to relationships containing auto-correlated error  
1261 terms, *Journal of the American Statistical Association*, 44: 245, 32-  
1262 61, <https://doi.org/10.1080/01621459.1949.10483290>, 1949 .
- 1263 DeLuisi, J. J., Longenecker, D. U., Mateer, C. L., Wuebbles, D. J.: An analysis of northern middle-latitude Umkehr  
1264 measurements corrected for stratospheric aerosols for 1979–1986, *J. Geophys. Res.*, 94, 9837–9846,  
1265 <https://doi.org/10.1029/JD094iD07p09837>, 1989.
- 1266 Diallo, M., Riese, M., Birner, T., Konopka, P., Müller, R., Hegglin, M. I., Santee, M. L., Baldwin, M., Legras, B., and  
1267 Ploeger, F.: Response of stratospheric water vapor and ozone to the unusual timing of El Niño and the QBO disruption  
1268 in 2015–2016, *Atmos. Chem. Phys.*, 18, 13055–13073, <https://doi.org/10.5194/acp-18-13055-2018>, 2018.  
1269
- 1270 Diallo, M. A., Ploeger, F., Hegglin, M. I., Ern, M., Groß, J.-U., Khaykin, S., and Riese, M.: Stratospheric water  
1271 vapour and ozone response to the quasi-biennial oscillation disruptions in 2016 and 2020, *Atmos. Chem. Phys.*, 22,  
1272 14303–14321, <https://doi.org/10.5194/acp-22-14303-2022>, 2022.  
1273
- 1274 EEAP (Environmental Effects Assessment Panel): 2022 Quadrennial Assessment - Environmental effects of  
1275 stratospheric ozone depletion, UV radiation, and interactions with climate change, 2023,  
1276 <https://ozone.unep.org/system/files/documents/EEAP-2022-Assessment-Report-May2023.pdf>, last access March 5,  
1277 2024.  
1278



- 1279 Evans, R.D., Irina Petropavlovskikh, Audra McClure-Begley, Glen McConville, Dorothy Quincy, and Koji  
1280 Miyagawa, Technical note: The US Dobson station network data record prior to 2015, re-evaluation of NDACC and  
1281 WOUDC archived records with WinDobson processing software, *Atmospheric Chemistry and Physics*, 17, 12051–  
1282 12070, <https://doi.org/10.5194/acp-17-12051-2017>, 2017.  
1283
- 1284 Fioletov, V. E., Labow, G., Evans, R., Hare, E. W., Köhler, U., McElroy, C. T., Miyagawa, K., Redondas, A.,  
1285 Savastiouk, V., Shalamyansky, A. M., Staehelin, J., Vanicek, K., and Weber, M.: Performance of the ground-based  
1286 total ozone network assessed using satellite data, *J. Geophys. Res.*, 113, D14313,  
1287 <https://doi.org/10.1029/2008JD009809>, 2008.  
1288
- 1289 Frith, S. M., Kramarova, N. A., Stolarski, R. S., McPeters, R. D., Bhartia, P. K., G. J. Labow: Recent changes in total  
1290 column ozone based on the SBUV Version 8.6 Merged Ozone Data Set, *J. Geophys. Res. Atmos.*, 119, 9735-9751,  
1291 <https://doi.org/10.1002/2014JD021889>, 2014.
- 1292 Frith, S. M., Kramarova, N. A., Bhartia, P. K., McPeters, R. D., Labow, G. J., J. R. Ziemke, J. R., Haffner, D.: Recent  
1293 Advances in the SBUV Merged Ozone Dataset (MOD) for LOTUS Phase 2 Analysis of Stratospheric Ozone Trends  
1294 and Uncertainties, LOTUS Phase 2 Workshop (Virtual), May 28, 2020.
- 1295 Godin-Beekmann, S., Azouz, N., Sofieva, V., Hubert, D., Petropavlovskikh, I., Effertz, P., Ancellet, G., Degenstein,  
1296 D., Zawada, D., Froidevaux, L., Frith, S., Wild, J., Davis, S., Steinbrecht, W., Leblanc, T., Querel, R., Tourpali, K.,  
1297 Damadeo, R., Maillard Barras, E., Stübi, R., Vigouroux, C., Arosio, C., Nedoluha, G., Boyd, I., van Malderen, R.:  
1298 Updated trends of the stratospheric ozone vertical distribution in the 60° S–60° N latitude range based on the LOTUS  
1299 regression model, *Atmos. Chem. Phys.*, 22, 11657–11673, <https://doi.org/10.5194/acp-22-11657-2022>, 2022.  
1300
- 1301 Harris, N.R.P., B. Hassler, F. Tummon, G. E. Bodeker, D. Hubert, I. Petropavlovskikh, W. Steinbrecht, J. Anderson,  
1302 P. K. Bhartia, C. D. Boone, A. Bourassa, S. M. Davis, D. Degenstein, A. Delcloo, S. M. Frith, L. Froidevaux, S.  
1303 Godin-Beekmann, N. Jones, M. J. Kurylo, E. Kyrölä, M. Laine, S. T. Leblanc, J.-C. Lambert, B. Liley, E. Mahieu, A.  
1304 Maycock, M. de Mazière, A. Parrish, R. Querel, K. H. Rosenlof, C. Roth, C. Sioris, J. Staehelin, R. S. Stolarski, R.  
1305 Stübi, J. Tamminen, C. Vigouroux, K. A. Walker, H. J. Wang, J. Wild, and J. M. Zawodny, Past changes in the vertical  
1306 distribution of ozone – Part 3: Analysis and interpretation of trends, *Atmos. Chem. Phys.*, 15, 9965-9982,  
1307 <https://doi.org/10.5194/acp-15-9965-2015>, 2015.  
1308
- 1309 Hassler, B., I. Petropavlovskikh, J. Staehelin, T. August, P. K. Bhartia, C. Clerbaux, D. Degenstein, M. De Mazière,  
1310 B. M. Dinelli, A. Dudhia, G. Dufour, S. M. Frith, L. Froidevaux, S. Godin-Beekmann, J. Granville, N. R. P. Harris,  
1311 K. Hoppel, D. Hubert, Y. Kasai, M. J. Kurylo, E. Kyrölä, J.-C. Lambert, P. F. Levelt, C. T. McElroy, R. D. McPeters,  
1312 R. Munro, H. Nakajima, A. Parrish, P. Raspollini, E. E. Remsberg, K. H. Rosenlof, A. Rozanov, T. Sano, Y. Sasano,  
1313 M. Shiotani, H. G. J. Smit, G. Stiller, J. Tamminen, D. W. Tarasick, J. Urban, R. J. van der A, J. P. Veefkind, C.  
1314 Vigouroux, T. von Clarmann, C. von Savigny, K. A. Walker, M. Weber, J. Wild, and J. M. Zawodny, Past changes in  
1315 the vertical distribution of ozone – Part 1: Measurement techniques, uncertainties and availability, *Atmos. Meas.*  
1316 *Techn.*, 7, 1395-1427, <https://doi.org/10.5194/amt-7-1395-2014>, 2014.



- 1317
- 1318 Hassler, B., Kremser, S., Bodeker, G. E., Lewis, J., Nesbit, K., Davis, S. M., Chipperfield, M. P., Dhomse, S. S., and  
1319 Dameris, M.: An updated version of a gap-free monthly mean zonal mean ozone database, *Earth Syst. Sci. Data*, 10,  
1320 1473–1490, <https://doi.org/10.5194/essd-10-1473-2018>, 2018.
- 1321
- 1322 Hassler, B., P. Young, P. (Lead Authors), Ball, W. T., Damadeo, R., Keeble, J., Maillard Barras, E., Sofieva, V.,  
1323 Zeng, G.: Update on Global Ozone: Past, Present, and Future, Chapter 3 in *Scientific Assessment of Ozone Depletion:*  
1324 *2022*, GAW Report No. 278, 509 pp., WMO, Geneva, 2022.
- 1325
- 1326 Hubert, D., Lambert, J.-C., Verhoelst, T., Granville, J., Keppens, A., Baray, J.-L., Bourassa, A. E., Cortesi, U.,  
1327 Degenstein, D. A., Froidevaux, L., Godin-Beekmann, S., Hoppel, K. W., Johnson, B. J., Kyrölä, E., Leblanc, T.,  
1328 Lichtenberg, G., Marchand, M., McElroy, C. T., Murtagh, D., Nakane, H., Portafaix, T., Querel, R., Russell III, J. M.,  
1329 Salvador, J., Smit, H. G. J., Stebel, K., Steinbrecht, W., Strawbridge, K. B., Stübi, R., Swart, D. P. J., Taha, G.,  
1330 Tarasick, D. W., Thompson, A. M., Urban, J., van Gijssel, J. A. E., Van Malderen, R., von der Gathen, P., Walker, K.  
1331 A., Wolfram, E., and Zawodny, J. M.: Ground-based assessment of the bias and long-term stability of 14 limb and  
1332 occultation ozone profile data records, *Atmos. Meas. Tech.*, 9, 2497–2534, <https://doi.org/10.5194/amt-9-2497-2016>,  
1333 2016.
- 1334
- 1335 E. Kalnay, Kanamitsu, M., Kistler, R., Collins, W., Deaven, D., Gandin, L., Iredell, M., Saha, S., White, G., Woollen,  
1336 J., Zhu, Y., Chelliah, M., Ebisuzaki, W., Higgins, W., Janowiak, J., Mo, K.C., Ropelewski, C., Wang, J., Leetmaa,  
1337 A., Reynolds, R., Jenne, R., and Joseph, D., The NCEP/NCAR 40-year reanalysis project, *Bull. Amer. Meteor. Soc.*,  
1338 77, 437–470, [https://doi.org/10.1175/1520-0477\(1996\)077<0437:TNYRP>2.0.CO;2](https://doi.org/10.1175/1520-0477(1996)077<0437:TNYRP>2.0.CO;2), 1996.
- 1339
- 1340 Knudsen, B. M., and J. U. Grooss, Northern midlatitude stratospheric ozone dilution in spring modeled with simulated  
1341 mixing. *J. Geophys. Res.*, 105, 6885–6890, <https://doi.org/10.1029/1999JD901076>, 2000.
- 1342
- 1343 Koukouli, M. E., Zara, M., Lerot, C., Fragkos, K., Balis, D., van Roozendaal, M., Allart, M. A. F., and van der A, R.  
1344 J.: The impact of the ozone effective temperature on satellite validation using the Dobson spectrophotometer network,  
1345 *Atmos. Meas. Tech.*, 9, 2055–2065, <https://doi.org/10.5194/amt-9-2055-2016>, 2016.
- 1346
- 1347 Kramarova, N. A., Frith, S. M., Bhartia, P. K., McPeters, R. D., Taylor, S. L., Fisher, B. L., Labow, G. J., DeLand,  
1348 M. T.: Validation of ozone monthly zonal mean profiles obtained from the version 8.6 Solar Backscatter Ultraviolet  
1349 algorithm, *Atmos. Chem. Phys.*, 13, 6887–6905, <https://doi.org/10.5194/acp-13-6887-2013>, 2013a.
- 1350 Kramarova, N. A., Bhartia, P. K., Frith, S. M., McPeters, R. D., and Stolarski, R. S.: Interpreting SBUV smoothing  
1351 errors: an example using the quasi-biennial oscillation, *Atmos. Meas. Tech.*, 6, 2089–2099,  
1352 <https://doi.org/10.5194/amt-6-2089-2013>, 2013b.



- 1353 Lary, D.J., Chipperfield, M.P., Pyle, J.A., Norton, W.A. Riishøjgaard, L.P. (1995), Three-dimensional tracer  
1354 initialization and general diagnostics using equivalent PV latitude–potential–temperature coordinates, Q.J.R.  
1355 Meteorol. Soc., 121: 187–210, <https://doi.org/10.1002/qj.49712152109>, 1995.
- 1356
- 1357 Lawrence, Z. D., Perlwitz, J., Butler, A. H., Manney, G. L., Newman, P. A., Lee, S. H., & Nash, E. R., The  
1358 remarkably strong Arctic stratospheric polar vortex of winter 2020: Links to record-breaking Arctic Oscillation and  
1359 ozone loss. *Journal of Geophysical Research: Atmospheres*, 125, e2020JD033271.  
1360 <https://doi.org/10.1029/2020JD033271>, 2020.
- 1361
- 1362 Lee, H., and Smith, A. K., Simulation of the combined effects of solar cycle, quasi-biennial oscillation, and volcanic  
1363 forcing on stratospheric ozone changes in recent decades, *J. Geophys. Res.*, 108, D2, 4049,  
1364 <https://doi.org/10.1029/2001JD001503>, 2003.
- 1365
- 1366 Madronich, S., Lee-Taylor, J. M., Wagner, M., Kyle, J., Hu, Z., & Landolfi, R. (2021). Estimation of skin and ocular  
1367 damage avoided in the United States through implementation of the Montreal Protocol on Substances that Deplete the  
1368 Ozone Layer. *ACS Earth and Space Chemistry*, 5(8), 1876–1888. <https://doi.org/10.1021/acsearthspacechem.1c00183>.
- 1369
- 1370 Maillard Barras, E., Haefele, A., Stübi, R., Jouberton, A., Schill, H., Petropavlovskikh, I., Miyagawa, K., Stanek, M.,  
1371 and Froidevaux, L.: Dynamical linear modeling estimates of long-term ozone trends from homogenized Dobson  
1372 Umkehr profiles at Arosa/Davos, Switzerland, *Atmos. Chem. Phys.*, 22, 14283–14302, [https://doi.org/10.5194/acp-](https://doi.org/10.5194/acp-22-14283-2022)  
1373 [22-14283-2022](https://doi.org/10.5194/acp-22-14283-2022), 2022.
- 1374
- 1375 Manney, G. L., and M. I. Hegglin, 2018: Seasonal and Regional Variations of Long-Term Changes in Upper-  
1376 Tropospheric Jets from Reanalyses. *J. Climate*, 31, 423–448, <https://doi.org/10.1175/JCLI-D-17-0303.1>.
- 1377
- 1378 Manney, G. L., and Coauthors, Unprecedented Arctic ozone loss in 2011. *Nature*, 478, 469–475,  
1379 <https://doi.org/10.1038/nature10556>, 2011.
- 1380
- 1381 McPeters, R. D., Bhartia, P. K., Haffner, D., Labow, G. J., Flynn, L.: The version 8.6 SBUV ozone data record: An  
1382 overview, *J. Geophys. Res. Atmos.*, 118, 8032–8039, <https://doi.org/10.1002/jgrd.50597>, 2013.
- 1383 Meng, L., Liu, J., Tarasick, D.W., Randel, W.J., Steiner, A.K., Wilhelmson, H., Wang, L., Haimberger, L., Continuous  
1384 rise of the tropopause in the Northern Hemisphere over 1980–2020, *Sci. Adv.* 7, eabi8065,  
1385 <https://doi.org/10.1126/sciadv.abi8065>, 2021.
- 1386 Millán, L. F., Hoor, P., Hegglin, M. I., Manney, G. L., Boenisch, H., Jeffery, P., Kunkel, D., Petropavlovskikh, I., Ye,  
1387 H., Leblanc, T., and Walker, K.: Exploring ozone variability in the upper troposphere and lower stratosphere using  
1388 dynamical coordinates, *EGUsphere [preprint]*, <https://doi.org/10.5194/egusphere-2024-144>, 2024.
- 1389 Petropavlovskikh, I., Bhartia, P. K., and DeLuisi, J.: New Umkehr ozone profile retrieval algorithm optimized for  
1390 climatological studies, *Geophys. Res. Lett.*, 32, L16808, <https://doi.org/10.1029/2005GL023323>, 2005.



- 1391 Petropavlovskikh, I., Miyagawa, K., McClure-Beegle, A., Johnson, B., Wild, J., Strahan, S., Wargan, K., Querel, R.,  
1392 Flynn, L., Beach, E., Ancellet, G., and Godin-Beekmann, S.: Optimized Umkehr profile algorithm for ozone trend  
1393 analyses, *Atmos. Meas. Tech.*, 15, 1849–1870, <https://doi.org/10.5194/amt-15-1849-2022>, 2022.
- 1394 Rodgers, C. D.: *Inverse Methods for Atmospheric Sounding : Theory and Practice.*, Series on Atmospheric, Oceanic  
1395 and Planetary Physics, World Scientific Publishing Company, Hackensack, N. J., <https://doi.org/10.1142/3171>, 2000.
- 1396 Savin, N. E., & White, K. J. (1978). Testing for Autocorrelation with Missing observations. *Econometrica* (Pre-1986),  
1397 46(1), 59.
- 1398 Smit, H. G. J. and the ASOPOS panel (Assessment of Standard Operating Procedures for Ozonesondes): Quality  
1399 assurance and quality control for ozonesonde measurements in GAW, World Meteorological Organization, GAW  
1400 Report #201, Geneva, Switzerland, available at: [https://library.wmo.int/doc\\_num.php?explnum\\_id=7167](https://library.wmo.int/doc_num.php?explnum_id=7167), 2014.  
1401
- 1402 Smit, H. G. J., Thompson, A. M. and the ASOPOS 2.0 panel (Assessment of Standard Operating Procedures for  
1403 Ozonesondes, v2.0): Ozonesonde measurement principles and best operational practices, World Meteorological  
1404 Organization, GAW Report #268, Geneva, Switzerland, available at:  
1405 [https://library.wmo.int/doc\\_num.php?explnum\\_id=10884](https://library.wmo.int/doc_num.php?explnum_id=10884), 2021.  
1406
- 1407 SPARC/IO3C/GAW, SPARC/IO3C/GAW Report on Long-term Ozone Trends and Uncertainties in the Stratosphere.  
1408 I. Petropavlovskikh, S. Godin-Beekmann, D. Hubert, R. Damadeo, B. Hassler, V. Sofieva (Eds.), SPARC Report No.  
1409 9, GAW Report No. 241, WCRP-17/2018, <https://doi.org/10.17874/f899e57a20b>, available at [www.sparc-](http://www.sparc-climate.org/publications/sparc-reports/sparc-report-no9)  
1410 [climate.org/publications/sparc-reports/sparc-report-no9](http://www.sparc-climate.org/publications/sparc-reports/sparc-report-no9), 2019.  
1411
- 1412 Staehelin, J., Pierre Viatte, Rene Stübi, Fiona Tummon, and Thomas Peter, 2018, Stratospheric ozone measurements  
1413 at Arosa (Switzerland): history and scientific relevance, *Atmospheric Chemistry and Physics*, 18, 6567–6584,  
1414 <https://doi.org/10.5194/acp-18-6567-2018>.  
1415
- 1416 Stauffer, R.M., Thompson, A. M., Kollonige, D. E., Tarasick, D. W., Van Malderen, R., Smit, H. G. J., Vömel, H.,  
1417 Morris, G.A., Johnson, B.J., Cullis, P.D., Stübi, R., Davies, J., Yan, M.M., An Examination of the Recent Stability of  
1418 Ozonesonde Global Network Data, *EArth and Space Science*, 9, e2022EA002459.  
1419 <https://doi.org/10.1029/2022EA002459>, 2022.  
1420
- 1421 Stauffer, R. M., Thompson, A. M., Kollonige, D. E., Komala, N., Al-Ghazali, H. K., Risdianto, D. Y., Dindang, A.,  
1422 Fairud bin Jamaluddin, A., Sammathuria, M. K., Zakaria, N. B., Johnson, B. J., and Cullis, P. D.: Dynamical drivers  
1423 of free-tropospheric ozone increases over equatorial Southeast Asia, *EGUsphere* [preprint],  
1424 <https://doi.org/10.5194/egusphere-2023-2618>, 2023.  
1425



- 1426 Stauffer, R. M., Thompson, A. M., Oman, L. D., & Strahan, S. E., The effects of a 1998 observing system change on  
1427 MERRA-2-based ozone profile simulations. *Journal of Geophysical Research: Atmospheres*, 124, 7429–7441,  
1428 <https://doi.org/10.1029/2019JD030257>, 2019.
- 1429
- 1430 Steinbrecht, W., U. Köhler, H. Claude, M. Weber, J. P. Burrows, and R. J. van der A, Very high ozone columns at  
1431 northern mid-latitudes in 2010, *Geophys. Res. Lett.*, 38, L06803, <https://doi.org/10.1029/2010GL046634>, 2011.
- 1432
- 1433 Sterling, C. W., Johnson, B. J., Oltmans, S. J., Smit, H. G. J., Jordan, A.F., Cullis, P. D., Hall, E. G., Thompson, A.  
1434 M., Jacquelyn C. Witte, J. C.: Homogenizing and estimating the uncertainty in NOAA's long-term vertical ozone  
1435 profile records measured with the electrochemical concentration cell  
1436 ozonesonde, *Atmos. Meas. Tech.*, 11, 3661–3687, <https://doi.org/10.5194/amt-11-3661-2018>, 2018.
- 1437
- 1438 Szelag, M. E., Sofieva, V. F., Degenstein, D., Roth, C., Davis, S., and Froidevaux, L.: Seasonal stratospheric ozone  
1439 trends over 2000–2018 derived from several merged data sets, *Atmospheric Chemistry and Physics*, 20, 7035–7047,  
1440 <https://doi.org/10.5194/acp-20-7035-2020>, 2020.
- 1441
- 1442 Tarasick, D. W., Davies, J., Smit, H. G. J., Oltmans, S. J.: A re-evaluated Canadian ozonesonde record: measurements  
1443 of the vertical distribution of ozone over Canada from 1966 to 2013, *Atmos. Meas. Tech.*, 9, 195–214,  
1444 <https://doi.org/10.5194/amt-9-195-2016>, 2016.
- 1445
- 1446 Thompson, A. M., Witte, J. C., Sterling, C., Jordan, A., Johnson, B. J., Oltmans, S. J., Fujiwara, M., Vömel, H.,  
1447 Allaart, M., PETERS, A., Coetzee, G. J. R., Posny, F., Corrales, E., Diaz, J. A., Félix, C., Komala, N., Lai, N., Nguyen,  
1448 H. T. A., Maata, M., Mani, F., Zainal, Z., Ogino, S., Paredes, F., Penha, T. L. B., da Silva, F. R., Sallons-Mitro, S.,  
1449 Selkirk, H. B., Schmidlin, F. J., Stübi, R., Thiongo, K.: First reprocessing of Southern Hemisphere ADDitional  
1450 OZonesondes (SHADOZ) Ozone Profiles (1998-2016). 2. Comparisons with satellites and ground-based instruments,  
1451 *J. Geophys. Res.*, 122, <https://doi.org/10.1002/2017JD027406>, 2017.
- 1452
- 1453 Thompson, A. M., H. G. J. Smit, J. C. Witte, R. M. Stauffer, B. J. Johnson, G. Morris, P. von der Gathen, R. Van  
1454 Malderen, J. Davies, A. PETERS, M. Allaart, F. Posny, R. Kivi, P. Cullis, N. Thi Hoang Anh, E. Corrales, T. Machinini,  
1455 F. R. da Silva, G. Paiman, K. Thiong'o, Z. Zainal, G. B. Brothers, K. R. Wolff, T. Nakano, R. Stübi, G. Romanens,  
1456 G.J. R. Coetzee, J. A. Diaz, S. Mitro, M. Mohamad and S.-Y. Ogino, Ozonesonde Quality Assurance: The JOSIE–  
1457 SHADOZ (2017) Experience, *Bulletin of the American Meteorological Society*, 100, 1, 155-171, 10.1175/BAMS-D-  
1458 17-0311.1, 2019.
- 1459
- 1460 Thompson, A. M., Stauffer, R. M., Wargan, K., Witte, J. C., Kollonige, D. E., & Ziemke, J. R.: Regional and seasonal  
1461 trends in tropical ozone from SHADOZ profiles: Reference for models and satellite products, *J. Geophys. Res.-  
Atmos.*, 126, e2021JD034691. <https://doi.org/10.1029/2021JD034691>, 2021.



- 1462 Torres, O., Herman, J. R., Bhartia, P. K., and Ahmad, Z.: Properties of Mount-Pinatubo Aerosols as Derived from  
1463 Nimbus-7 Total Ozone Mapping Spectrometer Measurements, *J. Geophys. Res.-Atmos.*, 100, 14043–14055,  
1464 <https://doi.org/10.1029/95JD01224>, 1995.
- 1465 Tweedy, O. V., Kramarova, N. A., Strahan, S. E., Newman, P. A., Coy, L., Randel, W. J., Park, M., Waugh, D. W.,  
1466 and Frith, S. M.: Response of trace gases to the disrupted 2015–2016 quasi-biennial oscillation, *Atmos. Chem. Phys.*,  
1467 17, 6813–6823, <https://doi.org/10.5194/acp-17-6813-2017>, 2017.
- 1468 Van Malderen, R., Marc A. F. Allaart, M. A. F., Hugo De Backer, H., Herman G. J. Smit, H. G. J., Dirk De Muer, D.  
1469 D.: On instrumental errors and related correction strategies of ozonesondes: possible effect on calculated ozone trends  
1470 for the nearby sites Uccle and De Bilt, *Atmos. Meas. Tech.*, 9, 3793–3816, <https://doi.org/10.5194/amt-9-3793-2016>,  
1471 2016.  
1472
- 1473 Wallace, J.M., The general circulation of the tropical lower stratosphere. *Rev. Geophys. Space Phys.*, 11, 191–222,  
1474 <https://doi.org/10.1029/RG011I002P00191>, 1973.  
1475
- 1476 Wallace, J.M., L. Panetta, and J. Estberg, Representation of the equatorial stratospheric quasi-biennial oscillation in  
1477 EOF phase space. *J. Atmos. Sci.*, 50, 1751–1762, [https://doi.org/10.1175/1520-0469\(1993\)050<1751:ROTESQ>2.0.CO;2](https://doi.org/10.1175/1520-0469(1993)050<1751:ROTESQ>2.0.CO;2), 1993.  
1478  
1479
- 1480 Wargan, K., C. Orbe, S. Pawson, et al. J. R. Ziemke, L. D. Oman, M. A. Olsen, L. Coy, and K. E. Knowland. 2018.  
1481 Recent decline in extratropical lower stratospheric ozone attributed to circulation changes *Geophysical Research*  
1482 *Letters*, <https://doi.org/10.1029/2018gl077406>.  
1483
- 1484 Wasserstein, R. L., Schirm A.L., Lazar, N.A., Moving to a World Beyond “ $p < 0.05$ ”, *The American Statistician*,  
1485 73:sup1, 1-19, <https://doi.org/10.1080/00031305.2019.1583913>, 2019.  
1486
- 1487 Weber, M., Arosio, C., Coldewey-Egbers, M., Fioletov, V. E., Frith, S. M., Wild, J. D., Tourpali, K., Burrows, J. P.,  
1488 and Loyola, D.: Global total ozone recovery trends attributed to ozone-depleting substance (ODS) changes derived  
1489 from five merged ozone datasets, *Atmos. Chem. Phys.*, 22, 6843–6859, <https://doi.org/10.5194/acp-22-6843-2022>,  
1490 2022a.  
1491
- 1492 Weber, M., W. Steinbrecht, C. Arosio, R. van der A, S. M. Frith, J. Anderson, L. Ciasto, M. Coldewey-Egbers, S.  
1493 Davis, D. Degenstein, V. E. Fioletov, L. Froidevaux, D. Hubert, D. Loyola, C. Roth, A. Rozanov, V. Sofieva, K.  
1494 Tourpali, R. Wang, and J. D. Wild: Stratospheric Ozone [in “State of the Climate in 2020“], *Bull. Amer. Meteor.*, 103  
1495 (8), S90–S92, <https://doi.org/10.1175/BAMS-D-22-0092.1>, 2022b.  
1496



- 1497 Wild, J.D., S.-K. Yang, and C.S. Long, Ozone Profile Trends: An SBUV/2 Perspective (QOS2016-133), in  
1498 Proceedings of the Quadrennial Ozone Symposium, Edinburgh, Scotland,  
1499 <https://meetingorganizer.copernicus.org/QOS2016/QOS2016-133.pdf>, last access February 6, 2024, 2016.  
1500
- 1501 Witte, J. C., Thompson, A. M., Herman G. J. Smit, H. G. J., Fujiwara, M., Posny, F., Coetzee, G. J. R., Northam, E.  
1502 T., Johnson, B. J., Sterling, C. W., Mohamad, M., Ogino, S-Y., Jordan, A., da Silva, F. R.: First reprocessing of  
1503 Southern Hemisphere ADDitional OZonesondes (SHADOZ) profile records (1998-2015) 1: Methodology and  
1504 evaluation, *J. Geophys. Res.*, 122, <https://doi.org/10.1002/2016JD026403>, 2017.  
1505
- 1506 Witte, J. C., Thompson, A., M., Smit, H. G. J., Vömel, H., Posny, F., Stübi, R.: First reprocessing of Southern  
1507 Hemisphere Additional Ozonesondes (SHADOZ) Profile Records. 3. Uncertainty in ozone profile and total column,  
1508 *J. Geophys. Res.*, 123(6), 3243-3268, <https://doi.org/10.1002/2017JD027791>, 2018.  
1509
- 1510 Witte, J. C., Thompson, A. M., Schmidlin, F. J., Northam, E. T., Wolff, K. R., Brothers, G. B.: The NASA Wallops  
1511 Flight Facility digital ozonesonde record: Reprocessing, uncertainties, and dual launches. *J. Geophys. Res.*, 124, 3565–  
1512 3582, <https://doi.org/10.1029/2018JD030098>, 2019.  
1513
- 1514 WMO (World Meteorological Organization), Scientific Assessment of Ozone Depletion: 2014, Global Ozone  
1515 Research and Monitoring Project-Report No. 55, 416 pp., WMO: Geneva, Switzerland,  
1516 available at: <https://www.esrl.noaa.gov/csd/assessments/ozone/2014/>, 2014.  
1517
- 1518 WMO (World Meteorological Organization), Scientific Assessment of Ozone Depletion: 2018, Global Ozone  
1519 Research and Monitoring Project-Report No. 58, 588 pp., WMO: Geneva, Switzerland,  
1520 <https://library.wmo.int/idurl/4/56362>, 2018.  
1521
- 1522 WMO (World Meteorological Organization), Scientific Assessment of Ozone Depletion: 2022, GAW Report No. 278,  
1523 509 pp.; WMO: Geneva, Switzerland, <https://ozone.unep.org/science/assessment/sap>, 2022.  
1524
- 1525 Wohltmann, I., Rex, M., Brunner, D., and Mäder, J., Integrated equivalent latitude as a proxy for dynamical changes  
1526 in ozone column, *Geophys. Res. Lett.*, 32, L09811, <https://doi.org/10.1029/2005GL022497>, 2005.  
1527
- 1528 Wolter, K., and M. S. Timlin, El Niño/Southern Oscillation behaviour since 1871 as diagnosed in an extended  
1529 multivariate ENSO index (MEI.ext). *Intl. J. Climatology*, 31, 14pp., 1074-1087, <https://doi.org/10.1002/joc.2336>,  
1530 2011.  
1531



- 1532 Yoon, S., Kotsakis, A., Alvarez, S. L., Spychala, M. G., Klovenski, E., Walter, P., Morris, G., Corrales, E., Alan, A.,  
1533 Diaz, J. A., and Flynn, J. H., Development and testing of a novel sulfur dioxide sonde, *Atmos. Meas. Tech.*, 15, 4373–  
1534 4384, <https://doi.org/10.5194/amt-15-4373-2022>, 2022.
- 1535
- 1536 Zhang, J., and Coauthors, Influence of the Arctic Oscillation on the Vertical Distribution of Wintertime Ozone in the  
1537 Stratosphere and Upper Troposphere over the Northern Hemisphere. *J. Climate*, 30, 2905–2919,  
1538 <https://doi.org/10.1175/JCLI-D-16-0651.1>, 2017.
- 1539
- 1540 Zerefos, C., Kapsomenakis, J., Eleftheratos, K., Tourpali, K., Petropavlovskikh, I., Hubert, D., Godin-  
1541 Beekmann, S., Steinbrecht, W., Frith, S., Sofieva, V., and Hassler, B.: Representativeness of single lidar  
1542 stations for zonally averaged ozone profiles, their trends and attribution to proxies, *Atmos. Chem. Phys.*,  
1543 18, 6427–6440, <https://doi.org/10.5194/acp-18-6427-2018>, 2018.